Characterizing a novel viral sensitizer BI-D1870

By

Margaret Watson

Thesis submitted to the

Faculty of Graduate and Postdoctoral Studies

in partial fulfillment of the requirements

for the degree of Master of Science

Department of Biochemistry, Microbiology, and Immunology

Faculty of Medicine

University of Ottawa

Abstract

Oncolytic viruses (OVs) are an emerging cancer therapy that use an oncotropic virus to selectively infect and kill cancer cells, as well as stimulate long-lasting anti-tumor immune responses. In order to achieve high therapeutic efficacy, OVs need sufficient replication within the tumor tissue to mediate these effects. However, OV's infectivity varies between different tumors and the host's immune system can rapidly clear the virus, hampering treatment efficiency. Oncolytic virus sensitizers are chemical compounds that specifically enhance OV's infectivity and efficacy. In our lab, I found that treatment of various cancer cell lines with BI-D1870, a pan-RSK (ribosomal S6 kinase) inhibitor, resulted in augmented Herpes Simplex Virus-1 (HSV1) and Vesicular Stomatitis Virus (VSVΔ51) infectivity. I also demonstrated that the effects of BI-D1870 on viral infection are virus-specific, and that RSK inhibition is not the primary target causing the enhancement of HSV1 and VSVΔ51 infection. Finally, BI-D1870 structural analogs were generated in an attempt to enhance the efficacy and selectivity of BI-D1870-based OV sensitizers. One of the analogs synthesized, KA-019, showed an improvement in the augmentation of OV infection over BI-D1870. As a genetically engineered strain of HSV1 has been approved by FDA for treatment of melanoma, the results of my project propose a novel viral sensitizer to improve viral replication within tumour cells with the hope of improving therapeutic efficacy.

Acknowledgements

I would like to express my most sincere gratitude towards my advisor, Dr. Tommy Alain, for providing me the opportunity to undertake this project, allowing me to grow and develop as a scientist and researcher. I am extremely grateful for his continuous teaching, support, motivation, and understanding.

To Dr. Chris Boddy, thank you for taking the time to go through the chemistry with me, supporting me, checking in with me and always answering my questions. To the members of the Boddy lab, especially Graham, Jesse and Puneet, thank you for teaching me organic chemistry, cheering me up when things went wrong, and for always lending a helping hand.

To Dr. Jean-Simon Diallo, thank you for being a part of my thesis advisory committee, your expertise, advice and feedback has been greatly appreciated. I could not have chosen better anyone better to guide me along with my research.

To my lab mates, Huy-Dung, Roberta, Vickey, Nasana, Jian-Jun, Bruno, Tyson and An-Dao, a big thank you for helping me along as I learned all new techniques (and eventually mastered the western blot), and for providing advice, support and encouragement through all my experiments, troubles and woes.

A huge shout out to the members of the Cowan lab, Anna, Stephen, Xiao, and Marie-Eve. I am so grateful for your friendship, love, and support my entire time at the CHEORI. Thank you for putting up with my raging pregnancy hormones, and OCD in the tissue culture room.
I am forever grateful to Marie Albert for all her help through my pregnancy and after. You put a smile on my face when I was feeling low, and took care of me through it all.
To my parents, thank you for your never ending love and support, the extra food, hugs and advice, and for being the best grandparents in the world.

And above all, to my wonderful husband, for your understanding (especially with my mood swings), endless love, support and delicious food; for wiping my tears, making me laugh, holding my hand and telling me everything was going to be okay. And especially for helping me bring our little baby girl into this world and taking care of the two of us. Thank you.

This is for you Abigail.

TABLE OF CONTENTS

List of Abbreviations

ADP	Adenosine diphosphate
AGC	Protein A, G, C family
Akt	Also known as PKB – protein kinase B
AMP	Adenosine monophosphate
AMPK	AMP-activated protein kinase
ATCC	American Type Culture Collection
ATP	Adenosine triphosphate
BSA	Bovine serum albumin
cAMP	Cyclic AMP
CAS	Chemical Abstracts Service
CK1	Casein kinase 1
CREB	cAMP response element-binding protein
CRISPR	Clustered regularly interspaced short palindromic repeats
DCM	Dichloromethane
DMEM	Dulbecco's Modified Eagle's Medium
DMF	Dimethylformamide
DMSO	Dimethyl sulfoxide
DNA	Deoxyribonucleic acid
DYRK1a	Dual specificity tyrosine-phosphorylation-regulated kinase 1A
EDTA	Ethylene-diamine-tetra-acetic acid
FBS	Fetal bovine serum
5-FU	5-fluorouracil
GM-CSF	Granulocyte-macrophage colony-stimulating factor
GMP	Guanosine monophosphate
HCl	Hydrochloric acid

HIV	Human immunodeficiency virus
IC	Inhibitory concentration
ICP	Infected cell protein
IFN	Interferon
IL	Interleukin
IRAK4	Interleukin-1 receptor-associated kinase 4
JNK	c-Jun N-terminal kinase
Lck	Lymphocyte-specific protein tyrosine kinase
LDL	Low density lipoprotein
LKB1	Liver kinase B1
Lok	Lymphocyte oriented kinase
MAPKAP-K3	MAP kinase-activated protein kinase 3
MARK	MAP/microtubule affinity-regulating kinase 3
MEK	Mitogen-activated protein kinase kinase
MELK	Maternal embryonic leucine zipper kinase
MOI	Multiplicity of infection
mRNA	Messenger ribonucleic acid
MST	Macrophage stimulating kinase
mTORC1	Mammalian target of rapamycin complex 1
NEK	NIMA related kinase
NFκB	Nuclear factor kappa-light-chain-enhancer of activated B cells
NK	Natural killer cell
OV	Oncolytic virus
PD-L1	Programmed death ligand 1
Pfu	Plaque forming unit
PIM	Proto-oncogene serine/threonine kinase
PHK	Phosphorylase kinase
RFP	Red fluorescent protein

RNA	Ribonucleic acid
RT	Room temperature
SDS-PAGE	Sodium dodecyl sulfate–polyacrylamide gel electrophoresis
SGK1	Serum and glucocorticoid-regulated kinase 1
SMC	Smac mimetic compounds
SmMLCK	Smooth muscle myosin light chain kinase
THF	Tetrahydrofuran
TLC	Thin layer chromatography
TNF	Tumour necrosis factor
WT	Wild type

List of Figures

Chapter 1 Introduction

1.1 Overview

1.1.1 Cancer

Cancer is defined as the uncontrollable growth of cells that form a tumour, and is one of the leading causes of death in Canada.[1] With the prevalence of cancer today, it is imperative that novel therapeutic approaches are discovered. Cancer cells are resilient in many ways, and are known to resist apoptosis (programmed cell death) and translation suppression. They also have defects in their regulatory signaling pathways that govern normal cell proliferation and homeostasis.[2,3] Hanahan and Weinberg's original 'hallmarks of cancer' include six alterations in cell physiology that dictate cancerous growth: self-sufficiency in growth signals, the ability to block growth-inhibitory signals, evasion of apoptosis, limitless replication, sustained angiogenesis, tissue invasion and metastasis.[3] Two new hallmarks have recently been suggested – the reprogramming of energy metabolism and the evasion of immune destruction.[4]

1.1.2 Cancer metabolism

Cancer cells commonly have an ability to acquire essential nutrients from a nutrient-poor environment and use them to proliferate.[5,6] Tumours have an increased amount of growth factors which stimulate two key signaling pathways: the mitogen-activated protein kinase (MAPK)/extracellular signal-regulated kinase (ERK) pathway and the phosphoinositide 3-kinase (PI3K) pathway which activates the mammalian target of rapamycin (mTOR) to stimulate cell growth.[6] mTOR is a serine/threonine kinase activated downstream of the PI3K/Akt pathway and

enhances cap-dependent mRNA translation and cell growth, as well as inhibiting catabolic reactions mediated by autophagy.[6]

1.1.3 Cancer treatments

Treatments for cancer have evolved over the years, with the first successful surgical procedure under general anesthesia having been performed by Seishu Hanaoka in 1804.[7] Surgery is one of the leading treatments for localized cancer by completely removing the tumour. It can potentially cure the patient if the cancer has been detected early enough and has not yet spread throughout the body. In 1895, radiation therapy emerged as a new treatment for cancer with the discovery of the x-ray by Wilhelm Roentgen.[8] This type of therapy uses high doses of radiation to damage DNA therefore blocking the ability of the cancer cell to divide.[9] Later, in 1903, S.W. Goldberg and Efim London used radium to achieve a complete positive response in two patients with basal cell carcinoma.[10] Surgery and radiation therapy were the standard of care for cancer treatment until the late 1940s when anti-metabolites, such as methotrexate, and alkylating agents, like nitrogen mustard, were discovered and used as chemotherapy agents for the treatment of cancer.[11] These drugs act by inhibiting DNA and/or the cell cycle, inducing cell death, but cannot distinguish between normal cells and cancer cells.[12] By the 1950s, chemotherapy was successfully being used in the treatment of leukemia and lymphoma. At this time, physicians and researchers saw that chemotherapy did not acquire the same success rates of complete remission in advanced solid tumours as surgery.[13] As a result, new drugs and drug combinations and the use of chemotherapy after surgery was developed in the 1970s to improve overall survival. Since then, cancer treatment became more targeted and focused on specific pathways, including anti-angiogenesis, signaling and specific mutations.[13] Today, the standard of

care is chemotherapy and radiation, though there are limitations with these treatments as they cannot selectively target cancer cells, and can lead to high toxicity and resistance.[14] New therapies in clinical trials try to resolve this problem with specific targeting of cancer cells and pathways.

1.1.4 Oncolytic viruses as a cancer therapy

One such therapy is the use of oncolytic viruses (OVs), which were first used on their own in the 1950s. Live viruses were injected into cancer patients and showed promising results.[15] There are many different types of viruses, classified by phenotypic characteristics, but only a few are suitable as oncolytic agents. These viruses must be non-pathogenic, have intrinsic cancer selective killing ability, or the ability to be engineered to express attenuating or arming genes.[16] Viruses can usurp cellular apoptotic programs and deregulate cellular energetics, making them ideal as a cancer therapy. Oncolytic viruses are known to initiate systemic and anti-tumour immune responses specifically against cancer cells and not normal cells.[17] This specificity towards the tumour of the OV can be at the level of receptor-mediated cell entry, intracellular anti-viral responses and/or restriction factors that determine how susceptible the infected cell is to support viral gene expression and replication[14,16,17]

Oncolytic viruses on their own cannot lead to massive tumour cell death – the tumours need to be completely void of viral defense systems so the therapeutic agent can outpace the innate and adaptive anti-viral immune response.[14, 17] This innate anti-viral response represents a hurdle the oncolytic virus must overcome so that it can facilitate action against the tumour.[14] In order to do so, OVs have been used in combination with chemotherapeutic agents, radiation and

other therapies like immunomodulators.[16] These combination treatments mix potent viral oncolysis with effective and long lasting anti-tumour response.[17] This balance between anti-tumour and anti-viral immunity is a priority in the research of OV therapy.[14]

1.2 Oncolytic viruses

1.2.1 Overview of oncolytic viruses

Oncolytic viruses (OVs) include a wide range of DNA and RNA viruses that are naturally tumour-selective or can be genetically engineered, providing a diverse platform for immunotherapy.[18] Viruses that naturally replicate in tumour cells are non-pathogenic in normal cells because there is an increased sensitivity of the innate anti-viral signaling pathways or a dependence on oncogenic signaling pathways.[19] Viruses in this first class include parvoviruses, myxoma virus, Newcastle disease virus, reovirus and Seneca Valley virus. The second class of viruses include genetically-manipulated viruses that are used as vaccine vectors such as attenuated measles virus, polio virus and vaccinia virus (VACV). Also included in this class of viruses are those which have been genetically-engineered with mutations or deletions within essential genes that restrict replication in normal cells, but not tumour cells. Examples include: adenovirus, herpes simplex virus 1 (HSV1), vaccinia virus, vesicular stomatitis virus (VSVΔ51) and Maraba.[20] Certain features of OVs provide an advantage over current cancer therapies. For example, there is a low probability that OVs will generate resistance as they can target multiple oncogenic pathways, can bring about cytotoxicity in several different ways, replicate in a tumour-selective fashion, are non-pathogenic and have minimal systemic toxicity.[21] Encoded transgenes inserted into the viral genome can enhance the anti-tumour response or tumour cell.[22]

Before activating the immune system, viral dose in the tumour increases over time due to the amplification of viral replication, in contrast to the pharmacokinetics of chemotherapy drugs which decrease in dose over time.[19] While these features have an edge over current therapies, there are still problems with OV therapy. The most important issue is to resolve delivery – systemic intravenous administration is simpler than an intratumoural injection and is able to target multiple tumours. However, this results in a lack of extravasation into tumours and viral sequestration into the liver which limits the effectiveness of OVs.[21] Neutralization antibodies in the circulation system can also inactivate OVs. Cell carriers such as mesenchymal stromal cells, myeloid-derived suppressor cells (MDSCs), neural stem cells, T cells, cytokine-induced killer cells or irradiated tumour cells can shield the virus from neutralization and help with delivery to the tumour.[19] Another obstacle in OV therapy include physical barriers that are involved in reducing the spread of OVs such as necrosis, calcification, hypoxia, acidosis, increased proteolytic activity and high interstitial pressures. Many clinical trials with OVs have used intratumoural injections to bypass the tumour architectural barriers, but this limits application to tumours that are physically inaccessible.[23] Other barriers include tumour size and heterogeneity which limit virus bio-distribution, and the blood-brain barrier which may limit the ability of some viruses to reach primary brain tumours and brain metastases, but this can be overcome by direct injection into central nervous system tumours.[23] One other main issue to overcome with OV therapy is the interaction with the immune system which can affect the therapeutic outcome in two different ways: 1) positively by inducing an anti-tumour immune response, or 2) negatively by limiting the replication and/or spread of the virus.[21]

1.2.2 OVs activate anti-tumor immune response

Oncolytic viruses promote anti-tumour responses through a dual mechanism of action: selective tumour cell killing and induction of systemic anti-tumour immunity. Abnormalities in the cancer cell response to stress, cell signaling and homeostasis provide an advantage for viral replication.[23] The dysregulation of some signaling pathways in cancer cells leads to higher infection rates and cell death. The RAS signaling pathway, which regulates carcinogenesis (the resistance to cell death and proliferation) can be over-active in cancer cells. The protein kinase R (PKR) pathway is not activated in these cells, leading to viral infection as mRNA translation is not inhibited. Some viruses, such as reovirus and vaccinia virus, have a natural selectivity for these cancer cells.[23] Other viruses have mutations that allow them to replicate in cells with defective PKR signaling, leading to the preferential lysis of tumour cells. For example, HSV1 has deletions of the ICP34.5 gene and glycoprotein US11 and is unable to block PKR phosphorylation.[24] Cancer cells also have dysregulation of their anti-viral mechanisms, based around type I interferon (IFN) signaling, giving an advantage to viruses like VSV. Type I IFNs are critical for the anti-viral and anti-tumour response in healthy cells as they promote an immune response to clear the virus, and reduce proliferation.[25]

Oncolytic viruses can induce immunogenic cell death (ICD) – a particular form of apoptosis where the death of cancer cells can induce an effective anti-tumour immune response through the recruitment and activation of dendritic cells and the stimulation of specific T lymphocytes.[14] ICD triggers the endoplasmic reticulum to release metabolites called damage-associated molecular patterns (DAMPs) such as calreticulin, ATP and high mobility group protein B1 (HMGB1).[14,26] Antigen presenting cells in the tumour microenvironment will recognize DAMPs and generate an immune response. This primary immune response can create

anti-tumour immunological memory with long term benefits to protect the host against relapse.[2,14,21] There are several aspects of the OV-tumour/host interaction that are important in explaining the effectiveness of OV therapy: the innate immune responses and degree of inflammation that is induced; the different types of virus-induced cell death; the inherent tumour physiology (like infiltrating and resident immune cells); vascularity and hypoxia; lymphatics and stromal architecture; and the tumour cell phenotype, which includes alterations in IFN signaling, oncogenic pathways, cell surface immune markers (such as major histocompatibility test (MHC) and natural killer cell (NK) receptors) and the expression of immunosuppressive factors.[27–29]

1.2.3 Anti-viral innate immunity

The anti-viral response is made up of several pathways (**Figure 1**) that are activated after the detection of a virus. The innate immune system is the first line of defense against viruses, and produces cytokines like IFNs, interleukins and tumour necrosis factor.[30] The recognition of the virus by the cell occurs through pattern recognition receptors that detect viral proteins, cytosolic DNA or double stranded RNA.[31] Cellular pathways that are activated in response to viral infection lead to formation of IFN related factor 3 (IRF-3), the histone acetyltransferases p300/CREB-binding protein (CBP) and transcriptional cofactors like activator protein 1 (AP-1), nuclear factor kappa-light-chain-enhancer of activated B cells (NFκB), and high mobility group protein I/Y (HMGI(Y)).[32,33] NFκB is a transcription factor activated through phosphorylation by IκB (inhibitor of κB) kinase (IKK) which controls the expression of type I IFN and is often dysregulated in cancer.[34] IKK3 and tumor necrosis factor receptor-associated factor family member-associated NFκB activator (TANK)-binding kinase 1 play a role in phosphorylating IRF-3 in response to viral infections.[30]

Many viruses have a way to disrupt the host immune response by interfering with IRF-3 activation, for instance, by producing a protein that will directly bind and disable IRF-3 or a protein that will interact with p300/CBP and alter interactions with IRF-3.[30] HSV1 infection is known to block the signaling effects of IFNs by reversing the effects of PKR,[35] and has been shown to block the phosphorylation of signal transducer and activator of transcription protein (STAT1 and STAT2).[36] Another pathway involved in the anti-viral response is the mTOR pathway. A previous study reported that the infection of DNA viruses induces the interaction of downstream mTOR effectors ribosomal protein S6 kinase (S6K1) and the signaling adaptor stimulator of interferon genes (STING) in a cyclic GMP-AMP (cGAMP)-synthase-dependent manner promoted by TANK-binding kinase 1 (TBK1). Furthermore, recent studies have shown that the mTORC1-S6K1 signaling axis modulates toll like receptor (TLR) pathways.[37]

TLRs are cell surface and intracellular pattern recognition receptors that are activated in response to pathogen-associated molecular patterns (PAMPs), including elements of viral capsids, DNA, RNA and viral protein products. The signaling of TLR activates the host cell anti-viral response and systemic innate immunity.[23] When the immune system is triggered, the virus will be cleared and the lytic effect of viral infection and anti-tumour immunity is decreased. The immune system detects viral infection and activates the adaptive immune system as well as the innate immune system to act against the virus.[14] Some downstream effectors involved in the clearance of OVs are TNF-associated factor 3 (TRAF3), IRF3, IRF7, and retinoic acid-inducible gene 1 (RIG1). These effectors activate the Janus kinase (JAK)/STAT pathway which coordinates the antiviral machinery in infected cells, reinforces IFN release leading to the activation of PKR which will recognize double stranded RNA and other viral elements. When activated, PKR will terminate mRNA translation via eIF2α phosphorylation and promote rapid cell death and clearance.[38]

Figure 1. The anti-viral response in normal cells and cancer cells. Modified from Kaufman et al.[23] In normal cells, after viral infection, the anti-viral pathway is activated. In cancer cells, the pathway is disrupted as they can downregulated certain components of the anti-viral response, such as IRF3 and IRF7 limiting the detection of viral particles. This leads cancer cells to be more susceptible to viral replication.

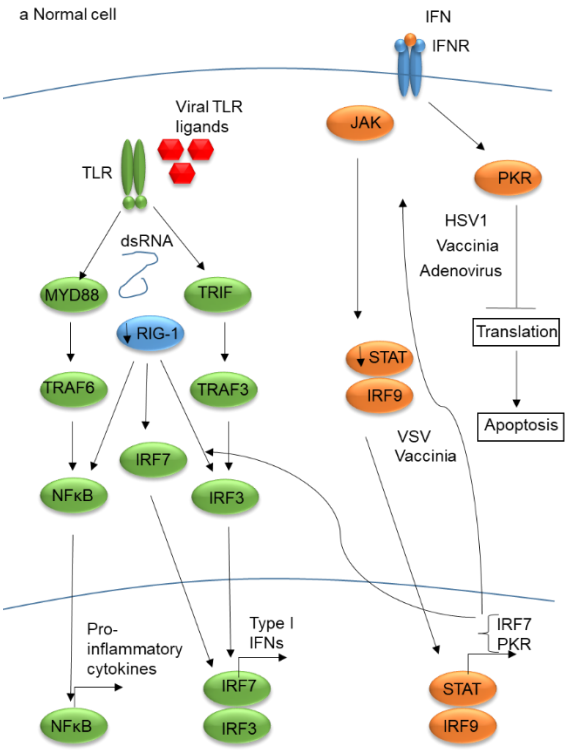
a Normal cell
IFN
IFNR
Viral TLR ligands
TLR
JAK
PKR
HSV1
Vaccinia
Adenovirus
dsRNA
MYD88
TRIF
RIG-1
Translation
STAT
IRF9
TRAF6
TRAF3
Apoptosis
VSV
Vaccinia
IRF7
NFκB
IRF3
Pro-inflammatory cytokines
Type I IFNs
IRF7
PKR
IRF7
IRF3
STAT
IRF9
NFκB

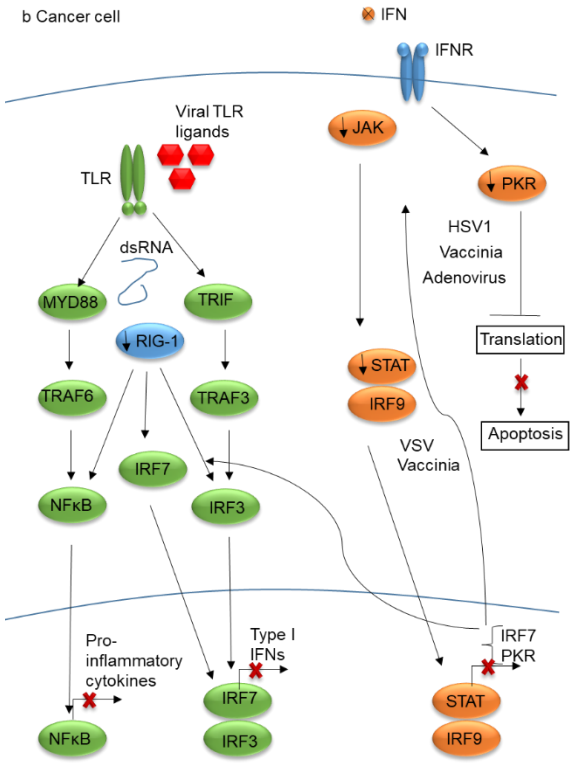
b Cancer cell
IFN
IFNR
Viral TLR ligands
TLR
JAK
PKR
HSV1
Vaccinia
Adenovirus
dsRNA
MYD88
TRIF
RIG-1
Translation
STAT
IRF9
TRAF6
TRAF3
Apoptosis
VSV
Vaccinia
IRF7
NFκB
IRF3
Pro-inflammatory cytokines
Type I IFNs
IRF7
PKR
IRF7
IRF3
STAT
IRF9
NFκB

During OV therapy, the aim of immune stimulation is to activate the T lymphocytes against tumour antigens. T cells can recognize tumour peptides and provide long-term immunity. OVs will generate the expression of cytokines leading to the recruitment of lymphocytes in order to break down the immune-suppressive environment. Oncolytic viral therapy will use this inflammatory response in order to target tumour cells.[14] Below I will introduce specific oncolytic viruses and their oncolytic properties.

1.2.4 Herpes Simplex Virus (HSV1)

Herpes Simplex Virus (HSV1) is a member of the alphaherpes virus family with a large genome and double stranded DNA that replicates in the nucleus of infected cells.[23] It was one of the first viruses to be developed into a recombinant oncolytic virotherapeutic vector as it has a large genome that is easy to control, allowing insertions of transgenes (such as granulocyte-macrophage colony-stimulating factor (GM-CSF)).[39] HSV1 is a major human pathogen that causes skin lesions and rashes and can infect peripheral nerves.[23,39] The symptoms of HSV1 infection include cold sores of the mouth and keratitis in the eyes, and is capable of causing life-threatening diseases in immunocompromised individuals such as newborns, patients with HIV, or patients undergoing immunosuppressive treatment.[40] HSV1 can infect many types of cells and enters through viral surface glycoproteins, herpesvirus entry mediator (HVEM) or surface nectins.[23] The process of infection starts when virions bind to heparan sulfate moieties on the host cell surface. This attachment triggers a cascade of molecular interactions that involve many viral and host cell proteins and receptors leading to the penetration of the viral nucleocapsid into the cytoplasm.[40] The nucleocapsid is transported to the nuclear membrane and the viral DNA is released for replication in the nucleus. HSV1 uses the glycoprotein D as the receptor binding

protein in order to enter the cell.[39] HSV1 can also use macropinocytosis and phagocytosis to enter the cell.[41] Penetration into the cell depends on the host cell type and the mode of entry in which HSV1 can pass into the cell. The virus may require fusion of the virion envelope with the plasma membrane or the membrane of an intracellular vesicle. After entry, the nucleocapsids dissociate and bind to a microtubule (MT)-dependent minus end-directed motor (dynein).[40] After the initial infection, the virus can remain latent in neurons, a key feature of alphaherpes viruses.[23,39,40]

HSV1 has been extensively engineered as a viral platform for oncolytic viruses. The viral toxicity of HSV1 is mediated partially by the gene product ICP34.5, which counteracts the type I IFN response and antagonizes PKR signaling pathway in non-dividing cells.[23] When ICP34.5 is deleted, the virus is unable to replicate in neurons or mediate a latent infection, reducing the overall pathogenesis of HSV1. The infected cell protein 0 (ICP0) is an immediate-early protein responsible for finding the balance between lytic replication and the reactivation from latency. ICP0 gives the virus a significant growth advantage during replication, especially at low multiplicity of infection (MOI). [42] ICP0-null mutants were shown to be attenuated for viral growth and impaired for viral reactivation. ICP0 can activate HSV1 promoters and viral gene expression, triggering the activation of IRF3, which, in the absence of ICP0, translocates to the nucleus to activate the IFN-ß promoter.[42] ICP0 can also prevent the activation of NFκB by TLRs that detect viral components.[30,42]

The most commercially advanced HSV1 based oncolytic virus used in the clinic is Talimogene laherparepvec (T-VEC), which includes deletions of ICP34.5 and ICP47.[23] The deletion of ICP47 results in the presentation of viral antigens by healthy and cancer cells, leading to the containment of infection in healthy tissues, and the immune-mediated destruction of

cancer cells that propagate HSV1.[23,39] This deletion induces the early activation of US11 promoter which blocks the phosphorylation of PKR preventing cancer cells from undergoing apoptosis when they have been infected. T-VEC also includes the human GM-CSF gene engineered into the viral genome in the place of the ICP34.5 gene, which bolsters the induction of anti-tumour immunity.[39] In preclinical studies, T-VEC demonstrated potent lytic effects against several different tumour cell lines, such as melanoma and pancreatic cancer.[43] In a phase II trial for the treatment of unresectable stage IIIC and IV melanoma, an initial dose of 10^6 pfu/ml was given, followed after three weeks by a dose of 10^8 pfu/ml given every two weeks until a maximum clinical response, unacceptable toxicity or disease progression was reached.[44] It was found that in 50 participants, there was a 26% response rate, with low-grade toxicity, including fever, fatigue and reactions at local site injections. In a phase III trial with 436 patients, the durable response rate (the response beginning within 12 months of treatment and lasting for at least 6 months) was 16.3 %, with an improved median survival of 23.3 months. These trials lead to the approval by the US Food and Drug Administration (FDA) of T-VEC for use as a cancer therapy for melanoma in 2015.[45] There are several other viruses that are currently in clinical trials, such as measles virus, reovirus, vaccinia virus, and Newcastle disease virus. An additional oncolytic virus that is promising for use in the clinic is vesicular stomatitis virus.

1.2.5 Vesicular Stomatitis Virus (VSV)

VSV belongs to the Rhabdoviridae family, which consists of large, genetically diverse single-stranded, negative sense RNA viruses.[46] They have a strong safety profile in humans, as well as vigorous immunogenicity and genetic malleability which are key features of these viruses. VSV is a cattle virus, not a human pathogen, and so pre-existing neutralizing antibodies

are rarely found in humans.[39,46] The rhabdoviridae genome consists of five genes: the nucleocapsid (N), the phosphoprotein (P), the matrix protein (M), the glycoprotein (G), and large polymerase (L). Many of these viruses are pantropic (like VSV and Maraba) and enter host cells through receptor-mediated (low-density lipoprotein (LDL) receptor) or clathrin-mediated endocytosis and replicate in the cytoplasm.[16,41,46] VSV cell entry has been made tumour selective through retargeting strategies – replacing the VSV glycoprotein with a more selective entry glycoprotein such as the measles F and H proteins.[16] Once inside the tumour cell, VSV replicates extremely quickly, expresses its gene products at high levels and elicits a strong humoral and cellular immune response towards their expressed foreign antigens.[46] The oncolytic VSV, can have one of two main M51 mutations: M51R (methionine to arginine) or ΔM51 (deletion of methionine 51). The amino acid point mutation or deletion of methionine in the viral matrix (M) protein at position 51 interferes with the ability of the virus to inhibit the host interferon response. The methionine in this position is essential for this, and its loss allows infected cells to produce and release IFN in response to infection. This leads to a sensitivity to IFN which inhibits viral replication in host cells.[47–49] Despite being rendered attenuated via these mutation, oncolytic VSVs are still capable of infection and lytic destruction of metastatic tumours, as the virus can infect multiple tumours simultaneously, offering the potential to restore immune surveillance mechanisms that can lead to a complete response in the patient and prevent recurrence.[50] The effectiveness of VSV oncolytic therapy is determined by the combination of two main factors: the type I IFN deficiency and the targeted viral replication in tumours.[51] mTORC1 can regulate type I IFN production and virus propagation through 4E-BPs and S6Ks. Thus, blocking type I IFN and antiviral cytokines by rapamycin in conjunction with treatment with viruses like VSV, myxoma, vaccinia or adenovirus, augments oncolysis. The inhibition of

type I IFN production by rapamycin is the primary mechanism that potentiates VSV therapeutic effect.[51]

The safety of VSV has been evaluated and found to have risk with strains that have mutations in the M or G gene which could revert back to the wildtype VSV upon passaging, but no neurological symptoms were detected when injected intra-hepatically into rhesus macaques, and was considered safe enough to proceed into phase I clinical trials.[39]

1.2.6 Vaccinia Virus (VACV)

The last OV to be covered in my thesis is the poxvirus used in the vaccination against smallpox, and one of the most developed viruses to be used in several different ways – vaccinia virus.[52] Vaccinia virus (VACV) has a large genome and shields its extracellular enveloped virions from the host immune system, which allows it to spread between tumours. It replicates and lyses cells quickly and induces a strong cytotoxic T lymphocyte response, recruiting neutralizing antibodies without causing significant disease in humans.[39] Viruses belonging to the vaccinia family take advantage of macropinocytosis in order to get into the cell, a process that is preceded by plasma membrane activity in the form of ruffling (motile protrusions of the cell membrane that are rich in actin filaments). Macropinocytosis is a growth factor-induced, actin-dependent endocytic process leading to the internalization of fluid and membrane into vacuoles.[41] Ruffling is induced by the activation of actin and microfilaments connected to the plasma membrane by growth factors that will activate signaling cascades inducing changes in the dynamics of the actin filaments. Viruses can induce this ruffling activity independently of growth factors.[41] p21-activating kinase 1 (PAK1) regulates the cytoskeleton dynamics and motility and

is essential for all stages of macropinocytosis. Upon activation, PAK1 will relocate to the plasma membrane where it activates the effectors needed for ruffling, blebbing and macropinosome formation.[41] Once inside the cell, VACV can stimulate the cell for enhanced viral replication through the epidermal growth factor receptor (EGFR) as it has the pro-vaccinia growth factor (VGF) protein homologous to the epidermal growth factor (EGF) and transforming growth factor alpha (TGFα) in humans. The deletion of the VGF gene results in VACV that targets cells with an inherent EGFR pathway activity, often found in cancerous cells. Clinical trials with VACV have reported good safety in regards to toxicity, with minor side effects such as low grade fever and local pain.[39] Active vaccinia particles have been found to shed from skin injection sites after vaccination-clinical trials have shown live JX-594 (also known as Pexa-Vec or pexastimogene devacirepvec) detected in throat swabs and skin pustules in patients up to one week after administration. The three main oncolytic vaccinia viruses in use in clinical trials are: JX-594, Transgene (or TG6002), and GeneLUX (or GL-ONC1/GLV-1h68).[16] Monotherapies with oncolytic viruses are in clinical trials, however combination treatments with chemotherapeutics, histone deacytelase (HDAC) inhibitors, mTOR inhibitors, and other small molecule inhibitors have been tested in order to find the best therapeutic outcome.

1.3 Combination treatments with oncolytic viruses

The first combination treatments with oncolytic viruses involved standard of care chemotherapeutics. Chemotherapy induces cytotoxicity through the inhibition of DNA replication, the cell cycle or the disruption of microtubules. It can be immunosuppressive, which can augment the infection of OVs.[53] Some of the main chemotherapies used in parallel with oncolytic viruses include cyclophosphamide, irinotecan, temozolomide, cisplatin, gemcitabine,

5-fluorouracil, doxorubicin and paclitaxel. There are several mechanisms of action proposed to explain the effects of chemotherapy drugs with oncolytic viruses. These include reducing the activation of complement proteins;[54] inhibiting tumour cell and systemic anti-viral responses;[55,56] suppressing the adaptive anti-viral immune response, and decreasing the levels of neutralizing antibodies;[57] synergistic cell killing;[58,59] stimulation of anti-tumour immune response through ICD[60] and dampening of immune cells.[61] A number of the chemotherapeutics tested either enhanced[62] or inhibited[63] viral replication and spread.

Combination therapies evolved from using chemotherapy to small molecules that target the anti-viral immune pathway, specifically the type I IFN pathway. Some of the first small molecules to be tested as enhancers of oncolytic viral activity were histone deacetylase inhibitors (HDACi). It was found that histone deacetylase will lead to the repression of IFN stimulated genes (ISGs) after type I IFN stimulation, allowing for viral replication.[64] Three main HDACi used in combination with OVs include valproic acid (VPA), trichostatin A (TSA), and Vorinostat.[65] They are less toxic than chemotherapy drugs[66] and have been shown to synergize with HSV1,[67] VACV,[68] and VSV.[25] Other small molecules used in combination with oncolytic viruses include mTOR inhibitors like rapamycin and its analogs. Rapamycin can augment the replication of adenovirus, myxoma virus, VACV, HSV1, VSVΔ51, Newcastle disease virus and reovirus.[69]

In 2010, a high-throughput screening assay using VSVΔ51 was developed to look for compounds that could be used to enhance OV replication. One main compound was identified, viral sensitizer 1 (VSe1), a chlorinated furanone-based compound. VSe1 was found to increase the replication of VSVΔ51 through the inhibition of type I IFN and other cellular anti-viral effects.[70]

There are new small molecule inhibitors such as TPCA-1 (an inhibitor of IKK and JAK1, shown to improve in vitro spread of HSV1 and VSVΔ51),[71] Tecfidera (also known as dimethyl fumarate, shown to block type I IFN production and signaling and enhance the spread of VSVΔ51, HSV1 and Sindbis virus in vitro)[72] and ruxolitinib (a JAK inhibitor which decreases the anti-viral response and increases the replication of oncolytic measles and HSV1).[73] Apoptosis, bystander killing and microtubule destabilization are a few other processes on which small molecules exert an effect and can be combined with oncolytic viral therapy. For example, smac mimetic compounds (SMC) are small molecules that bind cellular inhibitor of apoptosis (IAPs) and target them for degradation, sensitizing cancer cells of death by apoptosis. This process is dependent on immune triggers like TNFα, TNF-related apoptosis inducing ligand (TRAIL) and type I IFN.[74] Beug et al proposed that combining SMC with oncolytic viruses could lead to bystander killing of tumour cells exposed to these cytokines.[75] The SMC LCL161 in combination with VSVΔ51 showed the elimination of different types of tumour cells through CD8+ T cell production of IFNγ or TNFα.[76] Sunitinib, a multi-kinase inhibitor of PKR, vascular endothelial growth factor receptor (VEGFR) and the platelet-derived growth factor receptor (PDGFR), has been approved for the treatment of renal cell cancer and is known to augment the viral replication of VSV in mouse models and induces bystander killing, a process by which cytokines are released to act on surrounding cells, leading to cell death.[17] In combination with Pexa-Vec, it has shown durable complete response (>6 years) of a patient.[77] Colchicine, an arthritis drug, is a known microtubule destabilizer, and has been shown to increase synergistic killing when combined with VSV by decreasing type I IFN translation and promotes bystander killing.[78,79]

Recent research has been done with immune checkpoint inhibitors that target the anti-cytotoxic T-lymphocyte-associated protein 4 (CTLA4) or programmed death 1 (PD-1) protein – immune checkpoint proteins that downregulate the immune response. The humanized anti-CTLA4 antibody ipilimumab was approved by the FDA in 2011 for the treatment of melanoma, and has two major roles: downregulating helper T cells, and increasing T regulatory suppressor functions,[80] but it is not always effective.[81] Zamarin et al combined ipilimumab with oncolytic Newcastle disease virus and found an enhanced sensitization of mouse tumours to the CTLA4 blockade.[82] Clinical trials with ipilimumab in combination with T-VEC are in progress for the treatment of melanoma (NCT01740297).[83]

1.4 Clinical trials with oncolytic viruses

Initial clinical trials with OVs began in the 1950s,[84] and there are now three OVs currently approved for cancer therapy: Rigvir (approved in Latvia, Georgia and Armenia), Oncorine H101 (approved in China), and T-VEC (approved in the USA).[16] Rigvir is an unmodified enteric cytopathogenic human orphan type 7 (ECHO-7) picornavirus that was approved for the treatment of melanoma in Latvia in 2004 – the first oncolytic virus to get regulatory approval anywhere in the world.[16] There is limited data published describing its efficacy, but it seems to have an effect on tumour recurrence after the surgical resection of melanoma.[85] Oncorine, or ONYX-015, is an attenuated serotype 5 adenoviral vector with four deletions in the viral E3 gene, and in the E1B-55k gene. It selectively replicates in p53 deficient tumours as E1B-55k is a strong repressor of p53.[86] T-VEC was approved by the FDA in 2015 for the treatment of non-resectable metastatic melanoma, and then later in the EU for locally advanced or metastatic cutaneous melanoma and is the most recent OV to gain national regulatory approval. T-VEC is a recombinant human

herpes simplex virus type 1 with deletions of the ICP34.5 and ICP47 genes, and has human GM-CSF encoded under cytomegalovirus (CMV) promoters.[45] Many other viruses, like rhabdoviruses, are in clinical development, along with clinical trials combining OVs with small molecules.

1.4.1 Combination clinical trials

On clinicaltrials.gov there are 74 trials with oncolytic viruses, of which 27 are combination treatments. The first published combination clinical trial with an oncolytic virus combines 5-fluorouracil (5-FU). Out of 37 patients, 19 had better response rates with the combination treatment compared to chemotherapy alone.[87] Phase I trials of ONYX-015 with gastrointestinal tumours metastatic to the liver, unresectable pancreatic carcinoma and advanced sarcomas showed positive outcomes and no enhanced toxicity.[88,89] HSV1 strain NV1020 was used in a Phase I/II clinical trial in the liver in combination with standard chemotherapy for colorectal cancer, and showed anti-tumour effects.[90]

There are a few ongoing clinical trials with oncolytic viruses and chemotherapy: a phase III trial of reovirus (REO-018) with carboplatin and paclitaxel for the treatment of head and neck cancer (NCT01166542), and vaccinia (Pexa-Vec) in combination with sorafenib for the treatment of hepatocarcinoma (NCT02562755). However, many trials are heading away from chemotherapeutics and towards a combination of immunotherapy and oncolytic viruses. There is a phase Ib/II trial for the treatment of melanoma with T-VEC and ipilimumab that indicates higher response rates in combination than for either one as a monotherapy.[91] Ongoing research in labs worldwide look at *in vitro* and *in vivo* effects of other small molecule inhibitors in

combination with oncolytic viruses. For the best possible response in the clinic, elevated replication of the OV in tumours is imperative. Therefore, discovering compounds that can provide this boost in replication is of extreme importance. Recently, a new small molecule inhibitor of RSK, BI-D1870, was found to synergize with certain OVs.

1.5 BI-D1870 and the RSK pathway

1.5.1 The RSK pathway

The p90 ribosomal S6 kinase (RSK) family is a group of highly conserved serine/threonine (Ser/Thr) kinases that promote cell proliferation, growth, motility and survival and are almost exclusively activated downstream of ERK1/2. RSK inhibition is less likely to produce severe side effects as those observed following the inhibition of more upstream regulators like Raf and mitogen-activated protein kinase kinase (MEK).[92] RSKs are downstream effectors of the Ras/mitogen-activated protein kinase (MAPK) pathway in which mutations or the overexpression of the signaling components are found in many human cancers. The activation of RSK happens through a multistep phosphorylation cascade starting with ERK1/2-mediated activation of the C-terminal kinase domain, which then autophosphorylates a hydrophobic turn motif in RSK creating a docking site for phosphoinositide-dependent kinase 1 (PDK1) which will phosphorylate and activate the N-terminal kinase domain.[92,93] RSK has 4 isoforms, and is a member of the AGC subfamily which includes protein kinase A (PKA), protein kinase B (PKB or Akt), protein kinase C (PKC), p70 ribosomal S6 kinase (S6K), and mitogen-and-stress-activated protein kinase (MSK).[93,94] These kinases mediate many physiological processes and cellular effects of extracellular agonists by the phosphorylation of key regulatory proteins. Their

catalytic domains are approximately 40% identical, but all have unique non-catalytic domains and participate in diverse signaling pathways.[93]

RSK mediates the phorbol ester- and EGF-induced phosphorylation of glycogen synthase kinase 3B (GSK3B), liver kinase B1 (LKB1), and cAMP response element-binding protein (CREB),[93] and has several other targets including NFκB, eIF-4B (eukaryotic translation initiation factor 4B), and rpS6 (**Figure 2**).[92] Activated RSK is proposed to promote the progression of the cell cycle and survival by the phosphorylation and inactivation of cell cycle-regulatory and pro-apoptotic proteins such as cyclin dependent kinase (CDK) inhibitor p27, checkpoint kinase 1 (Chk1), Bcl-2-associated death promoter protein (BAD), Bcl-like protein 11 (BimEL), caspase-8 and p53 as well as the stimulation of actin-dependent endocytosis.[92,95–97]

1.5.2 BI-D1870, a small molecule inhibitor of RSK

BI-D1870 is a specific nanomolar inhibitor of RSK. It was originally developed to identify inhibitors of polo-like kinases (PLKs), but was found to inhibit RSK at a higher potency.[94] BI-D1870 is derived from a series of dihydropteridinones (heterocyclic compounds containing pteridine ring systems – fused pyrimidine and pyrazine rings),[98] and was identified in a kinase selectivity screen in the Division of Signal Transduction Therapy at the University of Dundee.[93] BI-D1870 inhibits RSK1-4 in vitro with an IC_{50} of 10 – 30 nM and is cell permeable. BI-D1870 has a >500 fold selectivity for RSK over nine other AGC kinases tested by Sapkota et al, and reduced the activity of several other kinases (see Table 1).[93] The most commonly reported concentration for BI-D1870 is 10 μM as concentrations of BI-D1870 lower than 2.5 μM were found to affect several biological functions.[99–103]

Chiu et al reported that BI-D1870 inhibits the RSK target Y box binding protein 1 (YB-1) causing apoptosis, shown through poly (ADP-ribose) polymerase (PARP) cleavage and the activation of the caspase cascade. They also found that BI-D1870 induces G2/M phase arrest by modulating the expression of p21 and other cell cycle regulators. BI-D1870 generates reactive oxygen species and increases endoplasmic reticulum stress and autophagy, as well as modulating the Akt and p38 MAPK cell survival signaling pathways.[104] The compound has also been reported to block TLR-mediated micropinocytosis through the inhibition of RSK.[97] Recently synthesized inhibitors of RSKs have been described as good candidates for anti-cancer drugs.[105]

Pambid et al found that BI-D1870 can be tolerated up to 100 mg/kg *in vivo,* and that it crosses the blood-brain barrier but has a low extraction efficiency from tissues. Pharmaco-kinetics and -dynamics were described to be low and metabolite production showed low levels.[103] More research must be done to improve the effect of BI-D1870 *in vivo* and discover how it is excreted from the tissue. The synthesis of this compound may give a better understanding of what is happening in this process.

Figure 2. The RSK signaling pathway. Modified from Chen et al.[106] RSK can inhibit and activate several different kinases and ultimately this pathway leads to translation and cell proliferation.

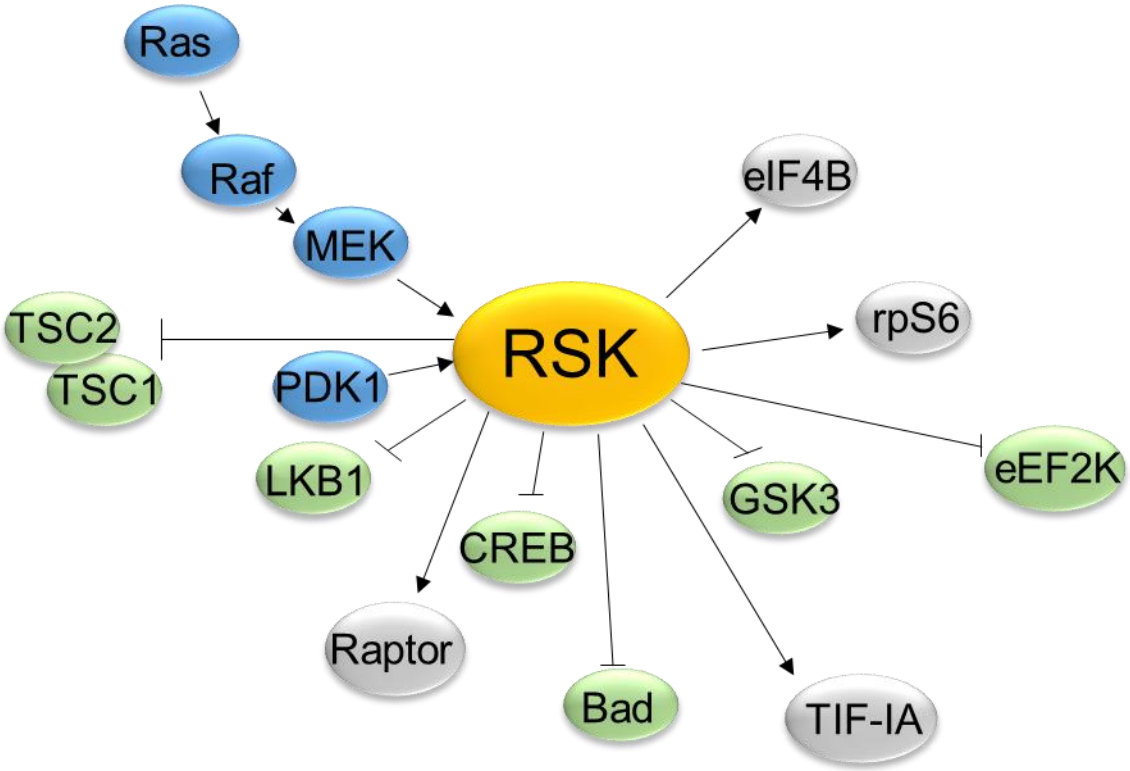
Ras
Raf
MEK
TSC2
TSC1
PDK1
RSK
eIF4B
rpS6
eEF2K
LKB1
GSK3
CREB
Raptor
Bad
TIF-IA

Table 1. Activity of RSK inhibitors on off target kinases extracted from a literature search.[93,94,102,107,108]

BI-D1870			SL0101		BIX-02565
<40% activity		>100% activity	<40% activity	>100% activity	
PKCa	PKB	ERK1	Aurora B	SGK1	Slk
GSKB	IRAK4	JNK1	PIM1	MAPKAP-K3	Lok
CDK2-A		p38γ MAPK	PIM3	SmMLCK	MST1
MARK3		SGK1		NEK6	
CK1		S6K1		NEK7	
Lck		MSK1			
MST2		MAPKAP-K3			
Aurora B		SmMLCK			
PLK1		PHK			
DYRK1a		AMPK			
MELK		NEK6			
PIM3		NEK7			
Slk		IKKb			
Lok					
MST1					

1.6 Rationale and Hypothesis

1.6.1 Rationale

Oncolytic viruses (OVs) have increasingly been used for the treatment of cancer over the past 20 years. OVs can selectively target and kill cancer cells, while inducing an anti-tumour immune response. These viruses can also induce direct cytopathic effects on the cancer cells and the disruption of blood vessels associated with the tumour. They can be very effective as a cancer treatment and have resulted in complete tumour regression in some patients. However, most patients show a limited response, with an inadequate amount of viral replication within the tumour. Researchers have found ways to help OV therapy by increasing replication of the virus, bystander killing of cancer cells, and/or stimulating a stronger and more specific anti-tumour immune response. In 2016, the FDA approved the first OV to be used in the clinic in the US and Canada when a 16.3% response rate was achieved – Talimogene laherparepvec (T-VEC). In order to improve this response rate, there are several barriers to overcome including sequestration by the liver, neutralizing antibodies, and the tumour microenvironment. Small molecule inhibitors and other drugs in combination with OVs have achieved an increase in therapeutic effectiveness. Several of these combinations have made their way to clinical trials – including T-VEC with paclitaxel, Pexa-Vec with ipilimumab, and measles virus with gemcitabine to name a few.

Through previous work done by members of the Alain lab with rapamycin and active site mTOR inhibitors (asTORi),[110] they discovered that there was an increase in the infection of HSV1-1716. Downstream target of mTORC1, rpS6, was found to be phosphorylated even in the presence of rapamycin when cells were infected with HSV1. Small molecule RSK inhibitor BI-D1870 also inhibits rpS6 through the RSK pathway, and it was originally thought that this

inhibitor could block the infection of HSV1. However, when tested in conjunction with HSV1-1716, there was a strong increase in infection. Therefore, the mechanism of action of BI-D1870 needed further investigation.

1.6.2 Hypothesis

- BI-D1870 can increase HSV1 and VSVΔ51 infection and spread within cancer cells tumour tissues. The generation of analogs can improve the effect of BI-D1870 upon HSV1-1716 and VSVΔ51 infection

1.6.3 Research Aims

- Aim 1: Assess BI-D1870 in combination with HSV1 and VSVΔ51 oncolysis and assess a mechanism of action
- Aim 2: Develop of novel sensitizers based on BI-D1870 structural analogs

Chapter 2: Materials and Methods

2.1 Cell lines, kinase inhibitors and viruses

2.1.1 Cell culture

Cell lines used included human glioblastoma (U343), prostate carcinoma (PC3), normal human fibroblasts (GM38), murine glioblastoma (K4622), murine breast carcinoma (4T1), human renal adenocarcinoma (786-0), murine breast carcinoma (EMT6), murine mammary epithelial cells (NMuMG), murine breast carcinoma (NT2196), human glioblastoma (LN-18), HER2+ breast carcinoma cells, and mouse embryonic fibroblasts (MEF). All cell lines, except LN-18, HER2+ and SLKΔ3-6 cells were obtained from ATCC. The LN-18 cells were obtained from Dr. Martin Roffe at the Hospital A.C. Camargo in Sao Paulo, Brazil. The HER2+ and SLKΔ3-6 cells were obtained from Dr. Luc Sabourin at the Ottawa Hospital Research Institute. The U343, K4622, PC3, NMuMG, NT2196, HER2+ cell lines were cultured using Dulbecco's Modified Eagle's Medium (DMEM) (GE HealthCare, cat. SH3002.01) containing 4500 mg/L glucose and 4.00mM L-glutamine, supplemented with 10% fetal bovine serum (FBS) (Sigma-Aldrich, cat. F1051) and 1% penicillin and streptomycin (GE HealthCare, cat. SH40003.01).

The GM38 cell line was cultured using the same media as previously described, but with 2% FBS. The LN-18 cell line was cultured using the same media as previously described, but with the addition of 1% pyruvate (Sigma-Aldrich, cat. P2256).

The 4T1 cells were cultured using RPMI-1640 (Roswell Park Memorial Institute) (Sigma-Aldrich, cat. R8758) containing 2.0 mM L-glutamine and sodium bicarbonate, supplemented with 10% FBS and 1% penicillin and streptomycin.

The cells were grown at 37°C and 5% CO_2 until a confluency of 80-90% was reached, then rinsed with in-house made phosphate buffered saline (PBS) (0.8% NaCl, 0.02% KCl, 0.144%

Na_2HPO_4, 0.024% KH_2PO_4, pH 7.4), lifted with 0.025% trypsin-EDTA (Life Technologies, CAS no. 9002-07-07) and collected by centrifugation (230 x g for 5 minutes) at room temperature (RT). Cells were then counted using a CASY cell counter (Innovatis). All cells were seeded and grown in tissue culture treated 10cm, 15cm, 6-well, 12-well, and 24-well plates (Corning).

2.1.2 Kinase inhibitors and nanoparticles

RSK inhibitors used included BI-D1870 (Enzo Life Sciences, cat. BML-EI407-0005), LJI308 (DC Chemicals, CAS. 1627709-94-7), BIX-02565 (ApexBio, cat. B1295), Fmk (Axon MedChem, CAS. 821794-92-7), or SL0101-1 (Adooq Bioscience, cat. A11160) were diluted in DMSO (Sigma-Aldrich, CAS. 67-68-5) to a stock concentration of 10 mM and stored at -20°C. Nanoparticles were provided and produced by Dr. Suresh Gadde, Department of Biochemistry, Microbiology and Immunology, University of Ottawa. BI-D1870- nanoparticles (BI-D-NPs) were synthesized via previously reported nanoprecipitation method.[111] Briefly, 100 µl of poly(lactic-co-glycolic acid-polyethylene glycol (PLGA-PEG) (10 mg/ml in Acetonitrile) and 100 µl of BI-D1870 (1mg/ml in acetonitrile) are mixed and added dropwise to 2.5 ml of water. The reaction mixture was stirred at room temperature for 6-7 hours to form self-assembly of BI-D-NPs. NPs were concentrated, and purified by centrifugal filters (50K or 100 K MWCO) and analyzed by Malvern Zetasizer (Dynamic light scattering (DLS)) and transmission electron microscopy (TEM).

2.1.3 Oncolytic viruses

Virus strains used include HSV1-1716-GFP (Herpes simplex virus type 1, Virttu Biologicals UK, Sorento Therapeutics), VSVΔ51-RFP and VSVΔ51-GFP (Vesicular stomatitis virus, Dr.

David Stojdl, CHEO Research Institute), VSV-G-GFP (G-less vesicular stomatitis virus, Dr. Jean-Simon Diallo, The Ottawa Hospital Research Institute), MG1-GFP (Maraba virus, Dr. David Stojdl, CHEO Research Institute), JX-594-GFP (vaccinia virus, Dr. John Bell, The Ottawa Hospital Research Institute), Myxoma (Grant McFadden - Biodesign Institute, Arizona State University) and Adenovirus-RFP (Dr. Robin Parks, The Ottawa Hospital Research Institute). Viral stocks were kept frozen at -80°C at 1.0 x 10^9 plaque forming units (pfu) in Opti-MEM (Thermo-Fisher, cat. 31985062).

HSV1-1716 infection was performed at a multiplicity of infection (MOI) of 0.1 with U343, GM38, K4622, PC3, NMuMG, NT2196, EMT6, 786-0 cells, and 0.01 with LN-18 cells. VSVΔ51 infection was performed at an MOI of 1 with GM38 cells, 0.1 for 4T1, NMuMG, and NT2196 cells, and 0.01 with EMT6 and 786-0 cells. VSV-G infection was performed at an MOI of 0.1 with 4T1 cells. Myxoma virus infection was performed at an MOI of 1 with U343 cells, JX-594 infection was performed at an MOI of 0.1 with U343 cells. All experiments with Adenovirus (10 MOI) were performed by students in the lab of Dr. Robin Parks at the Ottawa Hospital Research Institute.

2.2 Viral infection, kinase inhibitor and nanoparticle treatments

All cell lines were treated with the same protocol. The virus was diluted in media (DMEM or RPMI) to the correct MOI, then portioned out evenly into 6-well (3 mL), 12-well (2 mL), or 24-well plates (1 mL). BI-D1870 (or other RSK inhibitors, nanoparticles) were diluted in media (DMEM or RPMI) prior to being added to the well plates to concentrations of 0.1 mM, 0.5 mM, or 1 mM. Subsequently, 10 μL (for 24-well plates; 30 μL for 6-well plates, and 20 μL for 12-well plates) of each concentration was pipetted into one well of the plate to give a final concentration

of 1 μM, 5 μM, or 10 μM. DMSO was used as a control, and was diluted in media. The plates were then placed in the incubator, or the Incucyte S3 Live-Cell Analysis System (Essen Bioscience, cat. 4647). Images of the infection were taken 24 – 48 hours post infection on the EVOS microscope (Thermo-Fisher) and the Incucyte. Cell lysates were then collected for western blot analysis.

2.3 Extraction of cytosolic protein contents and protein quantification

Culture media was removed and the cells were rinsed using in-house PBS, and then lysed with in-house made lysis buffer (radioimmunoprecipitation assay buffer (RIPA buffer) (50 mM Tris, 150 mM NaCl, 1.0% IGEPAL-CA-630, 0.5% sodium deoxycholate, 0.1% SDS, pH 8.0), 50 mM NaF, 15 mM $NaVO_3$, Roche protease inhibitor) and then frozen at -80°C. Cell lysates are then thawed and centrifuged at 14,000xg for 10 minutes to remove phospholipid membranes, nucleic acids and other non-soluble matter. The remainder of the lysates undergo protein quantification with the BioRad DC Protein Assay. The working reagent is prepared by adding 20μl of reagent S to every mL of reagent A needed (to make working reagent A'). A standard curve containing 0.2 mg/mL, 0.5 mg/mL, 1.0 mg/mL, 1.5 mg/mL, and 2.0 mg/mL BSA in RIPA was prepared. 5μl of standards and 2 μl of each sample was pipetted in duplicate into a 96-well plate. 25 μl of reagent A' and 200 μl of reagent B was pipetted into each well. The plate was gently agitated to mix and then let rest for 15 mins before being read at an absorbance of 750 nm.

2.4 Western immunoblot analysis and antibodies

Quantified proteins were subjected to SDS-PAGE electrophoresis and were transferred onto a 0.45 μm nitrocellulose membrane (Bio-Rad, CAS 9004-70-0). For 15 well gels, 30 μg of protein

was loaded. The membranes were probed for proteins of interest using primary antibodies specific for HSV1 (Dako, cat. B011402), HSV-ICP0 (Santa Cruz, cat. 11060), GAPDH (Abcam cat. ab8245), VSVΔ51 (Dr. John Bell, The Ottawa Hospital Research Institute), and VACV (Quartett, cat. 12200100715). These antibodies were followed by a wash, and then a goat anti-rabbit or anti-mouse secondary polyclonal antibodies (BioRad). After blotting, the proteins of interest are visualized by chemiluminescence (ChemiDoc Imaging Systems, BioRad).

2.5 In vivo experiments

15 female BALB/c and 10 C57BL/6 mice were implanted with 4T1 and CT-2A cells respectively (injected subcutaneously). The mice were separated into two groups – those treated with vehicle and VSVΔ51-Fluc, and those treated with BI-D1870 and VSVΔ51-Fluc. 10 days post implantation, vehicle and BI-D1870 were injected intraperitoneally (i.p – 100mg/kg), and VSVΔ51-Fluc was injected intratumourally (i.t. – $1x10^8$ pfu in 50 μL). Day 2 and 3 post-treatment, mice were imaged with IVIS Spectrum In vivo Imaging System (Perkin Elmer, part 124262) in the morning, and injected with BI-D1870 and vehicle i.p. in the evening. Tumour size was measured via calipers 3 times a week starting 10 days post treatment. Animal weight was monitored 3 times a week and killed when symptoms developed (loss of >20% of body weight or difficulty moving, feeding, or grooming).

2.6 Synthesis of BI-D1870

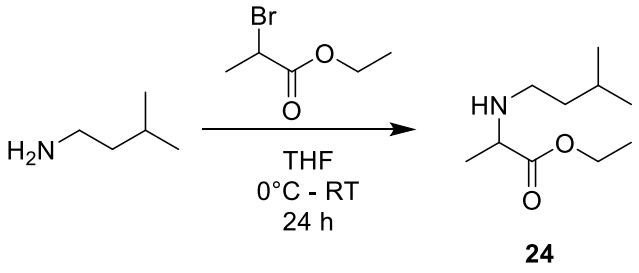

24

93%

A solution of isopentylamine (1.1 equivalent (eq)) (Sigma-Alridch, CAS 107-85-7) and triethylamine (1.1 eq) (Sigma-Aldrich, CAS 121-44-8) in tetrahydrofuran (THF) (1.7 M) (Sigma-Aldrich, CAS 109-99-9) was cooled to 0°C. Ethyl 2-bromopropionate (1.0 eq) (Sigma-Aldrich, CAS 535-11-5) in THF (1.7 M) was added dropwise over 2 hours as the solution gradually warmed to room temperature. The reaction solution was stirred for 24 more hours at room temperature before being filtered to remove the white precipitate that formed. The filtrate was concentrated under reduced pressure and purified by flash column chromatography (7:3 hexanes:ethyl acetate). The product, compound 24, was a dark orange oil with a 93% yield. **^{1}H NMR** (400 MHz, $CDCl_3$) δ 4.20 (q, *J*=7.1 Hz, 2H), 3.32 (q, *J*=6.9 Hz, 1H), 2.62-2.56 (m, 1H), 2.53-2.46 (m, 1H), 1.62 (sept, *J*=6.7 Hz, 1H), 1.51 (br s, 1H), 1.40-1.27 (m, 8H), 0.89 (dd, *J*=6.6 Hz, *J*=2.9 Hz, 6H). **^{13}C NMR** (100 MHz, $CDCl_3$) δ 175.9, 60.6, 56.8, 46.1, 39.2, 26.0, 22.8, 22.4, 19.1, 14.3.

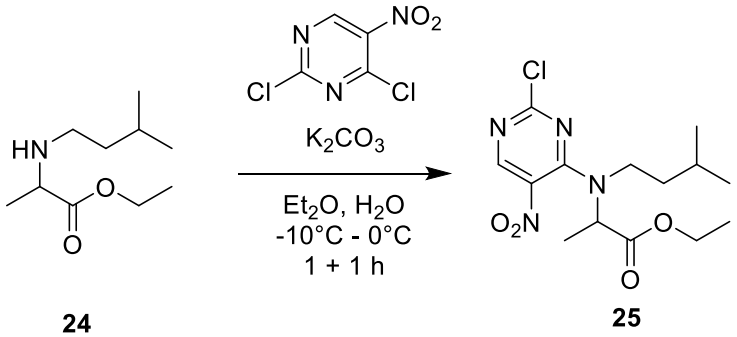

24 **25**

35%

To a solution of compound 24 (1.25 eq) in water (0.625 M) a solution of 2,4-dichloro-5-nitropyrimidine (1.0 eq) (Sigma-Aldrich, CAS 49845-33-2), in diethyl ether (0.250 M) (Sigma-Aldrich, CAS 69-29-7) was added. The mixture was cooled to 0°C before the addition of potassium carbonate (5.0 eq) (CAS 584-08-7) portionwise, and then stirred for 2 hours at this temperature. The reaction mixture was stirred for 2 more hours at room temperature until the thin layer chromatography (TLC) analysis showed no remaining amine. The organic phase was washed with water and dried with anhydrous magnesium sulfate (Sigma-Aldrich, CAS 7487-88-9), filtered, and evaporated under reduced pressure. The product, compound 25, was purified by flash column chromatography (9:1 hexanes:ethyl acetate) to get a dense yellow oil with a 35% yield. **^{1}H NMR** (400 MHz, $CDCl_3$) δ 8.67 (s, 1H), 4.49 (br d, *J*=6.1 Hz, 1H), 4.29-4.17 (m, 2H), 3.49-3.43 (m, 1H), 3.21-3.14 (m, 1H), 1.63 (d, *J*=7.0 Hz, 3H), 1.59-1.48 (m, 3H), 1.27 (t, *J*=7.1 Hz, 3H), 0.91 (dd, *J*=6.2 Hz, *J*=3.2 Hz, 6H). **^{13}C NMR** (100 MHz, $CDCl_3$) δ 170.3, 160.2, 156.3, 154.1, 131.5, 61.7, 58.9, 49.4, 35.5, 26.4, 22.4, 14.9, 14.1.

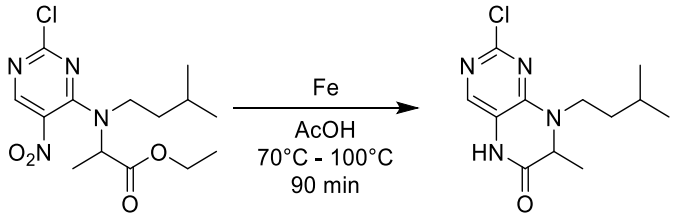

25 **26**

60%

Compound 25 (1.0 eq) was dissolved in glacial acetic acid (0.2 M) (Sigma-Aldrich, CAS 64-19-7) and heated to 70°C, then removed from the oil bath and 5.25 eq of iron powder (Iron (III) oxide, Sigma-Aldrich, CAS 1309-37-1)was added, resulting in an exothermic reaction. This reaction mixture was then placed back in the oil bath at 100°C and stirred for 3 hours. After cooling to

room temperature, the mixture was filtered over Celite (Sigma-Aldrich, CAS 61790-53-2) then extracted with dichloromethane (DCM) (Sigma-Aldrich, CAS 75-09-2) and 6N HCl (Sigma-Aldrich, CAS 7647-01-0). The product was extracted again with DCM, then the combined organic extracts were washed with water, aqueous ammonium hydroxide and brine before being dried with anhydrous magnesium sulfate, filtered, and evaporated under reduced pressure. The product, compound 26, was purified by flash column chromatography (100% ethyl acetate) to produce a white powder with a 60% yield. **^{1}H NMR** (400 MHz, $CDCl_3$) δ 8.50 (s, 1H), 7.63 (s, 1H), 4.24 (q, *J*=6.9 Hz, 1H), 4.18-4.11 (m, 1H), 3.14-3.07 (m, 1H), 1.64 (sept, *J*=6.6 Hz, 1H), 1.57-1.51 (m, 2H), 1.49 (d, *J*=6.8 Hz, 3H), 0.98 (dd, *J*=6.5 Hz, *J*=4.4 Hz, 6H). **^{13}C NMR** (100 MHz, $CDCl_3$) δ 166.0, 154.8, 151.1, 138.7, 117.2, 56.4, 43.2, 35.7, 25.9, 22.7, 22.3, 17.8.

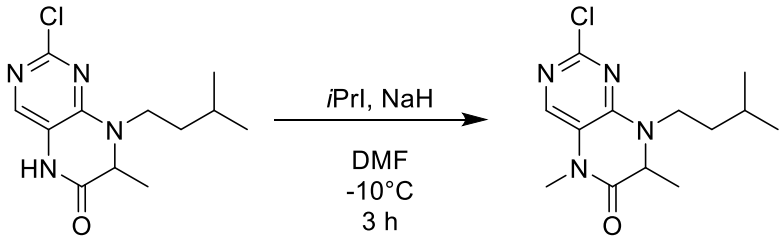

26 **27**

30%

A solution of compound 26 (1.0 eq) and 2-iodopropane (4.0 eq) (Sigma-Aldrich, CAS 75-30-9) in *N*,*N*-Dimethylformamide (DMF) (0.4 M) (Sigma-Aldrich, CAS 68-12-2) was cooled to -10°C, to which sodium hydride (60% suspension in mineral oil, 1.125 eq) (Sigma-Aldrich, CAS 7646-69-7) was added. The mixture was stirred for 4 hours and gradually warmed to room temperature The reaction was quenched with water and 6N HCl, and the product extracted with ethyl acetate (Sigma-Aldrich, CAS 141-78-6). The organic phase was washed with water, then dried with anhydrous magnesium sulfate, filtered and evaporated under reduced pressure. The product,

compound 27, was purified by flash column chromatography (9:1 DCM:MeOH) to get a yellow-ish solid with a 30% yield. **^{1}H NMR** (400 MHz, $CDCl_3$) δ 7.85 (1H, s), 4.88 (1H, q, J = 6.9 Hz), 3.61 (3H, s), 3.25-3.34 (2H, 3.30 (t, J = 7.5 Hz), 3.30 (t, J = 7.5 Hz)), 1.49 (1H, tsept, J = 7.7, 6.7 Hz), 1.26-1.43 (5H, 1.36 (dt, J = 7.7, 7.5 Hz), 1.28 (d, J = 6.9 Hz), 1.36 (dt, J = 7.7, 7.5 Hz)), 0.84-0.88 (6H, 0.86 (d, J = 6.7 Hz), 0.86 (d, J = 6.7 Hz)). **^{13}C NMR** (100 MHz, $CDCl_3$) δ 169.1, 154.5, 149.6, 140.5, 136.9, 53.9, 49.6, 38.4, 32.8, 27, 22.7, 17.9.

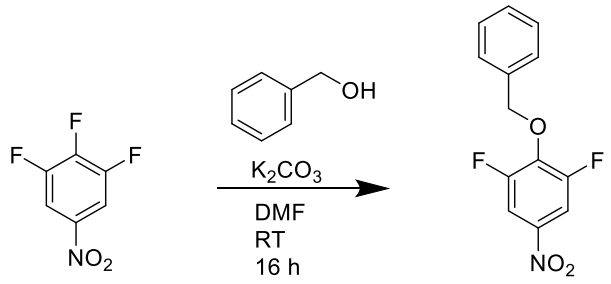

MW-040

55%

Potassium carbonate (2.0 eq) was added to a solution of 3,4,5-trifluoronitrobenzene (1.0 eq) and benzyl alcohol (1.05 eq) (Sigma-Aldrich, CAS 100-51-6) in DMF. The resultant mixture was stirred at room temperature overnight, and subsequently concentrated under reduced pressure. The residue was partitioned between ethyl acetate and water. The organic layer was separated and washed with brine, dried with anhydrous magnesium sulfate, filtered and evaporated under reduced pressure. The product, MW-040 (2-(benzyloxy)-1,3-difluoro-5-nitrobenzene), was purified by column chromatography (7:3 hexanes:ethyl acetate) to get a cream-coloured powder with a 55% yield. . **^{1}H NMR** (400MHz, $CDCl_3$) δ 7.00 (2H, d, J = 8.1, 1.4, 0.5 Hz), 7.17 (1H, t, J = 7.6, 1.4 Hz), 7.38 (2H, dd, J = 8.1, 7.6, 1.5, 0.5 Hz), 8.08 (2H, d, J = 1.9 Hz). **^{13}C NMR** (100 MHz, $CDCl_3$) δ 156, 152.1, 143.3, 133.9, 129.6, 123.6, 118.3, 112.5.

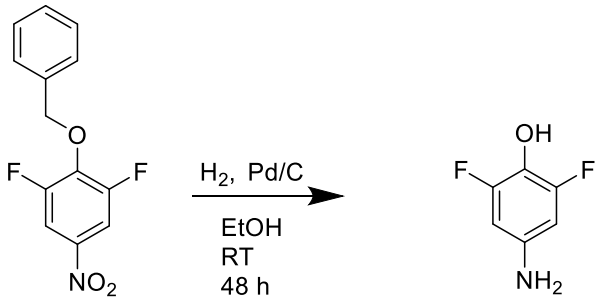

MW-040 **MW-045**

15%

To a solution of MW-040 (1.0 eq) in ethanol, 10% palladium on activated carbon was added (0.5 g). The mixture was hydrogenated (1 atm) at RT for 48 hours. The reaction mixture was filtered and the filtrate concentrated under reduced pressure to give 4-amino-2,6-difluorophenol (MW-45) with 15% yield. **^{1}H NMR** (400MHz, $CDCl_3$) δ 6.78 (2H, d, J = 1.8 Hz). **^{13}C NMR** (100 MHz, $CDCl_3$) δ 152.1, 142.4, 129.6, 103.4.

General procedure for final amination

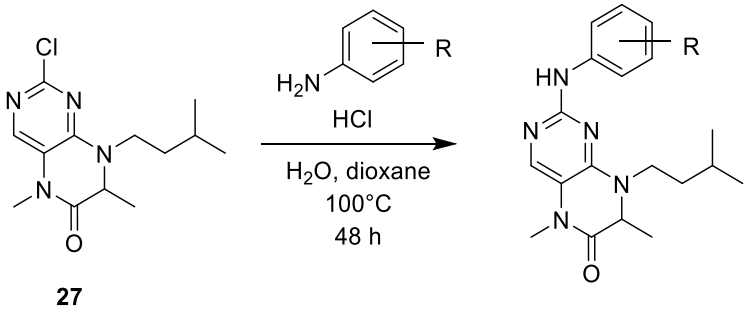

27

Concentrated hydrochloric acid (3.0 eq) was added to a mixture of compound 27 (1.0 eg), MW-45 (1.0 eq), water (0.83 M) and 1,4-dioxane (0.83 M) (Sigma-Aldrich, CAS 123-91-1) and then heated to reflux (100°C) and stirred for 48 hours. Once cooled to room temperature, the volatile components were removed by evaporation under reduced pressure and the product was isolated. Predicted spectra: **^{1}H NMR** (400MHz) δ 7.81 (1H, s), 6.97 (2H, d, *J* = 1.4 Hz), 4.88 (1H, q, *J* =

6.9 Hz), 3.61 (3H, s), 3.28-3.37 (2H, (t, *J* = 7.5 Hz), 1.49 (1H, sept, *J* = 7.7, 6.7 Hz), 1.21-1.33 (5H, (d, *J* = 6.9 Hz)) 0.84-0.88 (6H, (d, *J* = 6.7 Hz)).**^{13}C NMR** (100MHz) δ 169.1, 162.2, 152.1, 149.6, 140.5, 140.0, 136.9, 129.6, 105.6, 53.9, 49.6, 38.4, 32.8, 27, 22.7, 17.9.

2.7 Synthesis of series I analogs

2.7.1 Synthesis of KA-001

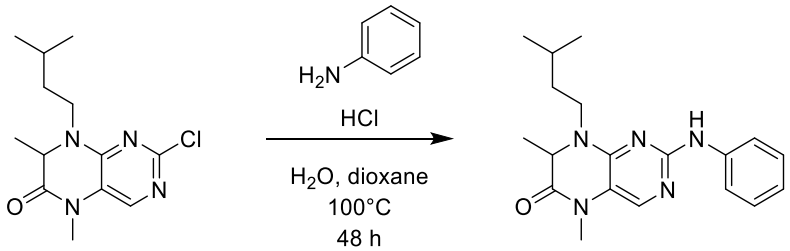

Compound **KA-001** was prepared following steps from **2.6**, with compound 27 and aniline (1.0 eq) (Sigma-Aldrich, CAS 62-53-3). The product was isolated by precipitation with a 43% yield as a cream-coloured powder. **^{1}H NMR** (400 MHz) δ 10.66 (s, 1H), 7.85 (s, 1H), 7.57 (d, *J*=7.7 Hz, 2H), 7.36 (dd, *J*=8.0 Hz, *J*=7.6 Hz, 2H), 7.14 (t, *J*=7.4 Hz, 1H), 4.50 (q, *J*=6.8 Hz, 1H), 3.93-3.86 (m, 1H), 3.36-3.29 (m, 1H), 3.18 (s, 3H), 1.68-1.55 (m, 2H), 1.46 (d, *J*=6.8 Hz, 4H), 0.89 (dd, *J*=9.8 Hz, *J*=6.3 Hz, 6H). **^{13}C NMR** (100 MHz) δ 163.2, 151.2, 149.3, 137.4, 128.8, 124.2, 123.9, 120.4, 115.0, 56.5, 45.1, 34.7, 28.1, 25.9, 22.4, 22.0, 18.6.

2.7.2 Synthesis of KA-004

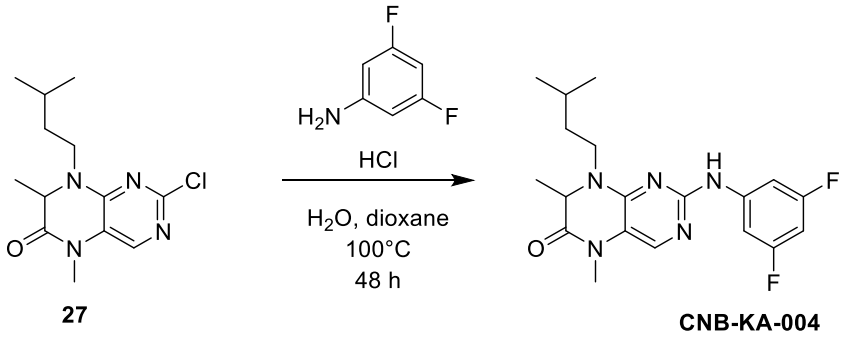

27 **CNB-KA-004**

55%

Compound **KA-004** was prepared following steps from **2.6**, with compound 27 and 3,5-difluoroaniline (1.0 eq) (Sigma-Aldrich, CAS 372-39-4)**.** A pale orange product was isolated by precipitation with a 55% yield. **^{1}H NMR** (400 MHz) δ 10.38 (s, 1H), 7.81 (s, 1H), 7.37 (dd, *J*=9.7 Hz, *J*=2.1 Hz, 2H), 6.88 (s, 1H), 4.45 (q, *J*=6.7 Hz, 1H), 3.96-3.88 (m, 2H), 3.21 (s, 3H), 1.66-1.59 (m, 2H), 1.3-1.45 (m, 1H), 1.41 (d, *J*=6.8 Hz, 3H), 0.89 (t or dd, *J*=6.2 Hz, 6H). **^{13}C NMR** (100 MHz) δ 163.6 (d, *J*=61.2 Hz), 163.3, 161.2 (d, *J*=61.2 Hz), 151.1, 149.5, 140.6, 115.7, 102.8 (d, *J*=115.2 Hz), 98.3, 56.6, 45.0, 34.8, 28.1, 25.8, 22.2, 22.0, 18.5.

2.7.3 Synthesis of KA-005

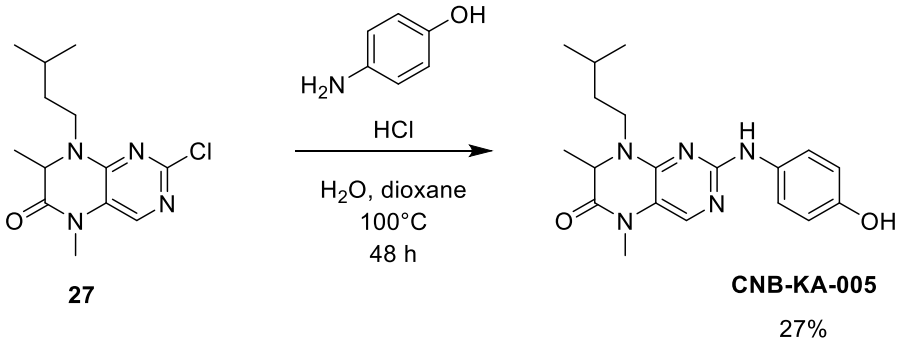

27 **CNB-KA-005**

27%

Compound **KA-005** was prepared following steps from **2.6**, with compound 27 and p-aminophenol (1.0 eq) (Sigma-Aldrich, CAS 123-30-8). A pale yellow powder was isolated by precipitation with a 27% yield. **^{1}H NMR** (400 MHz) δ 9.99 (s, 1H), 9.48 (br s, 1H), 7.62 (s, 1H), 7.26 (d, *J*=8.7 Hz, 2H), 6.77 (d, *J*=8.7 Hz, 2H), 4.46 (q, *J*=6.9 Hz, 1H), 3.87-3.79 (m, 1H), 3.29-3.22 (m, 2H), 3.17 (s, 3H), 1.63-1.48 (m, 2H), 1.43 (d, *J*=6.8 Hz, 3H), 0.86 (t or dd, *J*=6.2 Hz, 6H). **^{13}C NMR** (100 MHz) δ 163.2, 151.4, 149.5, 127.9, 123.7, 116.0, 115.3, 114.6, 56.4, 44.9, 34.7, 28.1, 25.8, 22.3, 22.0, 18.7.

2.7.4 Synthesis of KA-006

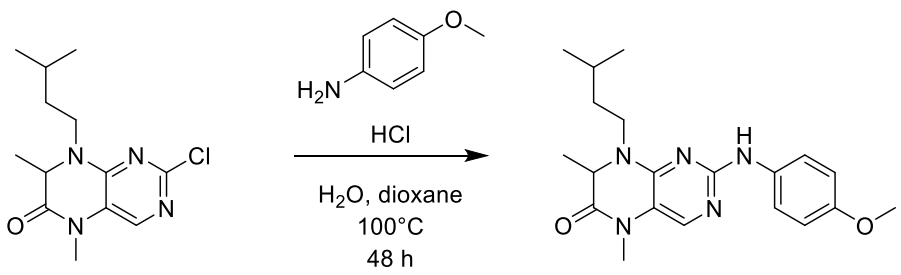

27 **CNB-KA-006**

13%

Compound **KA-006** was prepared following steps from **2.6**, with compound 27 and 4-methoxyaniline (1.0 eq) (Sigma-Aldrich, CAS 104=94-9). The product, a brown solid, was isolated by recrystallization with a 13% yield. This product was impure. **^{1}H NMR** (400 MHz) δ 7.80 (s, 1H), 7.53 (d, *J*=9.0 Hz, 2H), 6.94 (d, *J*=9.0 Hz, 2H), 4.52 (q, *J*=6.9 Hz, 1H), 4.09-4.02 (m, 1H), 3.80 (s, 3H), 3.49-3.42 (m, 1H), 3.33 (s, 3H), 1.77-1.64 (m, 3H), 1.58 (d, *J*=7.0 Hz, 3H), 0.94 (dd, *J*=12.5 Hz, *J*=6.3 Hz, 6H).

2.8 Synthesis of series I.II analogs

2.8.1 Synthesis of KA-013

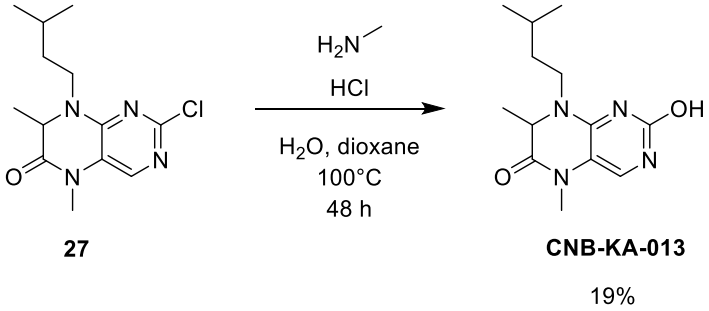

Compound **KA-013** was prepared following steps from **2.6**, with compound 27 and methylamine (1.0 eq) (Sigma-Aldrich, CAS 74-89-5) (but after 48 hours of reflux, there was no product formation. An acid catalyst (6 N HCl, 0.35 mL) was added and reflux continued for another 21 hours. The volatile components were evaporated under reduced pressure and the product was purified by flash column chromatography (5-10% gradient of methanol in DCM). The product was a dense brown oil with a 19% yield. **^{1}H NMR** (400 MHz, $CDCl_3$) δ 7.05 (s, 1H), 4.32-4.24 (m, 1H), 4.19 (q, *J*=6.9 Hz, 1H), 3.19 (s, 3H), 3.03-2.96 (m, 1H), 1.64-1.49 (m, 3H), 1.44 (d, *J*=6.9 Hz, 3H), 0.93 (dd, *J*=6. Hz, *J*=3.0 Hz, 6H). **^{13}C NMR** (100 MHz, $CDCl_3$) δ 164.1, 157.8, 154.4, 124.0, 112.0, 56.4, 43.5, 35.6, 28.2, 25.9, 22.6, 22.3, 18.5.

2.8.2 Synthesis of KA-019

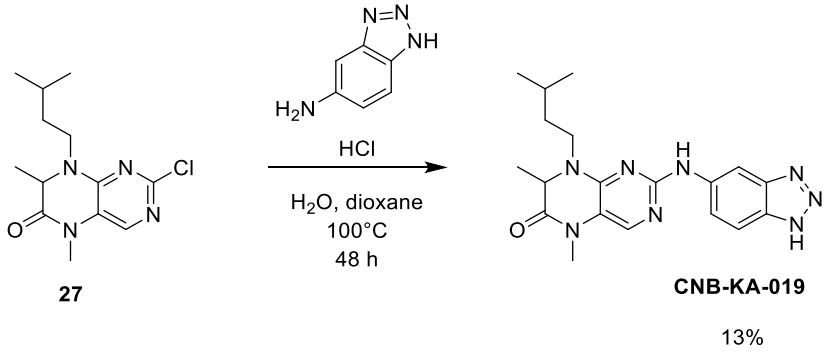

Compound **KA-019** was prepared following the steps from **2.6**, with compound 27 and 5-amino-1H-benzotriazole (1.0 eq) (Sigma-Aldrich, CDS000711). The product was purified by flash column chromatography (5-10-20% methanol in DCM) and a dense brown oil was isolated with a 13% yield. **^{1}H NMR** (400 MHz, $(CD_3)_2CO$) δ 10.58 (br s, 1H), 8.37 (s, 1H), 7.87 (d, *J*=8.8 Hz, 1H), 7.82 (s, 1H), 7.57 (dd, *J*=8.9 Hz, *J*=1.7 Hz, 1H), 4.42 (q, *J*=6.8 Hz, 1H), 4.09-4.02 (m, 1H), 3.46-3.38 (m, 1H), 3.32 (s, 3H), 1.73-1.65 (m, 2H), 1.62-1.54 (m, 1H), 1.51 (d, *J*=6.8 Hz, 3H), 0.86 (dd, *J*=17.5 Hz, *J*=6.2 Hz, 6H).

2.8.3 Synthesis of KA-020

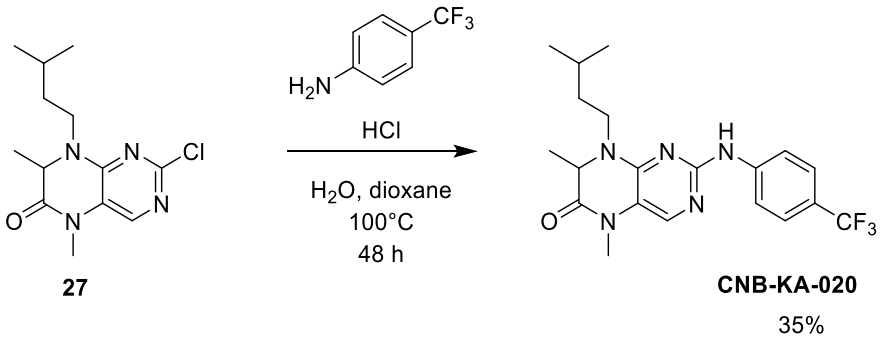

Compound **KA-020** was prepared following the steps from **2.6**, with compound 27 and 4-(trifluoromethyl)aniline (1.0 eq) (Sigma-Aldrich, CAS 455-14-1) and was purified by flash column chromatography (0-8% gradient of methanol in DCM). Two separate products were obtained: KA-020A – a pale orange powder with 35% yield. **^{1}H NMR** (400 MHz, $(CD_3)_2CO$) δ 7.93 (d, *J*=8.9 Hz, 2H), 7.82 (s, 1H), 7.68 (d, *J*=8.9 Hz, 2H), 4.53-4.48 (m, 1H), 4.21-4.14 (m, 1H), 3.50-3.42 (m, 1H), 3.33 (s, 3H), 1.80-1.62 (m, 3H), 1.54 (dd, *J*=6.9 Hz, *J*=2.1 Hz, 3H), 0.97 (dd, *J*=13.5 Hz, *J*=6.3 Hz, 6H). KA-020B – 20% yield. **^{1}H NMR** (400 MHz, $(CD_3)_2CO$) δ 8.03 (d, *J*=8.9 Hz, 2H), 7.80 (s, 1H), 7.57 (d, *J*=8.7 Hz, 2H), 4.28 (q, *J*=6.8 Hz, 1H), 4.19-4.11 (m,

1H), 3.31 (s, 3H), 3.26-3.20 (m, 1H), 1.73-1.54 (m, 3H), 1.36 (d, *J*=6.8 Hz, 3H), 0.97 (dd, *J*=10.5 Hz, *J*=6.4 Hz, 6H).

2.8.4 Synthesis of KA-021

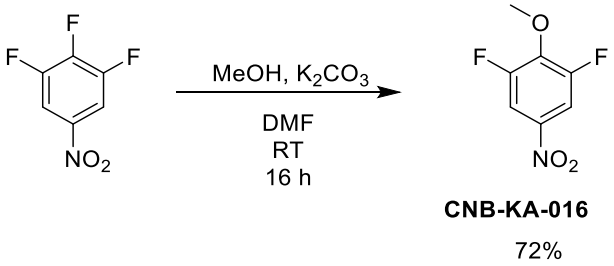

CNB-KA-016

72%

Potassium carbonate (5.0 eq) was added to a solution of 3,4,5-trifluoronitrobenzene (1.0 eq) (Sigma-Aldrich, CAS 66684-58-0) and methanol (1.05 eq) (Sigma-Aldrich, CAS 67-56-1) in DMF (0.4 M). The resulting reaction mixture was stirred at room temperature for 26 hours. The mixture was extracted with ethyl acetate and water, the aqueous phase saturated with sodium chloride before a second extraction. The combined organic phases were washed with brine and then dried with anhydrous magnesium sulfate, filtered and evaporated under reduced pressure. The product, **KA-016**, was purified by flash column chromatography (95:5 hexanes:acetone), and a bright yellow powder was produced with a 72% yield. **^{1}H NMR** (400 MHz, $CDCl_3$) δ 7.85 (d, *J*=8.6 Hz, 2H), 4.18 (dd, *J*=2.0 Hz, *J*=1.9 Hz, 3H). **^{13}C NMR** (100 MHz, $CDCl_3$) δ 155.2 (d, *J*=6.6 Hz), 152.7 (d, *J*=6.6 Hz), 142.5, 109.2, 108.9, 61.8 (dd, *J*=4.4 Hz, *J*=4.4 Hz).

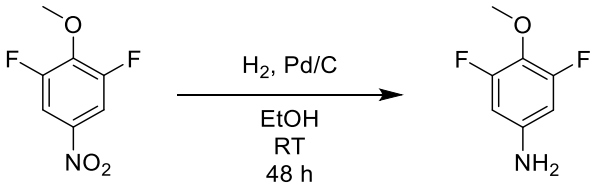

CNB-KA-016 **CNB-KA-018**

84%

Palladium on carbon (10% wt, 50% m/m) (Sigma-Aldrich, cat. 205699) was added to a solution of compound **KA-016** in ethanol (0.1 M) (Sigma-Aldrich, CAS 64-17-5), degassed and placed under argon. The solution was stirred at room temperature for 24 hours. The reaction mixture was filtered over Celite, and evaporated under reduced pressure. The product was purified by flash column chromatography (1:1 to 2:8 to 0:1 hexanes:DCM) to obtain compound **KA-018,** an off-white powder with an 84% yield. **^{1}H NMR** (400 MHz, $CDCl_3$) δ 6.21 (d, *J*=9.9 Hz, 2H), 3.87 (s, 3H), 3.65 (br s, 2H). **^{13}C NMR** (100 MHz, $CDCl_3$) δ 156.7 (dd, *J*=244 Hz, *J*=7.8 Hz), 142.4 (dd, *J*=12.4 Hz, *J*=12.4 Hz), 128.5, 98.8 (dd, *J*=17.9 Hz, *J*=7.7 Hz), 62.3 (dd, *J*=2.6 Hz, *J*=2.2 Hz).

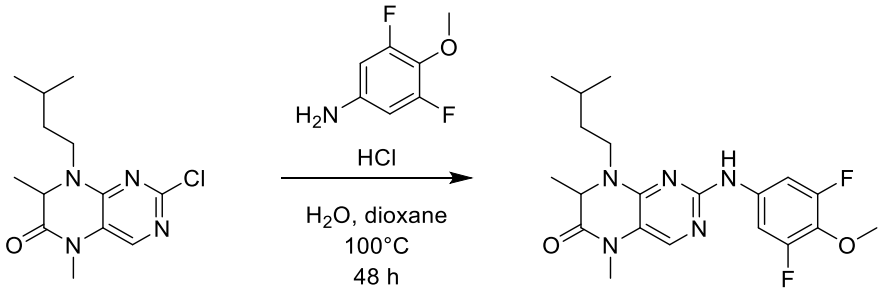

27 **CNB-KA-021**

50%

Compound **KA-021** was prepared by following the steps from **2.6**, with compound 27 and CNB-KA-018. The product was purified by flash column chromatography (0-10% gradient of methanol in DCM) and a pastel orange powder was formed with a 50% yield. . **^{1}H NMR** (400 MHz, DMSO-d_6, TMS) δ 9.37 (s, 1H), 7.38 (s, 1H), 7.52 (d, *J*=11.6 Hz, 2H), 4.27 (q, *J*=6.7Hz, 1H), 4.02-3.95 (m, 1H), 3.82 (s, 3H), 3.23 (s, 3H), 3.19-3.14 (m, 1H), 1.67-1.47 (m, 3H), 1.29 (d, *J*=6.8 Hz, 3H), 0.92 (dd, *J*=7.7 Hz, *J*=6.6 Hz, 6H). **^{13}C NMR** (100 MHz, DMSO-d_6, TMS) δ 163.8, 156.3 (d, *J*=8.0 Hz), 154.9, 153.9 (d, *J*=8.0 Hz), 150.5, 138.3, 137.3 (dd, *J*=13.5 Hz,

J=13.1 Hz), 128.7 (dd, *J*=15.3 Hz, *J*=14.9 Hz), 115.0, 101.4 (d, *J*=27.0 Hz), 61.9, 56.1, 43.0, 35.5, 27.7, 25.7, 22.4, 17.0.

2.8.5 Synthesis of KA-022

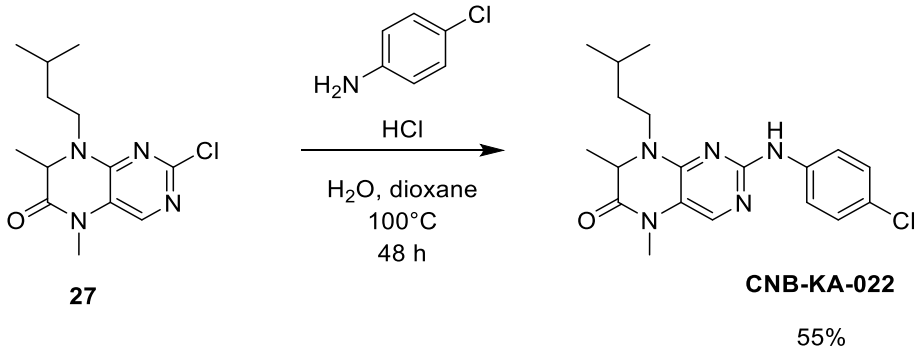

27

CNB-KA-022

55%

Compound **KA-022** followed the steps from **2.6**, with compound 27 and 4-chloroaniline (1.0 eq) (Sigma-Aldrich, CAS 106-47-8) and purified by precipitation. A beige powder was formed with a 55% yield. **^{1}H NMR** (400 MHz, DMSO-d_6, TMS) δ 10.34 (br s, 1H), 7.75 (s, 1H), 7.59 (d, *J*=8.5 Hz, 2H), 7.39 (d, *J*=8.6 Hz, 2H), 4.47 (q, *J*=6.8 Hz, 1H), 3.90-3.84 (m, 1H), 3.31-3.26 (m, 1H), 3.19 (s, 3H), 1.62-1.53 (m, 2H), 1.43 (d, *J*=6.6 Hz, 3H), 1.24 (br s, 1H), 0.87 (dd, *J*=7.4 Hz, *J*=6.6 Hz, 6H).

Chapter 3: Results

3.1: Assess BI-D1870 in combination with HSV1 and VSVΔ51 oncolysis

The mechanism of action of some oncolytic virus combination therapies with small molecule inhibitors are not all fully understood. With the work of previous members of the Alain lab,[110] BI-D1870 was identified and tested with HSV1-1716 and found to increase the amount of viral infection in comparison to the control. Testing the effect of BI-D1870 upon cancer cells, normal cells and various oncolytic viruses will help to understand the mechanism of action.

3.1.1 BI-D1870 is a small molecule inhibitor found to increase HSV1 infection

Cancer treatment is constantly undergoing evaluation in order to provide the best possible care to patients. Oncolytic viral therapy is a newer treatment in the clinic, with T-VEC (oncolytic HSV1) approved for use for melanoma. With only a 16.3% response rate, combining HSV1 with small molecule inhibitors or other compounds to improve upon the infection of the virus is essential. BI-D1870, a RSK inhibitor, was found to increase the infection of HSV1. To begin looking at how BI-D1870 increases infection, several types of cancer cells and normal cells will be tested with HSV1 in combination with BI-D1870.

Human glioblastoma cells (U343) were infected with HSV1-1716-GFP and HSV1-ICP0-null-GFP (**Figure 3 A, B**), murine glioblastoma (K4622) and normal human fibroblasts (GM38) were infected with HSV1-1716-GFP (**Figure 3 C – F**) at a multiplicity of infection (MOI) of 0.1. Concentrations of 10 μM have been reported to be optimal,[112] therefore concentrations of BI-D1870 used included 1 μM, 5 μM, and 10 μM with DMSO as a control. After 48 hours, the green fluorescent protein (GFP) signal was visualized using the EVOS microscope. The extent of

GFP signal seen is indicative of the amount of virus present in the cell. Both the human and murine glioblastomas (U343 and K4622) show increased GFP signaling when treated with BI-D1870 while the GM38 cells have little to no GFP signaling present in both the control and treated cells (**Figure 3 E, F**). Levels of HSV1-1716, ICP0 and GAPDH proteins were detected by western immunoblotting after 48 hours of infection. Viral proteins of HSV1 and ICP0 (an HSV1 protein indicative of the earliest stages of infection)[23] show an increase consistent with the amount of BI-D1870 (**Figure 3 A**). These results show that HSV1 (both HSV1-1716 and HSV1-ICP0-null) infection is increased in the presence of BI-D1870 in cancer cells, but not in normal cells.

3.1.2 BI-D1870 increases HSV1 infection in multiple cancer cell lines

To ensure that the effect BI-D1870 was consistent in other cancerous cell lines and normal cell lines, human renal cell adenocarcinoma cells (786-0) (**Figure 4 A-C**), murine breast carcinoma cells (EMT6) (**Figure 4 D-F**), normal murine mammary epithelial cells (NMuMG) (**Figure 5 A, B, D**) and murine breast carcinoma cells (NT2196) (**Figure 5 A, C - D**) were tested. All cell lines were infected with HSV1-1716-GFP at 0.1 MOI for 48 hours and treated with increasing concentrations of BI-D1870 (1 μM, 5 μM, 10 μM) with DMSO as a control. The GFP signal was visualized using the Incucyte and western blots performed with lysates collected after 48 hours. GraphPad Prism was used to calculate all p-values with an unpaired t-test. In Figure 4 A, the 786-0 cells show an increase in viral HSV1-1716 proteins, and a corresponding increase in ICP0 proteins. The GAPDH levels remain the same in the infected cells, however it looks like there is less GAPDH in the mock cells suggesting unequal loading or exposure issues. Figure 4 B shows a large increase in the extent of GFP signal produced between the control and

the 10 μM treated 786-0 cells**.** Figure 4 C confirms that the increase in infection seen between the DMSO and 10 μM treated cells is indeed significant with a p-value of <0.05. In Figure 4 D, the EMT6 cells show a large increase in viral HSV1-1716 proteins and only one band appearing for the ICP0 at the 10 μM. There are some unspecific bands seen in the mock and infected cells at 45 and 210 kDa. The GFP signaling between the DMSO and 10 μM treated EMT6 cells shows a small increase (**Figure 4 E**) and is not consistent with the western blot (**Figure 4 D**). However, the total GFP cluster area (the total amount of GFP signaling found in the entire well of the plate) was analyzed and found to have significant p-values <0.0001 between DMSO, 5 μM and 10 μM.

To directly compare the effect of BI-D1870 upon viral infection in normal cells and cancer cells, NMuMG (normal breast epithelial cells) and NT2196 (an *ex vivo* NMuMG tumor cell line overexpressing the Neu receptor)[113] were tested. Figure 5 A – C demonstrates that the infection of normal NMuMG cells in comparison to cancerous NT2196 cells is negligible. There is a strong increase in the viral infection of NT2196 cells treated with 10 μM BI-D1870 shown in the western (**Figure 5 A**) and the Incucyte images (**Figure 5 C**). This increase is significant between NT2196 (BI-D1870 at 10 μM) and DMSO as well as NMuMG (BI-D1870 at 10 μM) with a p-value <0.0001. These results show that between two related cell lines (one cancerous, one normal) there is a substantial increase in infection in the cancerous cells, and no increase of infection in the normal cells.

Figure 3. The effect of BI-D1870 on HSV1 infection. (A) Western blot analyses comparing HSV1-1716 and HSV1-ICP0-null proteins, ICP0 protein levels and GAPDH protein as a loading control, (B) Human glioblastoma cells (U343) were infected with HSV1-1716-GFP and HSV1-ICP0-null-GFP at 0.1 MOI in the presence of DMSO and 10 μM of BI-D1870, (C, D) murine glioblastoma (K4622) and (E, F) normal human fibroblasts (GM38) were infected with HSV1-1716-GFP at 0.1 MOI and treated with increasing concentrations of BI-D1870 (DMSO, 1 μM, 5 μM, 10 μM). Phase contrast and fluorescence microscopy imaging and western blot analysis on HSV1-1716, ICP0 and GAPDH proteins were performed on cell lysates 48 hours after infection.

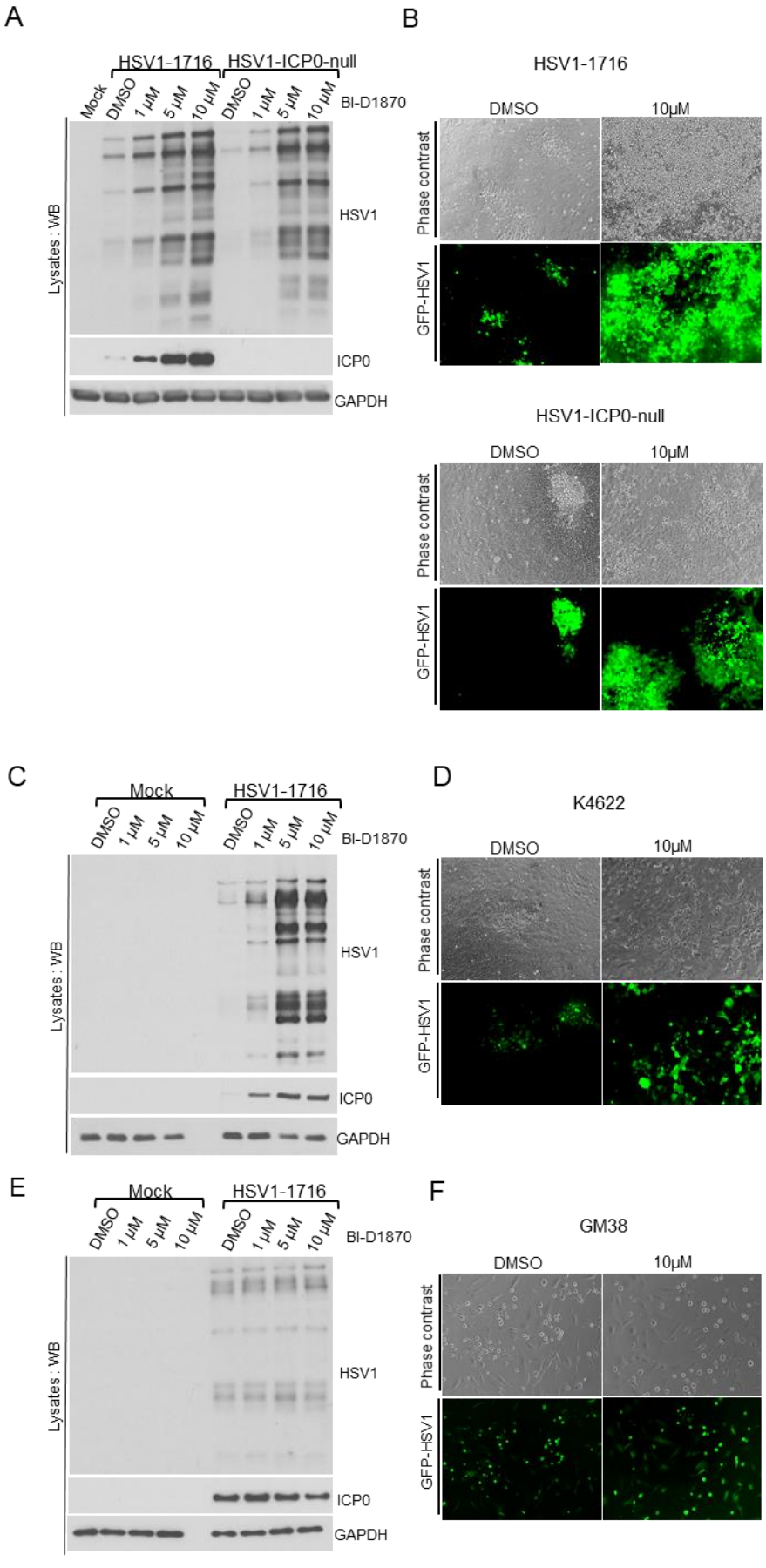
A
HSV1-1716
HSV1-ICP0-null
Mock
DMSO
1 μM
5 μM
10 μM
DMSO
1 μM
5 μM
10 μM
BI-D1870
Lysates : WB
HSV1
ICP0
GAPDH
B
HSV1-1716
DMSO
10μM
Phase contrast
GFP-HSV1
HSV1-ICP0-null
DMSO
10μM
Phase contrast
GFP-HSV1
C
Mock
HSV1-1716
DMSO
1 μM
5 μM
10 μM
DMSO
1 μM
5 μM
10 μM
BI-D1870
Lysates : WB
HSV1
ICP0
GAPDH
D
K4622
DMSO
10μM
Phase contrast
GFP-HSV1
E
Mock
HSV1-1716
DMSO
1 μM
5 μM
10 μM
DMSO
1 μM
5 μM
10 μM
BI-D1870
Lysates : WB
HSV1
ICP0
GAPDH
F
GM38
DMSO
10μM
Phase contrast
GFP-HSV1

Figure 4. The effect of BI-D1870 on HSV1 infection in 786-0 and EMT-6 cells (A, B) Human renal cell adenocarcinoma cells (786-0) were infected with HSV1-1716-GFP at 0.1 MOI in the presence of DMSO, 1 μM, 5 μM and 10 μM of BI-D1870. Phase contrast and fluorescence microscopy imaging and western blot analysis was performed 48 hours after infection. (C, D) Murine breast carcinoma cells (EMT6) were infected with HSV1-1716-GFP 0.1 MOI in the presence of DMSO, 1 μM, 5 μM, and 10 μM of BI-D1870. Phase contrast and fluorescence microscopy imaging and western blot analysis was performed 45 hours after infection.

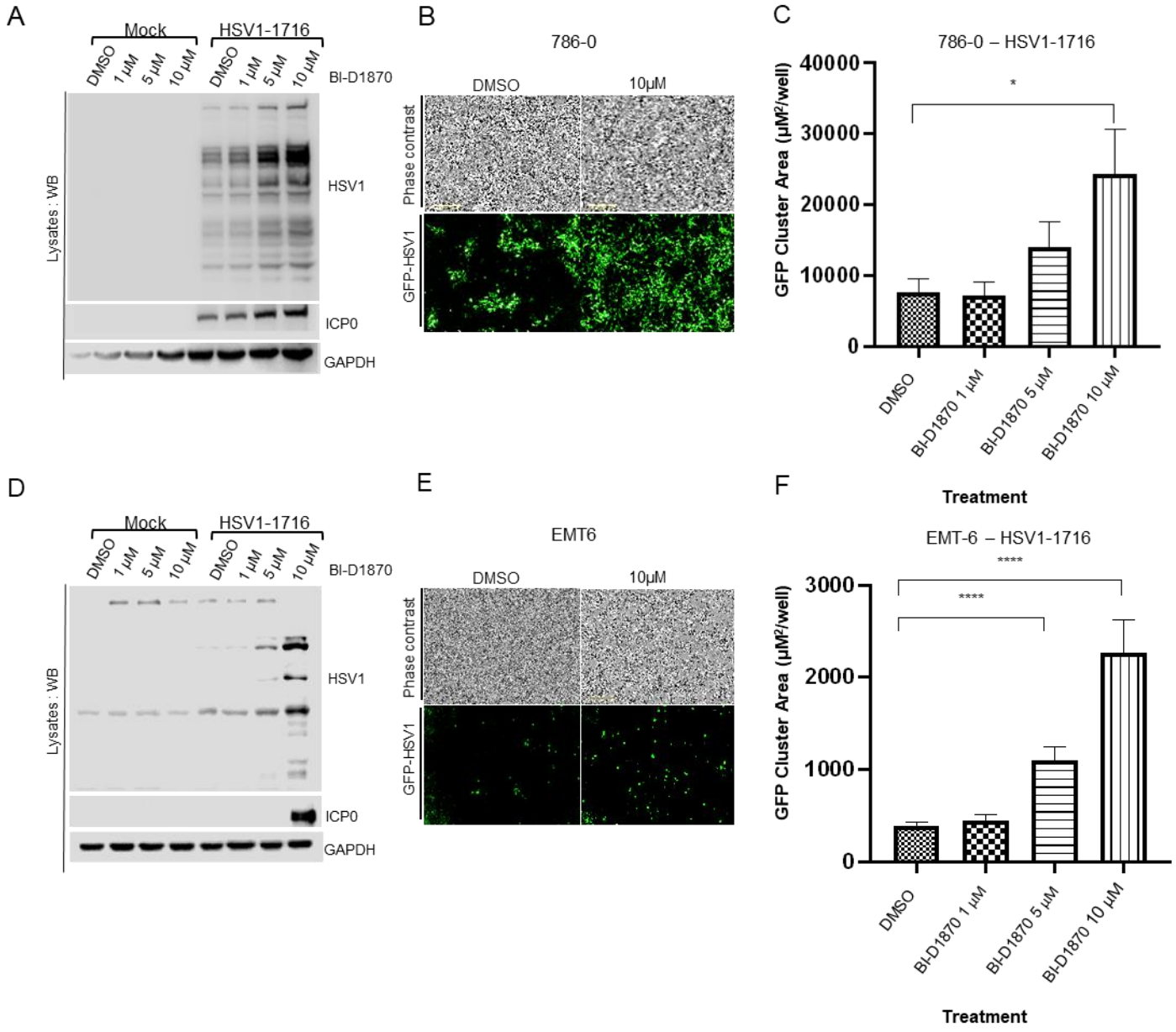
A
Mock
HSV1-1716
DMSO
1 μM
5 μM
10 μM
BI-D1870
Lysates : WB
HSV1
ICP0
GAPDH
B
786-0
DMSO
10μM
Phase contrast
GFP-HSV1
C
786-0 – HSV1-1716
GFP Cluster Area (μM²/well)
40000
30000
20000
10000
0
*
DMSO
BI-D1870 1 μM
BI-D1870 5 μM
BI-D1870 10 μM
Treatment
D
Mock
HSV1-1716
DMSO
1 μM
5 μM
10 μM
BI-D1870
Lysates : WB
HSV1
ICP0
GAPDH
E
EMT6
DMSO
10μM
Phase contrast
GFP-HSV1
F
EMT-6 – HSV1-1716
GFP Cluster Area (μM²/well)
3000
2000
1000
0
****
****
DMSO
BI-D1870 1 μM
BI-D1870 5 μM
BI-D1870 10 μM
Treatment

Figure 5. The effect of BI-D1870 on HSV1 infection in NMuMG and NT2196 cells. (A) Western blot analysis of cell lysates from murine mammary epithelial cells (NMuMG) and murine breast carcinoma cells (NT2196) with HSV1-1716, ICP0 and GAPDH proteins performed 48 hours after infection, (B) phase contrast and fluorescence microscopy of NMuMG cells treated with DMSO and 10 μM of BI-D1870, (C) phase contrast and fluorescence microscopy of NT2196 cells treated with DMSO and 10 μM of BI-D1870, (D) NMuMG and NT2196 cells infected with HSV1-1716 at 0.1 MOI and treated with 10 μM of BI-D1870 for 48 hours. p-values calculated with an unpaired t-test with **** <0.0001.

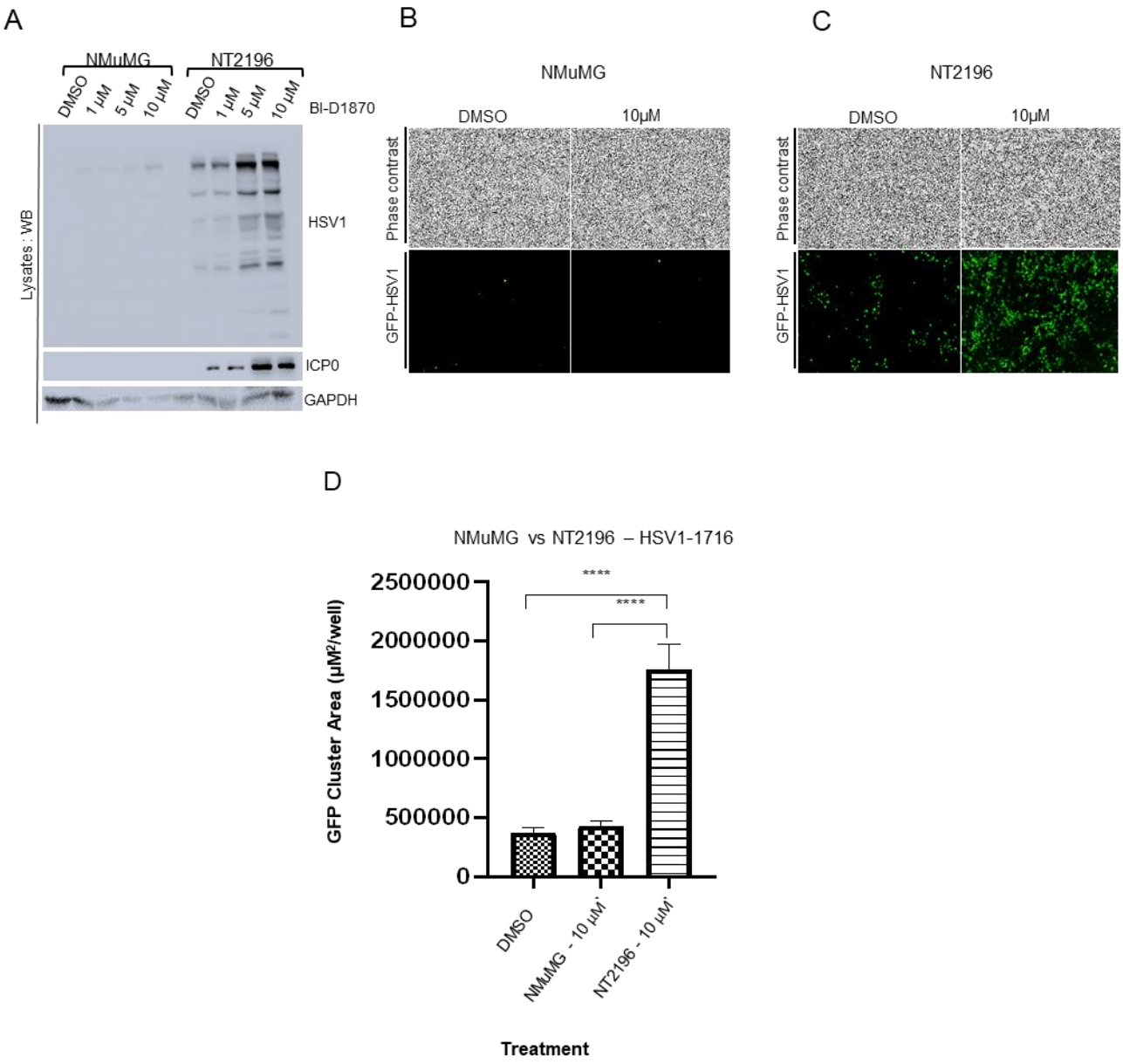
A
NMuMG
NT2196
DMSO
1 μM
5 μM
10 μM
DMSO
1 μM
5 μM
10 μM
BI-D1870
Lysates : WB
HSV1
ICP0
GAPDH
B
NMuMG
DMSO
10μM
Phase contrast
GFP-HSV1
C
NT2196
DMSO
10μM
Phase contrast
GFP-HSV1
D
NMuMG vs NT2196 – HSV1-1716
GFP Cluster Area (μM²/well)
2500000
2000000
1500000
1000000
500000
0
****
****
DMSO
NMuMG - 10 μM
NT2196 - 10 μM
Treatment

3.1.3 BI-D1870 increases the infection of rhabdoviruses

BI-D1870 was found to increase the viral infection of HSV1-1716 in several different cancer cells, but not in normal cells. Other oncolytic viruses like vesicular stomatitis virus (VSVΔ51) and Maraba (MG1) virus are currently being used in clinical trials (NCT02923466, NCT02285816) alone and in combination with other small molecules. The next steps was to test these viruses with BI-D1870 to see if the results are similar to those obtained with HSV1-1716.

4T1 cells were infected with VSVΔ51-GFP and Maraba MG1-GFP at 0.1 MOI for 24 hours and treated with increasing concentrations of BI-D1870 (1 μM, 5 μM, 10 μM) with DMSO as a control (**Figure 6 A, B, E**). There is an increase in VSVΔ51 infection as demonstrated in the western blot (**Figure 6 A**), and GFP images (**Figure 6 B, E**). This is consistent with the results seen in Figures 3 – 5 with HSV1-1716. In contrast to previous results with normal cells, human fibroblasts (GM38) infected with VSVΔ51-GFP at 1 MOI for 24 hours show an increase in viral proteins in the western blot (**Figure 6 C**), however, GFP images show no clear increase in fluorescence (**Figure 6 D**). Further testing with GM38 cells and VSVΔ51 must be done in order to discover whether or not BI-D1870 can increase viral infection in these normal cells. These results demonstrate that the infection of rhabdoviruses like VSVΔ51 and Maraba MG1 is increased in the presence of BI-D1870, however, whether this is cancer-specific and that normal cells are not affected will require additional experiments.

3.1.4 BI-D1870 enhances VSVΔ51 viral infection in multiple cell lines

Figures 4 and 5 showed that BI-D1870 increased the infection of HSV1-1716 in multiple different cancerous cell lines, but did not increase in the normal cell lines GM38 and NMuMG.

To determine if BI-D1870 and VSVΔ51 can obtain similar results to those with HSV1-1716, the same cells lines – 786-0, EMT-6, NT2196 and NMuMG were tested.

786-0 cells were infected with VSVΔ51-GFP at 0.01 MOI for 24 hours and treated with increasing concentrations of BI-D1870 (1 μM, 5 μM, 10 μM) with DMSO as a control (**Figure 7 A-C**). Interestingly, western immunoblotting shows a decrease in viral proteins present in cells treated with 1 μM and 5 μM of BI-D1870 in comparison to the control, however, the cells treated with 10 μM of BI-D1870 show an increase of viral proteins (**Figure 7 A**). GFP images also show an increase of viral infection in the cells treated with 10 μM BI-D1870 in comparison to those treated with DMSO (**Figure 7 B**). GFP data collected by the Incucyte and graphed with GraphPad was analyzed by an unpaired t-test which showed a significant increase in GFP fluorescence when cells are treated with 5 μM and 10 μM of BI-D1870 (p-values of <0.05 and <0.01 respectively).

EMT-6 cells were infected with VSVΔ51 at 0.01 MOI for 25.5 hours and treated with increasing concentrations of BI-D1870 (Figure 8 D-F). The western blot (**Figure 7 D**) and the GFP images (**Figure 7 E**) again demonstrate a positive effect: viral proteins of VSVΔ51 show a large increase – from barely any infection to lots of infection in BI-D1870 treated cells, but the GFP images show a smaller increase. To confirm that there was an increase in viral infection in the EMT-6 cells, data collected from the Incucyte was graphed with GraphPad and analyzed by an unpaired t-test. The results (**Figure 7 F**) show a significant p-value of <0.0001 between DMSO and 10 μM BI-D1870 treated cells.

The last two cell lines to be compared to previous experiments with HSV1-1716 are the ex vivo NMuMG tumour cell line NT2196 and NMuMG, These two cell lines can be directly compared in their responses to the virus and drug as they have a common lineage.[113] NMuMG

and NT2196 cells were infected with VSVΔ51 at 0.1 MOI and treated with BI-D1870 in increasing concentrations for 24 hours (**Figure 8 A-D**). Western immunoblotting (**Figure 8 A**) and GFP images (**Figure 8 B**) show no increase in infection in NMuMG cells when treated with BI-D1870. However, NT2196 cells have an increase in viral infection as demonstrated by the western blot (**Figure 8 A**) with an increase in VSVΔ51 proteins, and more fluorescence in the GFP images (**Figure 8 C**). GFP cluster area data was gathered from the Incucyte and analyzed with GraphPad. An unpaired t-test demonstrates a significant difference between NT2196 cells treated with DMSO and 10 μM of BI-D1870, as well as between NMuMG cells and NT2196 cells treated with 10 μM of BI-D1870 with a p-value of <0.0001. Overall, the results from Figure 7 and 8 show that VSVΔ51 infection can be enhanced by the presence of BI-D1870 in various cancerous cell lines, but has no effect on normal cell lines. This is in agreement with results from Figures 3 – 5 with HSV1-1716.

Figure 6. **The effect of BI-D1870 on rhabdoviruses** in (A, B) murine breast carcinoma cells (4T1) and (C, D) normal human fibroblasts (GM38). Each cell line was infected with VSVΔ51-GFP at 0.1 MOI and 1 MOI respectively and treated with increasing concentrations of BI-D1870 (DMSO, 1 μM, 5 μM and 10 μM). (E) 4T1 cells infected with Maraba MG1 at 0.1 MOI and treated with increasing concentrations of BI-D1870 (DMSO, 1 μM, 5 μM, 10 μM). Phase contrast and fluorescence microscopy imaging and western blot analysis was performed on cell lysates 24 hours after infection.

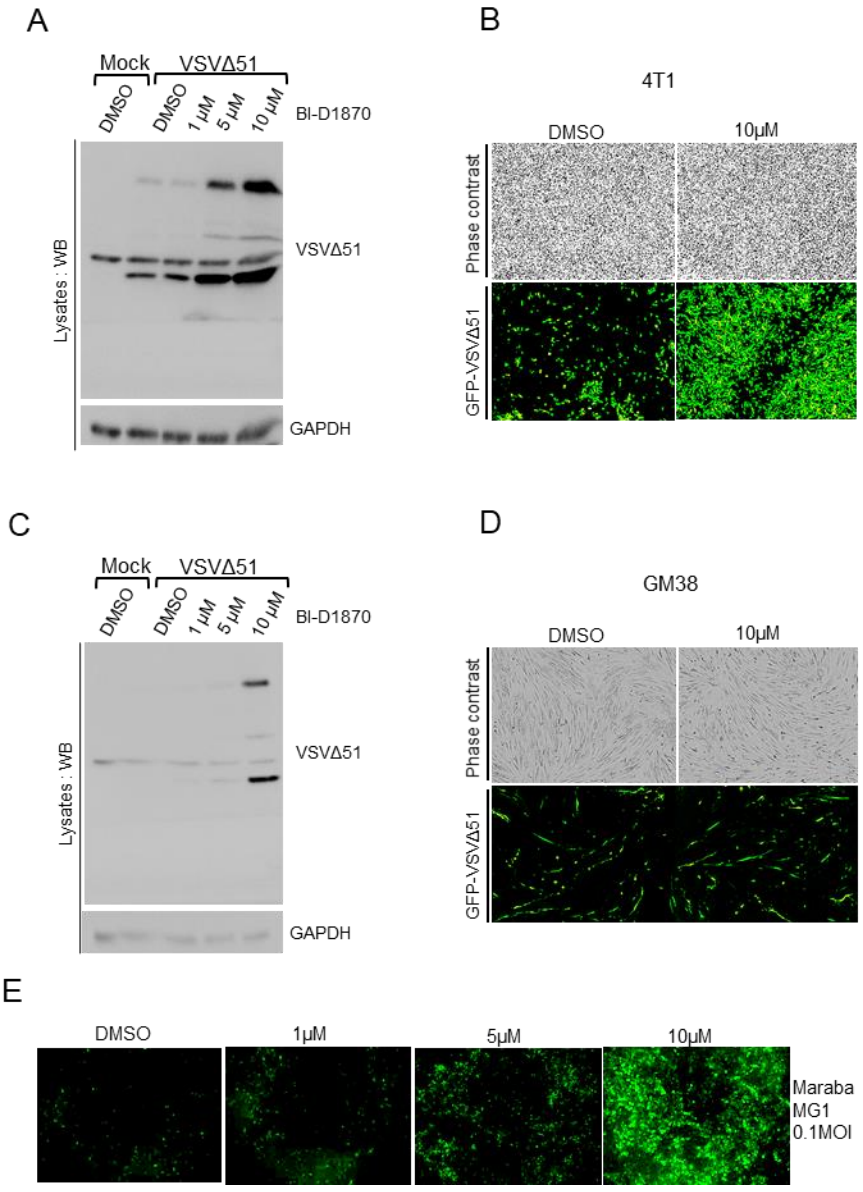
A
Mock
VSVΔ51
DMSO
DMSO
1 μM
5 μM
10 μM
BI-D1870
Lysates : WB
VSVΔ51
GAPDH
B
4T1
DMSO
10μM
Phase contrast
GFP-VSVΔ51
C
Mock
VSVΔ51
DMSO
DMSO
1 μM
5 μM
10 μM
BI-D1870
Lysates : WB
VSVΔ51
GAPDH
D
GM38
DMSO
10μM
Phase contrast
GFP-VSVΔ51
E
DMSO
1μM
5μM
10μM
Maraba
MG1
0.1MOI

Figure 7. The effect of BI-D1870 on VSVΔ51 infection in 786-0 and EMT-6 cells. (A, B) Human renal cell adenocarcinoma cells (786-0) were infected with VSVΔ51-GFP at 0.01 MOI in the presence of DMSO, 1 μM, 5 μM and 10 μM of BI-D1870. Phase contrast and fluorescence microscopy imaging and western blot analysis was performed 24 hours after infection. (C, D) Murine breast carcinoma cells (EMT-6) were infected with VSVΔ51-GFP 0.01 MOI in the presence of DMSO, 1 μM, 5 μM, and 10 μM of BI-D1870. Phase contrast and fluorescence microscopy imaging and western blot analysis was performed 25.5 hours after infection.

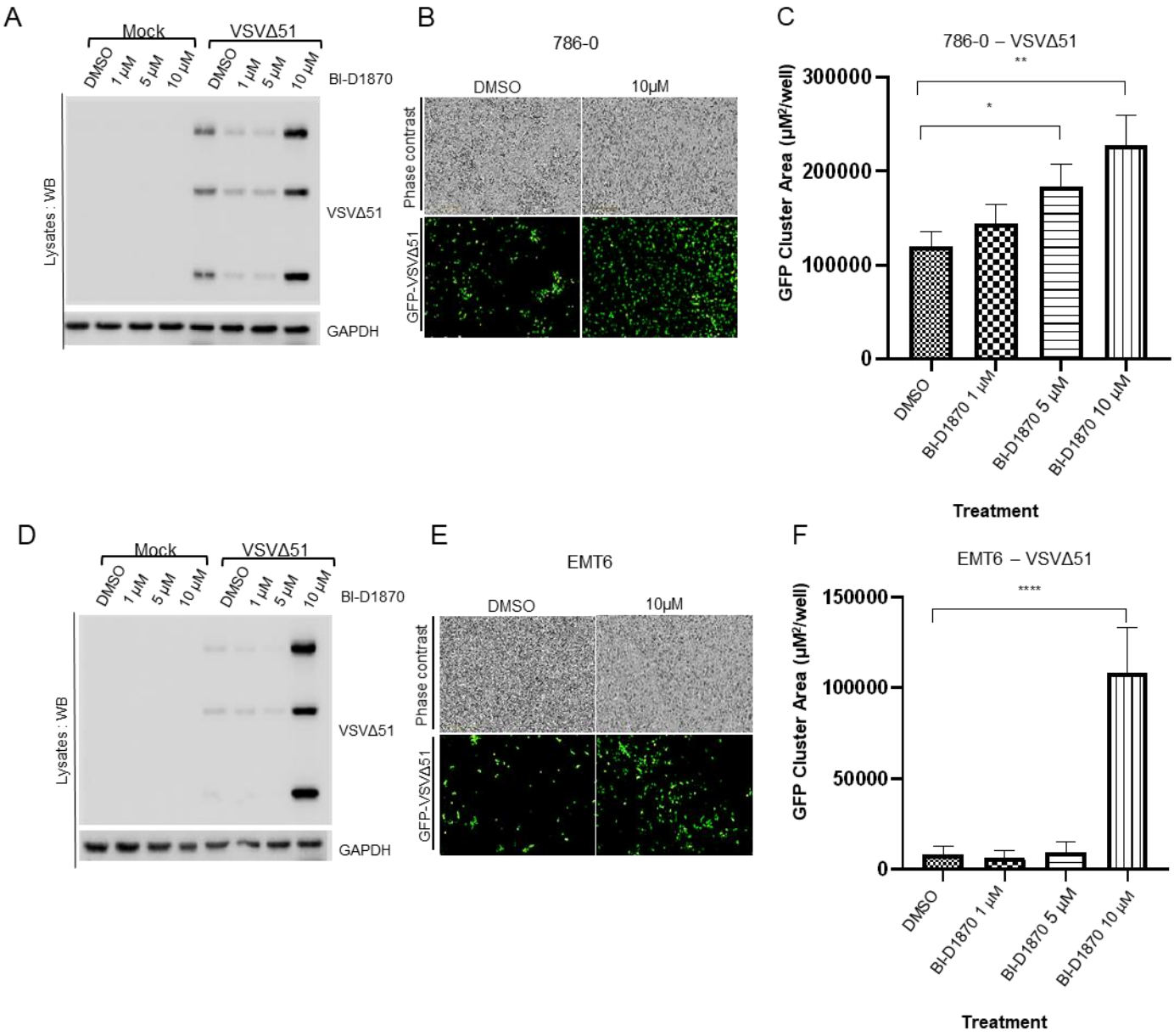
A
Mock
VSVΔ51
DMSO
1 μM
5 μM
10 μM
BI-D1870
Lysates : WB
VSVΔ51
GAPDH
B
786-0
DMSO
10μM
Phase contrast
GFP-VSVΔ51
C
786-0 – VSVΔ51
GFP Cluster Area (μM²/well)
300000
200000
100000
0
**
*
DMSO
BI-D1870 1 μM
BI-D1870 5 μM
BI-D1870 10 μM
Treatment
D
Mock
VSVΔ51
DMSO
1 μM
5 μM
10 μM
BI-D1870
Lysates : WB
VSVΔ51
GAPDH
E
EMT6
DMSO
10μM
Phase contrast
GFP-VSVΔ51
F
EMT6 – VSVΔ51
GFP Cluster Area (μM²/well)
150000
100000
50000
0
****
DMSO
BI-D1870 1 μM
BI-D1870 5 μM
BI-D1870 10 μM
Treatment

Figure 8. The effect of BI-D1870 on VSVΔ51 infection on NMuMG and NT2196 cells. (A) Western blot analysis of cell lysates from murine mammary epithelial cells (NMuMG) and murine breast carcinoma cells (NT2196) with VSVΔ51 and GAPDH proteins performed 24 hours after infection, (B) phase contrast and fluorescence microscopy of NMuMG cells treated with DMSO and 10 μM of BI-D1870, (C) phase contrast and fluorescence microscopy of NT2196 cells treated with DMSO and 10 μM of BI-D1870, (D) NMuMG and NT2196 cells were infected with VSVΔ51 at 0.1 MOI for 24 hours and treated with DMSO and 10 μM BI-D1870. p-values calculated with an unpaired t-test where **** <0.0001.

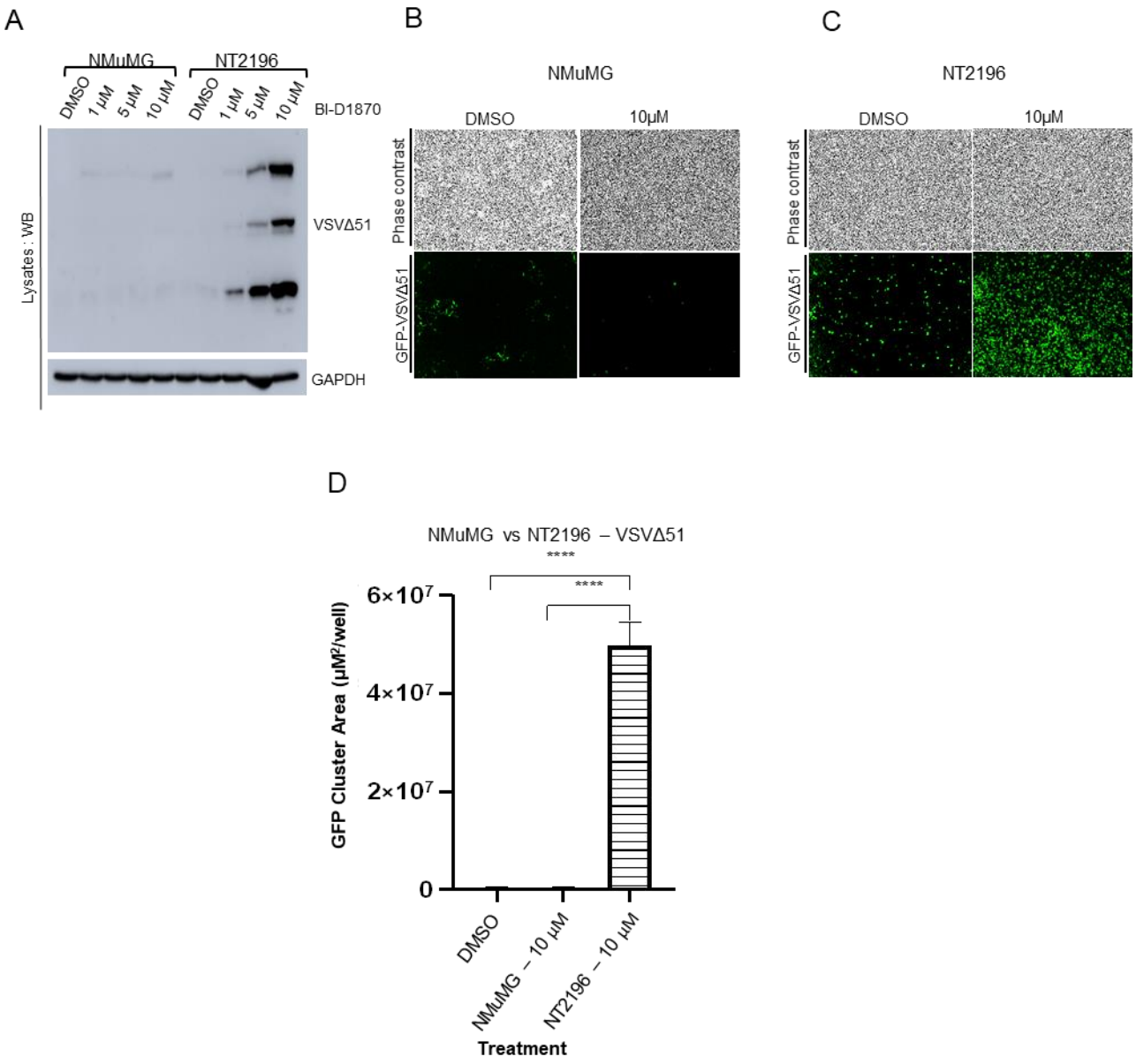
A
NMuMG
NT2196
DMSO
1 μM
5 μM
10 μM
DMSO
1 μM
5 μM
10 μM
BI-D1870
Lysates : WB
VSVΔ51
GAPDH
B
NMuMG
DMSO
10μM
Phase contrast
GFP-VSVΔ51
C
NT2196
DMSO
10μM
Phase contrast
GFP-VSVΔ51
D
NMuMG vs NT2196 – VSVΔ51
****
****
GFP Cluster Area (μM²/well)
6×10⁷
4×10⁷
2×10⁷
0
DMSO
NMuMG – 10 μM
NT2196 – 10 μM
Treatment

3.1.5 BI-D1870 can increase viral replication in mice

Figures 3 – 8 show that BI-D1870 can increase the infection of HSV1-1716, VSVΔ51 and Maraba MG1 *in vitro* in cancer cell lines. While these results are encouraging, the next steps are to determine whether BI-D1870 can exert a positive effect upon the infection of VSVΔ51 *in vivo*. These experiments are important to show if BI-D1870 is toxic in combination with oncolytic viruses, and if it can increase viral infection within tumour tissue *in vivo*.

Mice with the 4T1 subcutaneous breast cancer tumours were either treated with VSVΔ51-Fluc (5×10^8 pfu) intratumourally (i.t.) or a combination of BI-D1870 (100 mg/kg, intraperitoneally (i.p.)) and VSVΔ51-Fluc for 72 hours (**Figure 9 A-B**). 18 hours post infection (p.i.), the greatest amount of luciferase expression is found within the mice treated with BI-D1870 and slowly tapers off at 72 hours p.i. In the mice treated with BI-D1870, there is a larger amount of luciferase seen in both the injection site and the tumour, however, after 48 hours, the viral infection looks as if it has spread outside of the tumour tissue. Figure 9 C shows a dose response with mice tolerating up to 100 mg/kg of BI-D1870 with an increase in viral titer when VSV-Fluc (1×10^6 pfu) was administered i.t. 1491 mouse glioblastoma cells and mice implanted with 1491 cell intracranially were treated with VSVΔ51 (5×10^8 pfu intravenously (i.v.)) or BI-D1870 (100 mg/kg i.p.) and VSVΔ51 for 24 hours (**Figure 9 D-F**). Again, an increase in luciferase is detected in the brain tumours only in the presence of BI-D1870. This preliminary data indicates that BI-D1870 is able to potentiate a positive effect of VSVΔ51 infection *in vivo*, and is tolerated up to 100 mg/kg in mice. Further experiments must be completed to assess safety and specificity.

3.1.6 Nanoparticles carrying BI-D1870 can enhance the viral infection of HSV1

In the past few years, nanotechnology research has made great progress in drug delivery systems. Nanoparticles can provide stability in cancer treatments and are able to aid therapeutic efficacy[114] by enhancing drug delivery to cancerous tissue, reducing toxicity and side effects.[115,116] The naked drug can move in and out of the tumour through its leaky vasculature, while the encapsulated drug is able to move into the tumour microenvironment, but not out, allowing for greater uptake of the drug (**Figure 10 A**). I have hypothesized that nanoparticles can aid in delivering BI-D1870 to cancer cells and tissue, providing a more targeted approach.

Nanoparticles were used to deliver BI-D1870 in combination with HSV1-1716 to human glioblastoma (U343) and prostate carcinoma (PC3) cells (**Figure 10**). U343 and PC3 cells were infected with HSV1-1716-GFP at 0.1 MOI for 48 hours and treated with either DMSO, an empty nanoparticle, a nanoparticle with BI-D1870, or naked BI-D1870 (both with increasing concentrations of 1 μM, 5 μM, 10 μM) (**Figure 10 B-C**). Western immunoblotting of HSV1 proteins show an increase of both cell lines treated with nanoparticles and naked BI-D1870. These results demonstrate that nanoparticles are able to deliver BI-D1870 to cancer cells and increase viral infection of HSV1-1716. This targeted approach could be used in future *in vivo* experiments to provide better delivery of the drug to cancer tissues.

Figure 9. In vivo experiments with VSVΔ51 and BI-D1870. (A) Mouse breast cancer model (4T1 - subcutaneous) – mice treated with VSVΔ51-Fluc (5 x 10^8 pfu i.t.) compared to mice treated with BI-D1870 (100 mg/kg i.p.) + VSVΔ51-Fluc, (B, F) graphical representation of the total flux (p/s) and mice treated with VSVΔ51-Fluc (5 x 10^8 pfu i.t.) vs VSVΔ51-Fluc + BI-D1870 (100 mg/kg i.p.) (C) 4T1 mouse model – mice treated with VSVΔ51 and increasing doses of BI-D1870 (Vehicle, 50 mg/kg, 100 mg/kg), tumours were extracted and viral titer were performed by plaque assay viral titer, (D) murine glioma cells (1491) treated with HSV1-1716-GFP at 0.1 MOI with DMSO or BI-D1870 (10 μM) for 48 hours, (E) 1491 mouse glioma model – mice treated with VSVΔ51-Fluc (5 x 10^8 pfu i.t.) compared to mice treated with BI-D1870 (100 mg/kg i.p.) + VSVΔ51-Fluc for 24 hours.

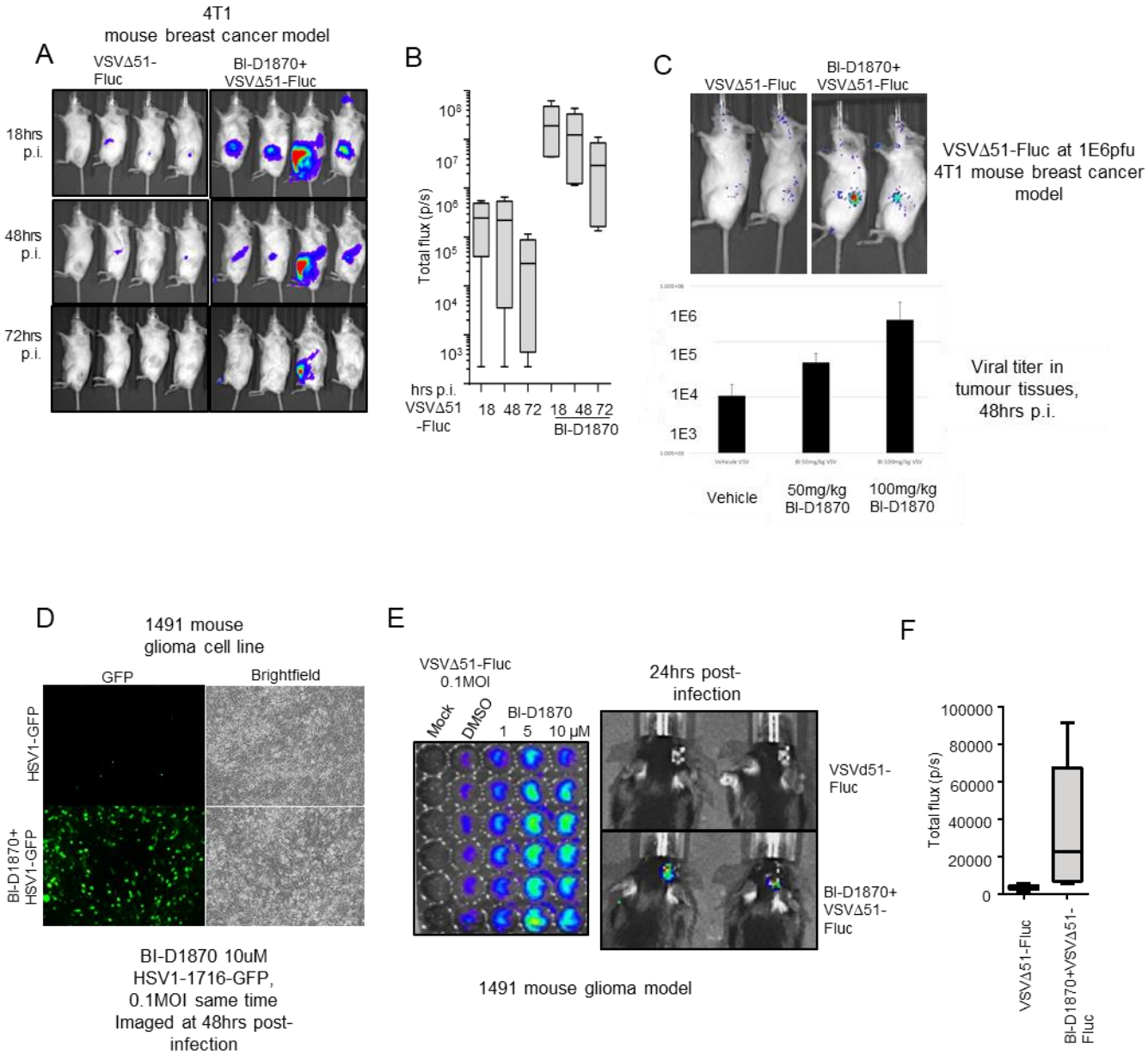
4T1
mouse breast cancer model
A
VSVΔ51-Fluc
BI-D1870+ VSVΔ51-Fluc
18hrs p.i.
48hrs p.i.
72hrs p.i.
B
Total flux (p/s)
hrs p.i.
VSVΔ51 -Fluc
18 48 72
18 48 72
BI-D1870
C
VSVΔ51-Fluc
BI-D1870+ VSVΔ51-Fluc
VSVΔ51-Fluc at 1E6pfu 4T1 mouse breast cancer model
1E6
1E5
1E4
1E3
Viral titer in tumour tissues, 48hrs p.i.
Vehicle
50mg/kg BI-D1870
100mg/kg BI-D1870
D
1491 mouse glioma cell line
GFP
Brightfield
HSV1-GFP
BI-D1870+ HSV1-GFP
BI-D1870 10uM
HSV1-1716-GFP,
0.1MOI same time
Imaged at 48hrs post-infection
E
VSVΔ51-Fluc 0.1MOI
Mock
DMSO
BI-D1870
1 5 10 μM
24hrs post-infection
VSVd51-Fluc
BI-D1870+ VSVΔ51-Fluc
1491 mouse glioma model
F
Total flux (p/s)
100000
80000
60000
40000
20000
0
VSVΔ51-Fluc
BI-D1870+VSVΔ51-Fluc

Figure 10. Nanoparticles (NP) carrying BI-D1870 enhances HSV1-1716 infection. (A) Pictoral representation of naked drug delivery vs nanoparticle delivery of drug to the tumour. (B) Human glioblastoma (U343) and (C) prostate carcinoma (PC3) cells were infected with HSV1-1716-GFP (0.1 MOI) and treated with DMSO, empty nanoparticles (NP-empty), nanoparticles containing BI-D1870 at 10 μM (NP-BI-D1870) or naked BI-D1870 at the corresponding concentrations (1μM, 5 μM, 10 μM). Fluorescence microscopy imaging and western blot analyses were performed on cell lysates 48 hours after infection.

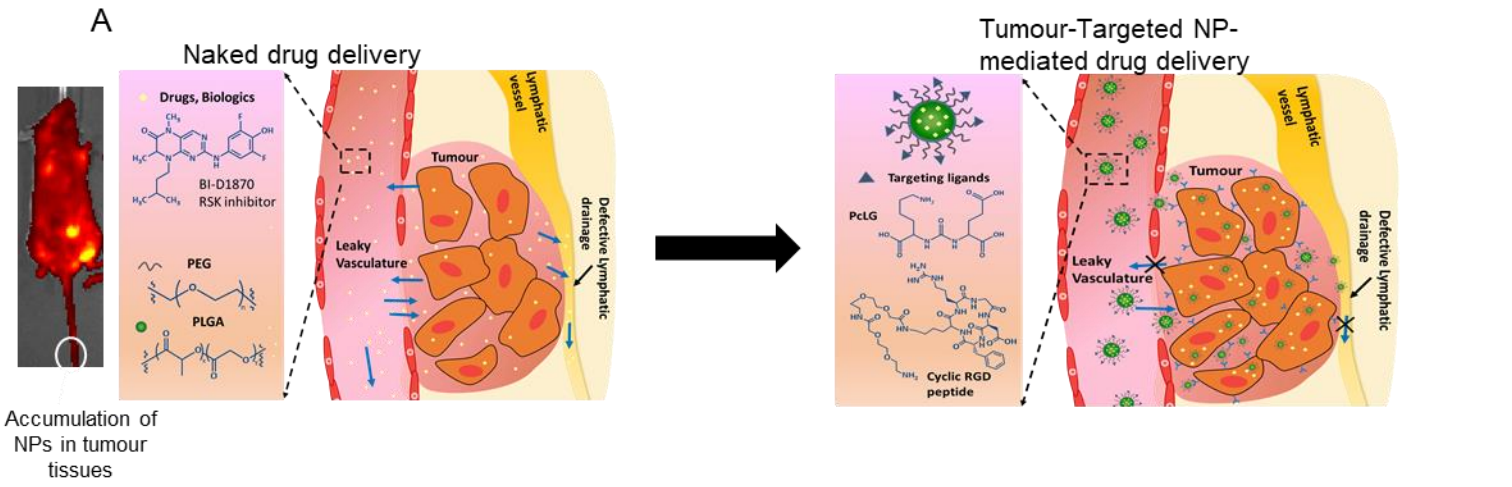
A
Naked drug delivery
Drugs, Biologics
BI-D1870
RSK inhibitor
PEG
PLGA
Tumour
Leaky Vasculature
Lymphatic vessel
Defective lymphatic drainage
Accumulation of NPs in tumour tissues
Tumour-Targeted NP-mediated drug delivery
Targeting ligands
PcLG
Cyclic RGD peptide
Tumour
Leaky Vasculature
Lymphatic vessel
Defective lymphatic drainage

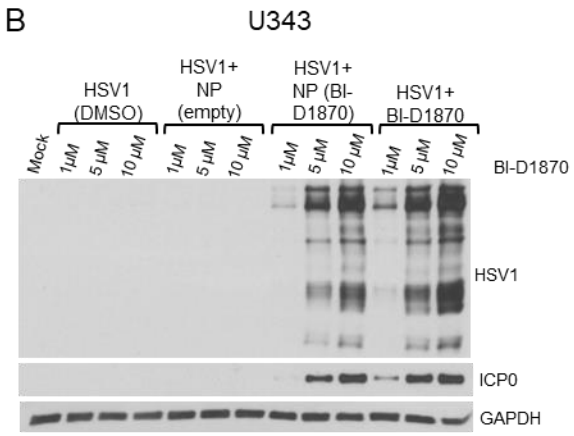
B
U343
HSV1 (DMSO)
HSV1+ NP (empty)
HSV1+ NP (BI-D1870)
HSV1+ BI-D1870
Mock
1μM
5 μM
10 μM
BI-D1870
HSV1
ICP0
GAPDH

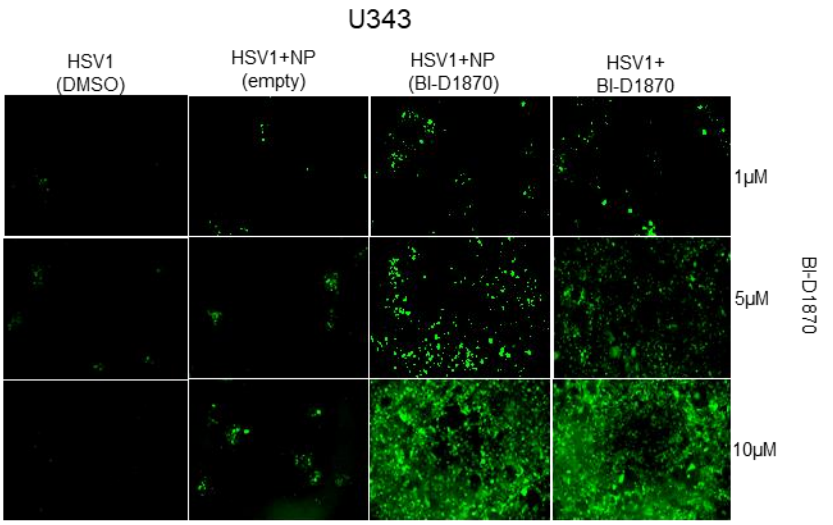
U343
HSV1 (DMSO)
HSV1+NP (empty)
HSV1+NP (BI-D1870)
HSV1+ BI-D1870
1μM
5μM
10μM
BI-D1870

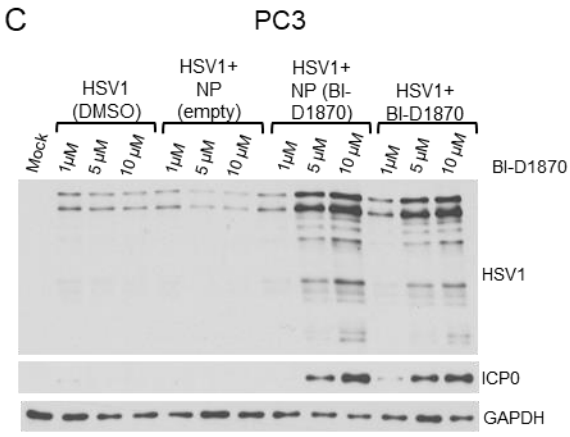
C
PC3
HSV1 (DMSO)
HSV1+ NP (empty)
HSV1+ NP (BI-D1870)
HSV1+ BI-D1870
Mock
1μM
5 μM
10 μM
BI-D1870
HSV1
ICP0
GAPDH

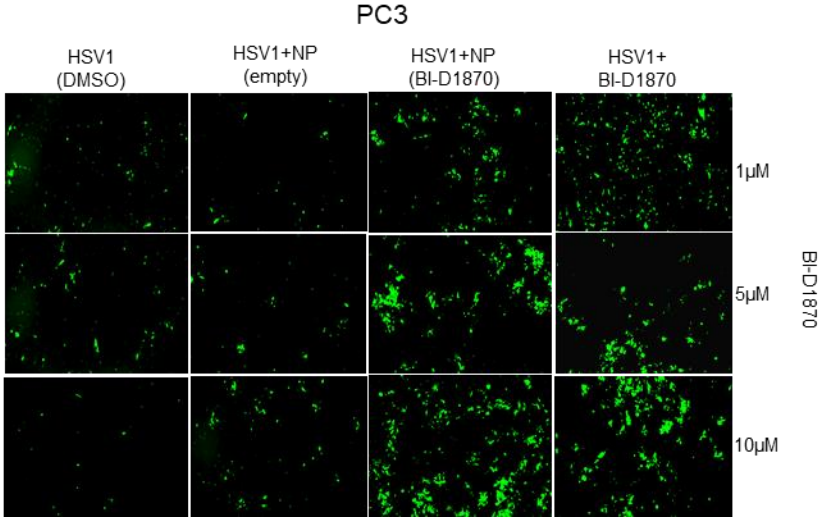
PC3
HSV1 (DMSO)
HSV1+NP (empty)
HSV1+NP (BI-D1870)
HSV1+ BI-D1870
1μM
5μM
10μM
BI-D1870

3.1.7 BI-D1870 represses viral infection in poxviruses and adenovirus

HSV1-1716, VSVΔ51 and Maraba MG1 were all found to have an increase in viral infection in cancer cells when treated with BI-D1870. To continue these experiments, other oncolytic viruses were considered for testing. Some of the main OVs found in clinical trials and combined with a drug include poxviruses[117] (NCT00554372) and adenovirus[118] (NCT0598129).

In contrast with HSV1-1716 and VSVΔ51, U343 cells infected with vaccinia virus (VACV-GFP) or myxoma virus (MYX-GFP) at an MOI of 1 and treated with increasing concentrations of BI-D1870 showed a repression of infection (**Figure 11 A-B**). Adenovirus (Ad-RFP), tested by members of the Parks lab at the Ottawa Hospital Research Institute, with an MOI of 10 was also repressed in the presence of 10 μM of BI-D1870 (**Figure 11 B**). Western immunoblotting shows a complete repression of VACV proteins in the presence of increasing concentrations of BI-D1870, a complete opposite to that of HSV1-1716 and VSVΔ51 (**Figure 8 A**). These results show that BI-D1870 does not increase all oncolytic viruses, but appears inhibitory to poxviruses and adenovirus. More experiments with other OVs must be done to see if there is a trend in positive or negative outcome.

Figure 11. BI-D1870 represses viral infection of poxviruses and adenovirus. (A) Western blot analysis of VACV proteins with increasing concentrations of BI-D1870 (DMSO, 1 μM, 5 μM, 10 μM) and GAPDH as loading control. (B) U343 cells were infected with vaccinia virus at 1 MOI, myxoma virus at 1 MOI and adenovirus at 10 MOI in the presence of increase concentrations of BI-D1870. Fluorescence microscopy and western blot analysis was performed 48 hours after infection.

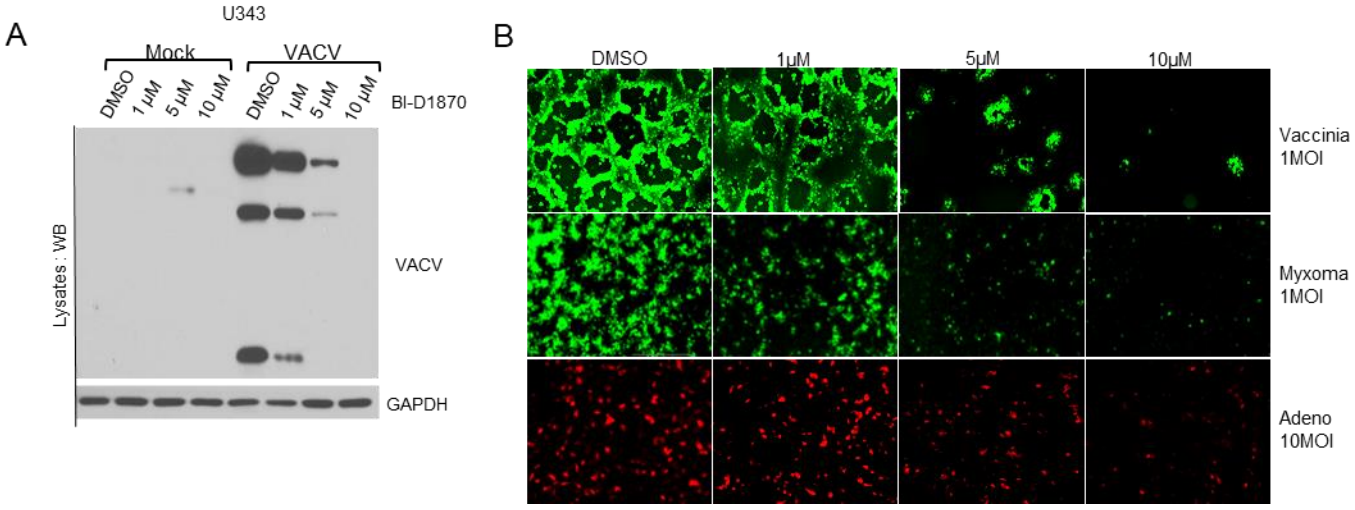
A
U343
Mock
VACV
DMSO
1 μM
5 μM
10 μM
DMSO
1 μM
5 μM
10 μM
BI-D1870
Lysates : WB
VACV
GAPDH
B
DMSO
1μM
5μM
10μM
Vaccinia
1MOI
Myxoma
1MOI
Adeno
10MOI

3.2: Determining the mechanism of action of BI-D1870

3.2.1 The inhibition of RSK by BI-D1870 is not the main mechanism of action

BI-D1870 is a known RSK inhibitor with many off target effects.[93,94,112] To determine whether or not the inhibition of RSK is the mechanism behind the increase in viral infection, other commonly used RSK inhibitors in the literature were tested: LJI308, BIX02565, Fmk and SL0101. U343 cells were infected with HSV1-1716-GFP at 0.1 MOI for 48 hours and treated with increasing concentrations (1 μM, 5 μM, and 10 μM) of each RSK inhibitor with DMSO as a control (**Figure 12**). Western immunoblotting (**Figure 12 A**) and GFP images (**Figure 12 B**) show that BI-D1870 is the only RSK inhibitor that increases the viral infection of HSV1-1716.

In order to rule out RSK as a main mediator of the mechanism of action, CRISPR-Cas9 was used upon human glioblastoma cells (LN-18) to knock out the two main isoforms of RSK present in these cells – RSK 1 and 2. The wild type (WT) RSK1/2 $^{+/+}$, RSK1$^{-/-}$, RSK 2$^{-/-}$ and RSK1/2$^{-/-}$ were infected with HSV1-1716-GFP at 0.01 MOI for 48 hours and treated with increasing concentrations of BI-D1870 (1μM, 5 μM, 10 μM) and DMSO (**Figure 13**). Western immunoblotting shows an increase in viral proteins in RSK1/2$^{+/+}$, RSK1$^{-/-}$, RSK 2$^{-/-}$ and RSK1/2$^{-/-}$ cells (**Figure 13 A**). The GFP images from the Incucyte display a correlative increase in fluorescence with BI-D1870 (**Figure 13 B**). To confirm that the RSK1 and 2 isoforms are not present in these cells, western immunoblotting of key proteins was performed (**Figure 13 C**). An analysis of GFP fluorescence done with Incucyte software shows an increase over time, however the RSK2$^{-/-}$ cells have a substantially smaller increase in comparison to the wild type, and is more similar to the cells treated with DMSO (**Figure 13 D**). The GFP cluster area for RSK1/2$^{+/+}$, RSK1$^{-/-}$, RSK 2$^{-/-}$ and RSK1/2$^{-/-}$ has been analyzed and graphed with GraphPad. Supplemental Figure 1C shows an increase in the amount of viral infection in RSK 2$^{-/-}$ cells as the

concentration of BI-D1870 increases, however when compared to RSK1/2$^{+/+}$, RSK1$^{-/-}$, and RSK1/2$^{-/-}$ cells, the total amount of viral infection is inferior. These results suggest that while these knock out cell lines show an increase in viral infection when treated with BI-D1870, the inhibition of RSK2 could still be a part of the mechanism of action of BI-D1870.

3.2.2 BI-D1870 has many off-target effects

In the literature, BI-D1870 has been reported to inhibit and activate many more proteins than just RSK.[93,94,112] In order to determine the specific off targets of BI-D1870, a literature search was done using keyword 'RSK inhibitor' on PubMed. All known targets of RSK inhibitors BI-D1870, LJI308, LJH608, BIX02565, Fmk, and SL0101 were catalogued and then inputted into Microsoft PowerPoint to create a Venn diagram (**Figure 14 A**).[93–95,108,112,119,120] The result of this comparison provided a list of suggested off targets of BI-D1870 (**Figure 14 B**).

The Sabourin lab at the Ottawa Hospital Research Institute works with the Ste-20 like protein (SLK) which was reported to be a specific off-target of BI-D1870. SLK is a caspase 3-activated kinase that has a role in the initiation of apoptosis, cell cycle progression, cell migration and the cytoskeleton.[121] An HER2+ cell line was used with a deletion of SLK Δ3-6 (as described in Pryce et al, 2017)[122] (SLK$^{fl/fl}$) to determine if the function of SLK is important in the mechanism of action of BI-D1870 (**Figure 15**). SLK$^{+/+}$ and SLK$^{fl/fl}$ were both infected with VSVΔ51-RFP at 0.01 MOI for 24 hours and treated with increasing concentrations of BI-D1870 (**Figure 15 A**). Western immunoblotting and GFP images show no increase in infection between SLK$^{+/+}$ and SLK$^{fl/fl}$. This experiment was repeated with HSV1-1716-GFP at 0.1 MOI and increasing concentrations of BI-D1870 for 48 hours (**Figure 15 B**). These results show no increase in infection in SLK$^{+/+}$ cells and SLK$^{fl/fl}$ cells treated with BI-D1870. This data shows that SLK does not play a role in the mechanism of action of BI-D1870.

Figure 12. RSK inhibition is not the main mechanism by which BI-D1870 increases viral infection. (A) Western blot analysis showing the levels of HSV1 proteins present in each sample comparing other RSK inhibitors to that of BI-D1870. (B) Human glioblastoma cells (U343) were infected with HSV1-1716-GFP (0.1 MOI) and treated with increasing concentrations (DMSO, 1 μM, 5 μM, 10 μM) of commonly used RSK inhibitors (BI-D1870, LJI308, BIX02565, Fmk, SL0101). Fluorescence microscopy imaging was performed 48 hours after infection.

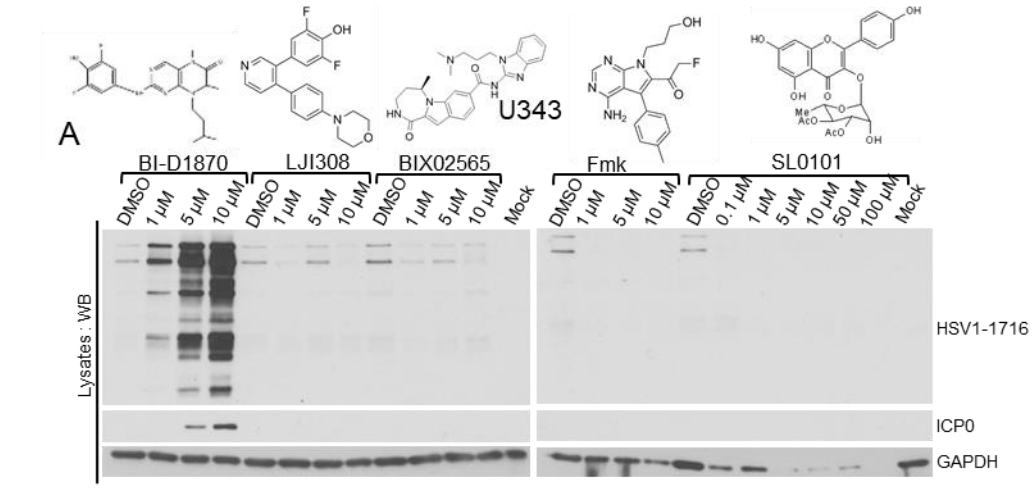
A
U343
BI-D1870
LJI308
BIX02565
Fmk
SL0101
DMSO
1 μM
5 μM
10 μM
Mock
0.1 μM
50 μM
100 μM
Lysates : WB
HSV1-1716
ICP0
GAPDH

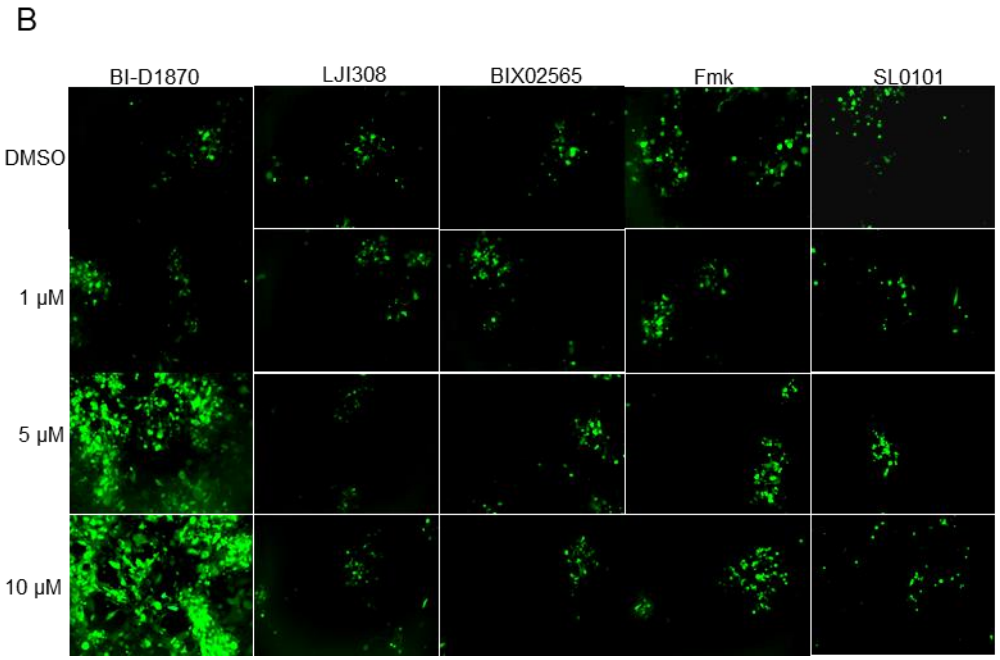
B
BI-D1870
LJI308
BIX02565
Fmk
SL0101
DMSO
1 μM
5 μM
10 μM

Figure 13. The RSK protein is not essential for the increase in infection when cells are treated with BI-D1870. (A) Western blot analysis showing the amount of HSV1 proteins present in increasing amounts of BI-D1870 in human glioblastoma (LN-18), ICP0, and GAPDH, (B) RSK1/2$^{+/+}$, RSK1$^{-/-}$ and RSK2$^{-/-}$ and RSK1/2$^{-/-}$ cells were infected with HSV1-1716-GFP (0.01 MOI) and treated with increasing concentrations (DMSO, 1 μM, 5 μM, 10 μM) of BI-D1870. Fluorescence microscopy imaging was performed 48 hours after infection. (C) Western blot analysis showing phosphorylation in LN-18 cells with RSK$^{-/-}$ of TSC2, RSK1, RSK2 and ERK1/2 protein levels, (D) GFP cluster analysis of RSK1/2$^{+/+}$, RSK1$^{-/-}$, RSK2$^{-/-}$ and RSK1/2$^{-/-}$ cells infected with HSV1-1716 and treated with 10 μM of BI-D1870 in comparison to DMSO.

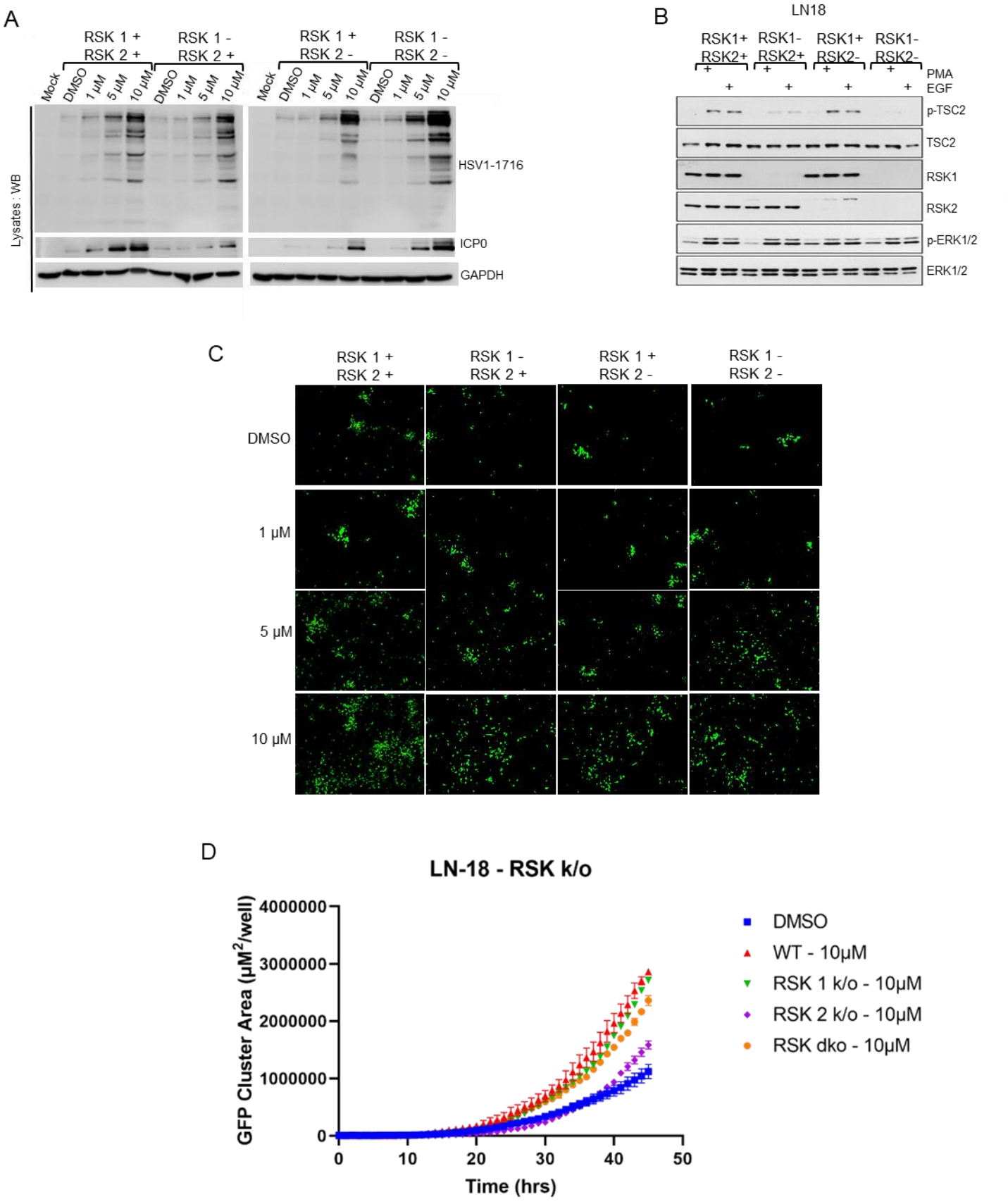
A
RSK 1 +
RSK 2 +
RSK 1 -
RSK 2 +
RSK 1 +
RSK 2 -
RSK 1 -
RSK 2 -
Mock
DMSO
1 μM
5 μM
10 μM
Lysates : WB
HSV1-1716
ICP0
GAPDH
B
LN18
RSK1+ RSK2+
RSK1- RSK2+
RSK1+ RSK2-
RSK1- RSK2-
PMA
EGF
p-TSC2
TSC2
RSK1
RSK2
p-ERK1/2
ERK1/2
C
RSK 1 +
RSK 2 +
RSK 1 -
RSK 2 +
RSK 1 +
RSK 2 -
RSK 1 -
RSK 2 -
DMSO
1 μM
5 μM
10 μM
D
LN-18 - RSK k/o
GFP Cluster Area (μM²/well)
4000000
3000000
2000000
1000000
0
0
10
20
30
40
50
Time (hrs)
DMSO
WT - 10μM
RSK 1 k/o - 10μM
RSK 2 k/o - 10μM
RSK dko - 10μM

Figure 14. BI-D1870 has many specific off target effects. (A) Venn diagram and table comparison of known off targets of RSK inhibitors BI-D1870, LJI308, LJH685, (B) table of off target proteins specific to BI-D1870 in comparison to RSK inhibitors LJI308, LJH685, BIX02565, Fmk, and SL0101.

A

Inhibitors	total	Kinases
BI-D1870 LJ1308 LJH685	12	IKK-beta PRKCE CSNK1D TIE2 MKNK2 AXL CSF1R ROCK2 TYK2(JH1-domain catalytic) RET PIK3CG FLT3
LJ1308 LJH685	3	PKAC-alpha BRAF(V600E) MKNK1
BI-D1870 LJH685	8	AURKB p38-beta JNK1 PDGFRB PLK4 MNK2 AEL1(T316I)-phosphorylated ALK
BI-D1870 LJ1308	9	VEGFR2 LOK JAK2(JH1-domain catalytic) PIK3C2B BMPR2 PAK2 JNK3 DYRK1B TRKA
LJH685	3	ACVR1B TSSK1B YANK3
LJ1308	19	DAPK2 ERBB4 IRAK1 HIPK3 DYRK1A MAP3K3 CSNK1E HIPK2 BRAF DAPK1 HIPK4 HIPK1 PIP5K2C IRAK3 CLK3 TRKC MEK4 PIK3CA DAPK3
BI-D1870 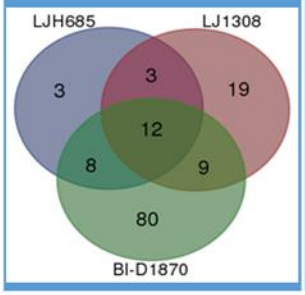	80	FAK PIM3 MEK2 p38-gamma MELK CK1 PRK2 KIT(V559D,T670I) PAK1 M-K1 MEKK1 NET CSK CHK1 INSR PDK1 CMGC ERK2 TKL SmMLCK IGF1R JNK2 GSK3-alpha MST2 PHK CHK2 CCR6 SRPK3 IRAK4 GSK3-beta PRAK EF2K MST1 SRPK1 CDK9 PLK2 PAK4 ABL1(T315I)-phosphorylated MSK1 p38-delta PKD1 MSK2 KIT M-K3 ULK2 NEK2a CSNK1G2 PKA ABL1(E255K)-phosphoyrlated SLK CDK7 PDGFRA PDPK1 SNARK ERK8 PIM2 MARK3 MNK1 LKB1 PLK3 CDK3 PCTK1 PLK1 AMPK AURKA MLK1 MAP3K4 TGFBR1 SRC CDK2 PIM1 MKK1 CaMK-1 p38-alpha NEK6 CK2 NEK7 JAK3(JH1-domain catalytic) EGFR(L858R) MEK1

B

Table 1. List of unique off target kinases specific to BI-D1870

Ser/Thr Kinases		Tyrosine Kinases	Other Kinases	
AMPK	NEK2a	ABL1	CaMK1	p38-δ
CDK2	NEK6	CSK	CCR6	p38-γ
CHK1	NEK7	IGF1R	CDK3	PDPK1
CHK2	PAK4	INSR	CDK9	PHKA2
CK2	PCTK1	JAK3	CK1	PRKACA
CSNK2A1	PIM2	KIT	CSNK1G2	PKD1
GSK3-a	PKA2	MET	ERK2	PRAK
LKB1	PLK1	MST1	ERK8	PRK1
MAPK12	PLK2	TLK	FAK	smMLCK
MAPK13	PLK3		MAP3K4	SNARK
MEKK1	SLK		MARK3	SRPK1
MST2			MLK1	SRPK3
			MKK1	ULK2

Figure 15. SLK is an off target of BI-D1870. (A) HER2+ cell line wild type cells (SLK) and with SLK Δ3-6 ($SLK^{fl/fl}$) deletion were infected with 0.01 MOI VSVΔ51-RFP and treated with increasing concentrations of BI-D1870 (DMSO, 1 μM, 5 μM, 10 μM). (B) SLK and $SLK^{fl/fl}$ cells were infected with 0.1 MOI HSV1-1716-GFP and treated with increasing concentrations of BI-D1870 (DMSO, 1 μM, 5 μM, 10 μM). Phase contrast and fluorescence microscopy imaging was performed 48 hours after infection.

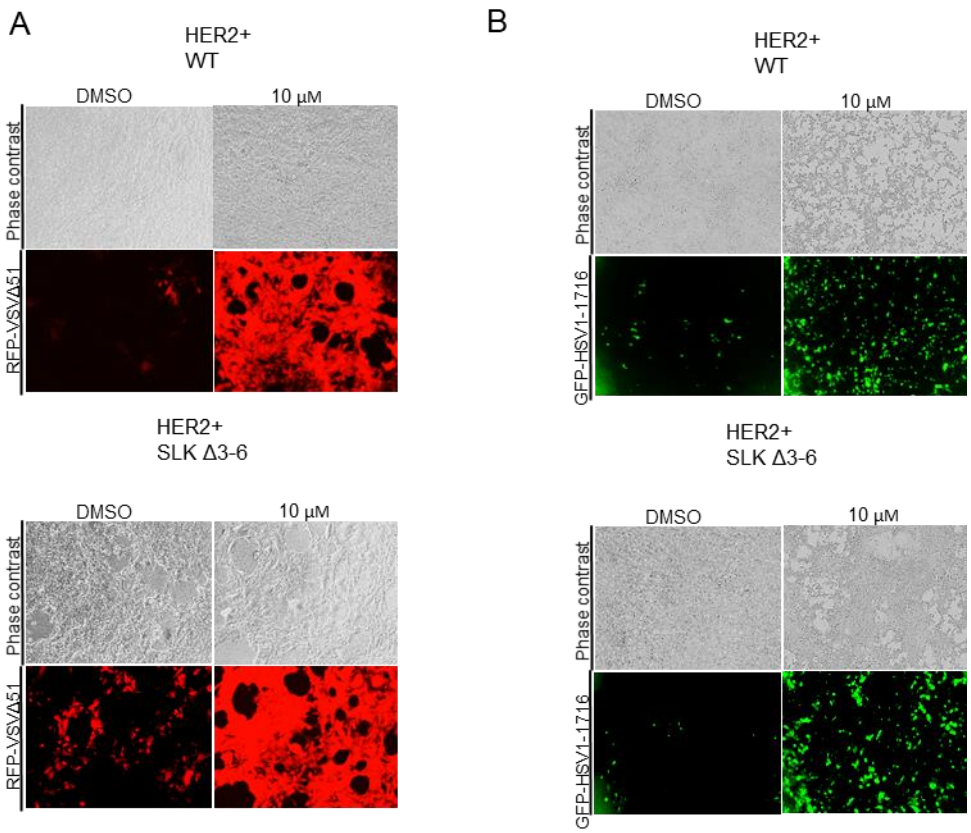
A
HER2+
WT
DMSO
10 μM
Phase contrast
RFP-VSVΔ51
HER2+
SLK Δ3-6
DMSO
10 μM
Phase contrast
RFP-VSVΔ51
B
HER2+
WT
DMSO
10 μM
Phase contrast
GFP-HSV1-1716
HER2+
SLK Δ3-6
DMSO
10 μM
Phase contrast
GFP-HSV1-1716

3.3 Aim 2: The development of structural analogs based on BI-D1870

3.3.1 The synthesis of BI-D1870 and synthetic route to produce analogs

BI-D1870 was synthesized by Matthias Hoffman et al at Boehringer Ingelheim Pharma Gmbh & Co. Kg as part of patent WO2003020722A1, the invention of novel dihdyropteridinones for the use as medicine. Pteridinone derivatives, like BI-D1870, have antiproliferative activity and can be used for the treatment of tumours and viral infections. The biological properties of the compounds created in the patent were found to be acceptable to be used as treatments for viral infections, inflammation and autoimmune diseases, bacterial, fungal and/or parasitic infections, cardiovascular diseases and cancer. These compounds inhibit proliferation of cells in the G2/M phase of the cell cycle, leading to programmed cell death.[109]

The original synthesis of BI-D1870, as part of the patent, included a step in which benzyl amine was used to add on to 2-bromopropionate leading to compound 23 which would undergo a reduction to remove the benzyl group to make compound 24. For a more efficient synthesis an addition reaction of the amine with 2-bromopropionate was substituted for this primary step. The final step was also modified by Dr. Kim Apperley as the original synthesis resulted in small amounts of starting material being converted into product. To change compound 27 into product, concentrated hydrochloric acid was added to compound 27 and an aniline in suspension with water and 1,4-dioxane, heated to 100°C and stirred for 48 hours (**Figure 16 A**). This modification to the final step enabled analogs to be synthesized using compound 27 and a variety of anilines to probe the function of the phenol group. Other sites on BI-D1870 will be subjected to modifications in order to determine if they are important to mechanism of action, and if any changes will improve the function of the drug upon viral infection (**Figure 16 B**).

Figure 16. The synthesis of BI-D1870. (A) The synthetic pathway modified from patent[109] to produce BI-D1870 and its analogs, (B) important functional groups on BI-D1870 with the ability to be modified.

A

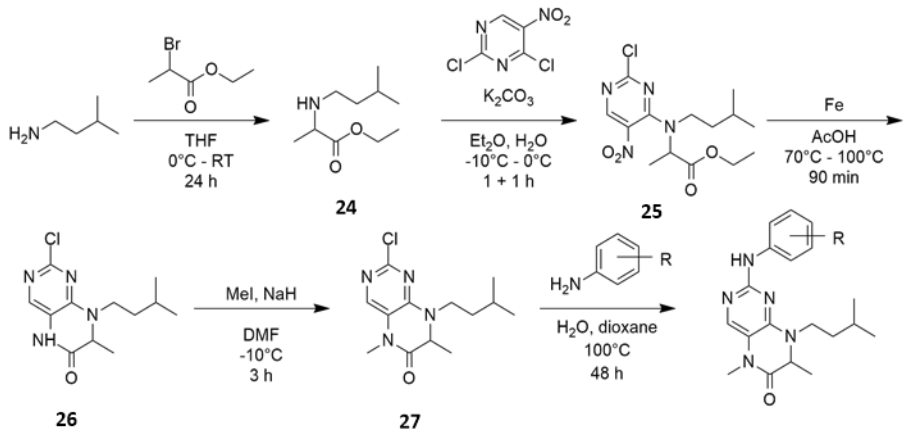
Br
THF
0°C - RT
24 h
24
K_2CO_3
Et_2O, H_2O
-10°C - 0°C
1 + 1 h
25
Fe
AcOH
70°C - 100°C
90 min
MeI, NaH
DMF
-10°C
3 h
26
27
H_2O, dioxane
100°C
48 h

B

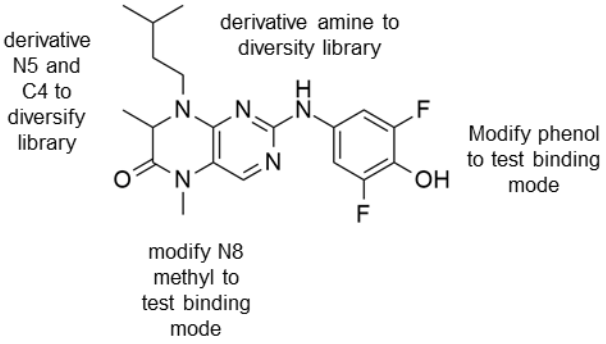
derivative N5 and C4 to diversify library
derivative amine to diversity library
Modify phenol to test binding mode
modify N8 methyl to test binding mode

3.3.2 The binding of BI-D1870 in proteins gives indications of areas of modification

The crystal structure and binding mode of RSK has been reported[126,127] with the phenol group buried deep within the binding pocket (**Figure 17 A**). The exposed portion of BI-D1870 has limited areas in which to modify the structure to improve RSK binding. When BI-D1870 is bound to JAK2 (a non-receptor tyrosine kinase that signals through the JAK/STAT pathway),[127] BI-D1870 is flipped around in comparison to when it is bound to RSK (**Figure 17 B**). In JAK2 the phenol group is exposed, with the rest of the molecule inside the pocket. It appears to not be bound quite as tightly as in RSK, allowing the structure of BI-D1870 to be modified more optimally.

3.3.3 Series I and II analogs are designed based on binding modes

In collaboration with the Boddy lab at the University of Ottawa, Series I and II analogs were designed (**Figure 18 B, C**). BI-D1870 (**Figure 18 A**), is modified at a few different points – in Series I (**Figure 18 B**), the phenol group is altered, and in Series II (**Figure 18 C**), the isopentyl chain and both methyl groups are modified. Series I analogs were made by Dr. Kim Apperley and split into two sections: Series I.I - KA-001, KA-004, KA-005 and KA-006, with KA-007 as the in-house made BI-D1870; and Series I.II - KA-013, KA-019, KA-020, KA-021 and KA-022.

Figure 17. Crystal structures of BI-D1870 in the binding pocket modified from Jain et al and Puleo et al.[126,127] (A) BI-D1870 bound in the pocket of RSK with the phenol group buried deep inside the pocket, (B) BI-D1870 bound in the pocket of JAK2 with the phenol group exposed.

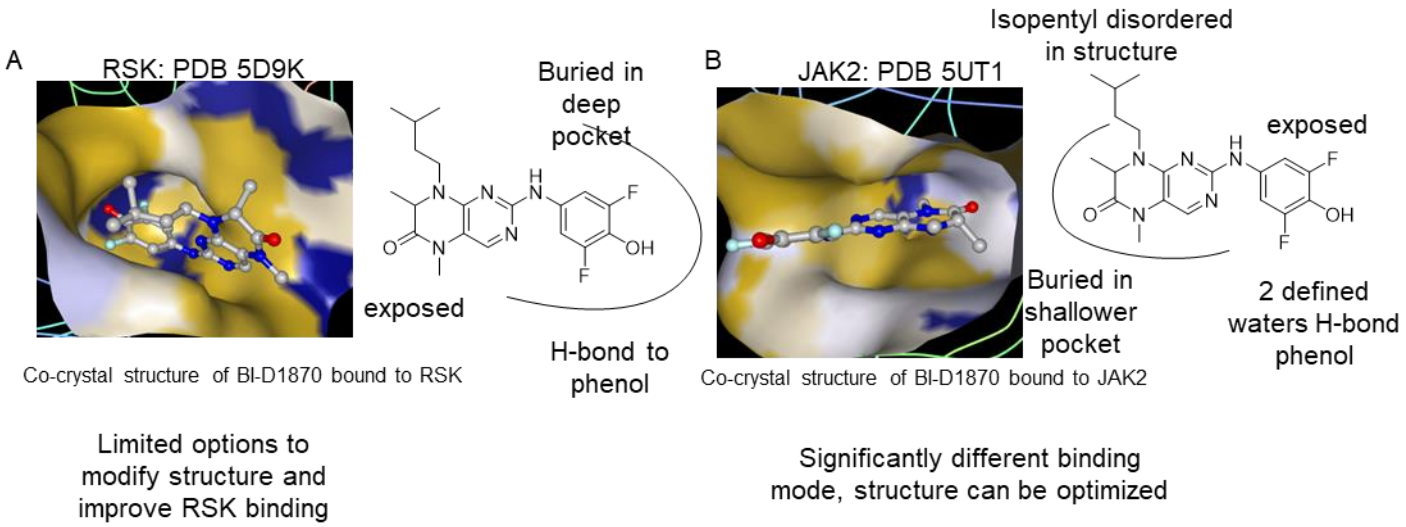
A
RSK: PDB 5D9K
Buried in deep pocket
exposed
H-bond to phenol
Co-crystal structure of BI-D1870 bound to RSK
Limited options to modify structure and improve RSK binding
B
JAK2: PDB 5UT1
Isopentyl disordered in structure
exposed
Buried in shallower pocket
2 defined waters H-bond phenol
Co-crystal structure of BI-D1870 bound to JAK2
Significantly different binding mode, structure can be optimized

Figure 18. **Series I and II analogs derived from BI-D1870**. (A) Structure of BI-D1870, (B) structures of Series I analogs – KA-001, KA-004, KA-005, KA-006, KA-007, KA-013, KA-019, KA-020, KA-021, KA-022. (C) Structures of Series II analogs

A

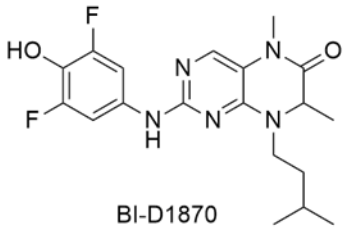

BI-D1870

B

Series I

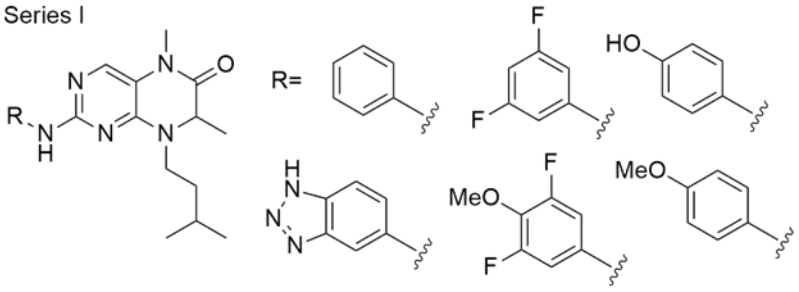

C

Series II

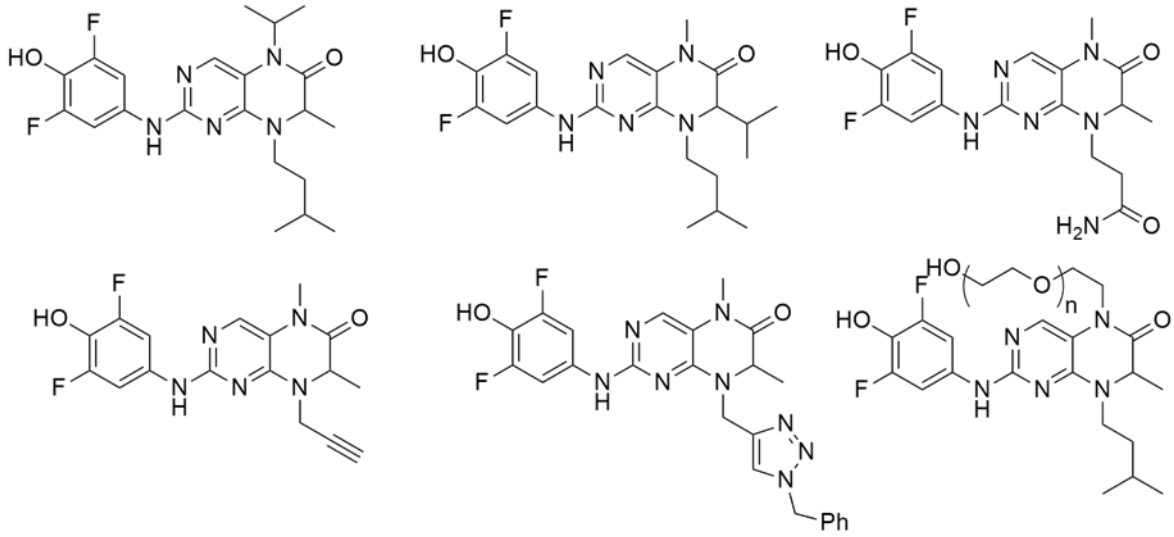

3.3.4 Series I.I analogs do no increase HSV1-1716 infection

Series I analogs were received in two groups, and so were tested separately. Series I.I analogs include KA-001, KA-004, KA-005, KA-006 and KA-007. Following the original experiments with BI-D1870 and HSV1-1716, Series I.I analogs were tested on U343 cells infected with 0.1 MOI HSV1-1716-GFP for 48 hours with increasing concentrations (1 μM, 5 μM, 10 μM) and compared to pharmaceutical made BI-D1870 (**Figure 19**). KA-001 shows a small increase in viral proteins on the western blot (**Figure 19 A**), but GFP cluster area analysis by the Incucyte of the infection over time (**Figure 19 B**) and GFP images (**Figure 19 C**) show an increase in infection similar to that of DMSO. KA-004 does not show any increase in infection on the western blot or the GFP images. The GFP cluster area analysis shows an increase over time that is even less than cells treated with DMSO. KA-005 and KA-006 show a small increase in the western blot, GFP cluster area analysis, and GFP images, however they are not comparable to the increase in infection by BI-D1870. KA-007 increases the infection HSV1-1716 in a similar manner to BI-D1870. Western immunoblotting indicates that HSV1 protein levels are similar between both BI-D1870 and KA-007, there is a comparable GFP cluster area over time, and fluorescence images show a similar increase in viral infection. These results show that none of the series I.I analogs, other than KA-007 (in-house BI-D1870), can increase HSV1-1716 infection.

Figure 19. The effect of Series I.I analogs on HSV1-1716 infection. (A) Western blot analyses of HSV1 proteins for Series I.I analogs (KA-001, KA-004, KA-005, KA-006, KA-007) compared to BI-D1870 with ICP0 as a control for infection, and GAPDH as a loading control, (B) graphical representation of GFP cluster area (μM^2/well over time) of each analog at 10 μM. Series I.I analogs compared to DMSO and BI-D1870 (10 μM). (C) Human glioblastoma cells (U343) were infected with HSV1-1716-GFP (0.1 MOI) and treated with varying concentrations (DMSO, 1μM, 5μM, 10μM) of series I.I analogs (KA-001, KA-004, KA-005, KA-006, KA-007) and BI-D1870. Fluorescence microscopy imaging was performed 48 hours after infection

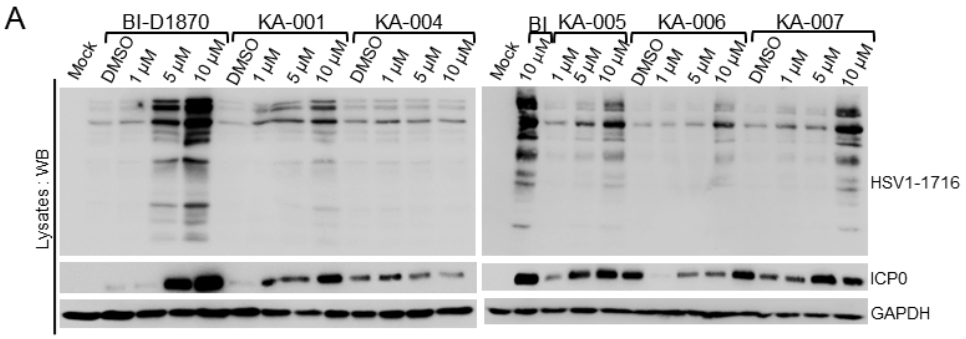
A
BI-D1870
KA-001
KA-004
BI
KA-005
KA-006
KA-007
Mock
DMSO
1 μM
5 μM
10 μM
Lysates : WB
HSV1-1716
ICP0
GAPDH

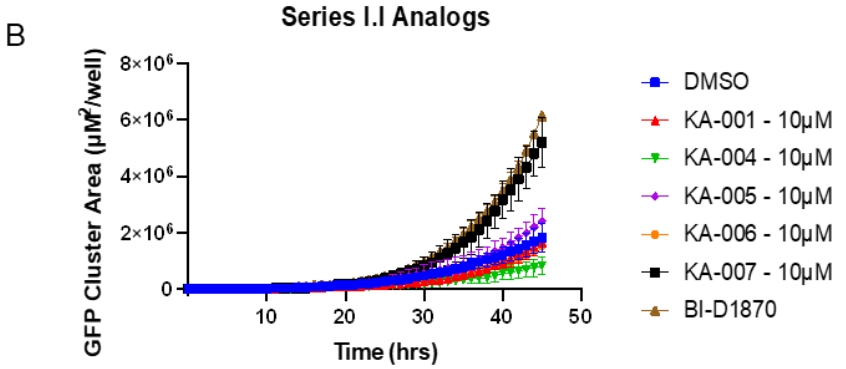
B
Series I.I Analogs
GFP Cluster Area (μM²/well)
8×10⁶
6×10⁶
4×10⁶
2×10⁶
0
10
20
30
40
50
Time (hrs)
DMSO
KA-001 - 10μM
KA-004 - 10μM
KA-005 - 10μM
KA-006 - 10μM
KA-007 - 10μM
BI-D1870

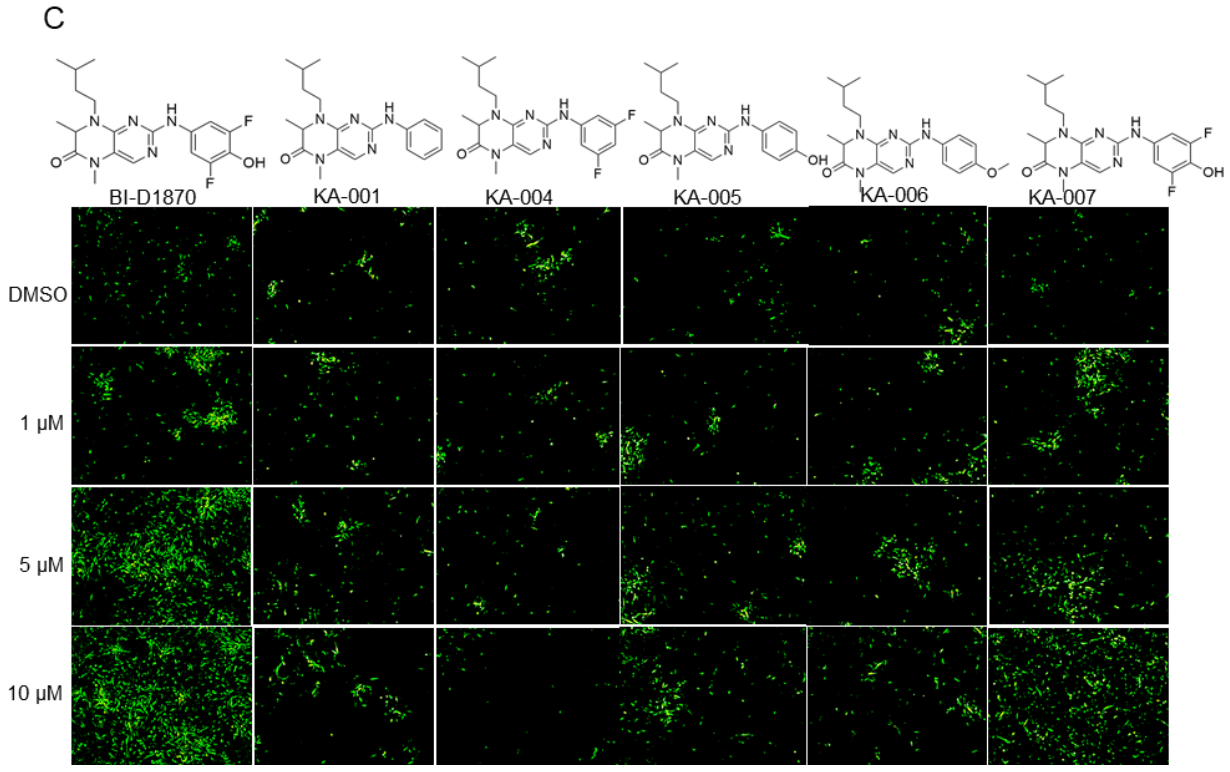
C
BI-D1870
KA-001
KA-004
KA-005
KA-006
KA-007
DMSO
1 μM
5 μM
10 μM

3.3.5 KA-019 from Series I.II exerts a greater effect upon HSV1 infection than BI-D1870

The second group of Series I analogs include KA-013, KA-019, KA-020, KA-021, and KA-022. These analogs were tested in the same manner as those in series I.I. U343 cells were infected with HSV1-1716-GFP at 0.1 MOI and treated with increasing concentrations of Series I.II analogs and BI-D1870 for 48 hours (**Figure 20**). KA-013, KA-020, KA-021 and KA-022 show no increase in viral infection as demonstrated in the western blot, GFP cluster area analysis and GFP images. KA-019, on the other hand, shows an even greater increase of viral infection than BI-D1870 as is seen in the increased amount of viral proteins (**Figure 20 A**), GFP cluster area analysis (**Figure 20 B**) and GFP fluorescence (**Figure 20 C**). This analog has a triazole group in place of the phenol **(Figure 21 A)**. In direct comparison to BI-D1870, KA-019 has a significant increase in viral infection compared to the DMSO control with a p-value of <0.01, and a p-value of <0.05 when compared to BI-D1870 calculated with an unpaired t-test through GraphPad (**Figure 21 B**). The fluorescence images of BI-D1870 and KA-019 show a similar increase at concentrations of 1 μM and 5 μM, but at a concentration of 10 μM, KA-019 shows a greater area of viral infection. These results show that out of all the Series I analogs, KA-019 was found to increase viral infection of HSV1-1716 to a greater extent than BI-D1870.

Figure 20. **The effect of Series I.II analogs on HSV1-1716 infection**. (A) Western blot analyses of HSV1 proteins for Series I.II analogs (KA-013, KA-019, KA-020, KA-021, KA-022) compared to BI-D1870 with ICP0 as a control for infection, and GAPDH as a loading control, (B) graphical representation of GFP cluster area (μM^2/well over time) of each analog at 10 μM. Series I.II analogs compared to DMSO and BI-D1870 (10 μM). (C) Human glioblastoma cells (U343) were infected with HSV1-1716-GFP (0.1 MOI) and treated with varying concentrations (DMSO, 1μM, 5μM, 10μM) of series I.II analogs (KA-013, KA-019, KA-020, KA-021, KA-022) and BI-D1870. Fluorescence microscopy imaging was performed 48 hours after infection.

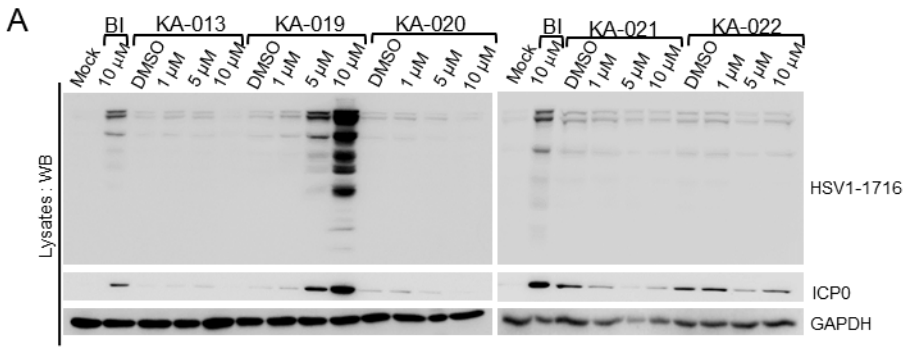
A
BI
KA-013
KA-019
KA-020
BI
KA-021
KA-022
Mock
10 μM
DMSO
1 μM
5 μM
10 μM
Lysates : WB
HSV1-1716
ICP0
GAPDH

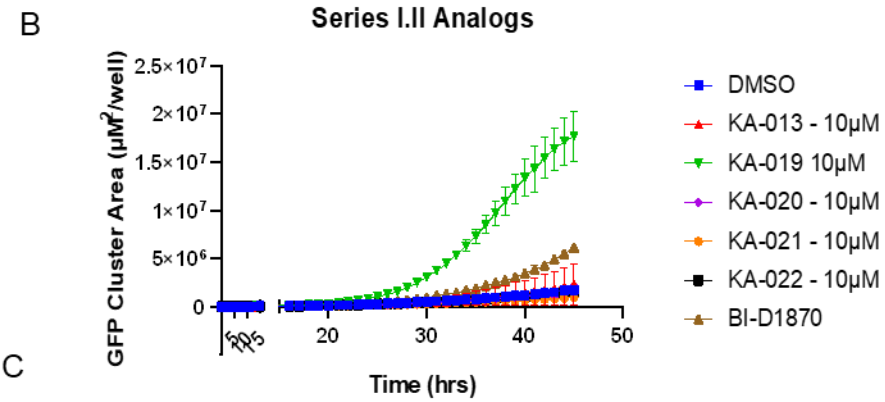
B
Series I.II Analogs
GFP Cluster Area (μM²/well)
2.5×10⁷
2×10⁷
1.5×10⁷
1×10⁷
5×10⁶
0
20
30
40
50
Time (hrs)
DMSO
KA-013 - 10μM
KA-019 10μM
KA-020 - 10μM
KA-021 - 10μM
KA-022 - 10μM
BI-D1870

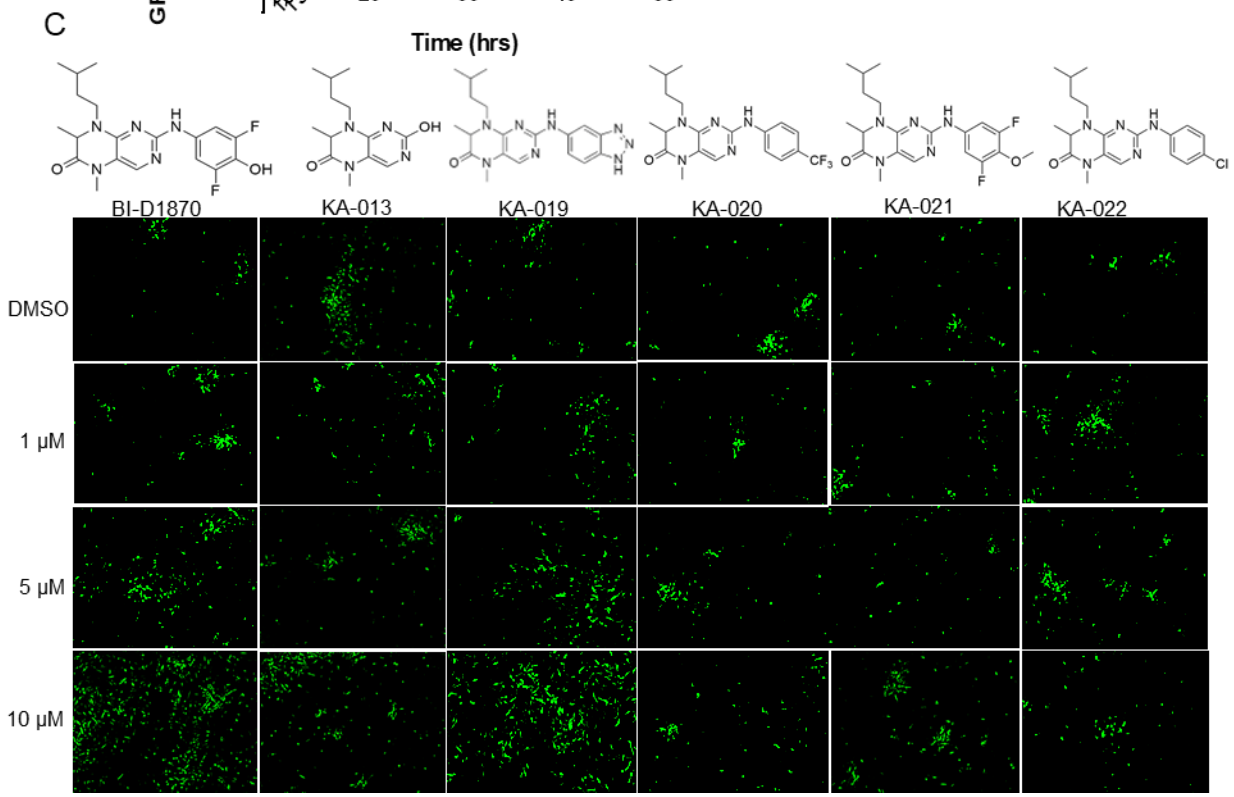
C
BI-D1870
KA-013
KA-019
KA-020
KA-021
KA-022
DMSO
1 μM
5 μM
10 μM

Figure 21. The effect of BI-D1870 vs KA-019. (A, B) U343 cells were infected with HSV1-1716-GFP at 0.1 MOI and treated with increasing concentrations (DMSO, 1 μM, 5 μM, 10 μM) of BI-D1870 and KA-019. p-values were calculated with an unpaired t-test, where ** < 0.01, * <0.05. Fluorescence microscopy images were taken 48 hours after infection.

A

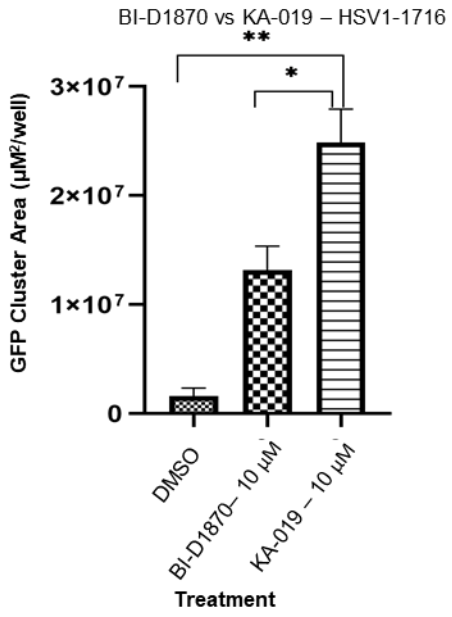
BI-D1870 vs KA-019 – HSV1-1716
**
*
3×10⁷
2×10⁷
1×10⁷
0
GFP Cluster Area (µM²/well)
DMSO
BI-D1870– 10 µM
KA-019 – 10 µM
Treatment

B

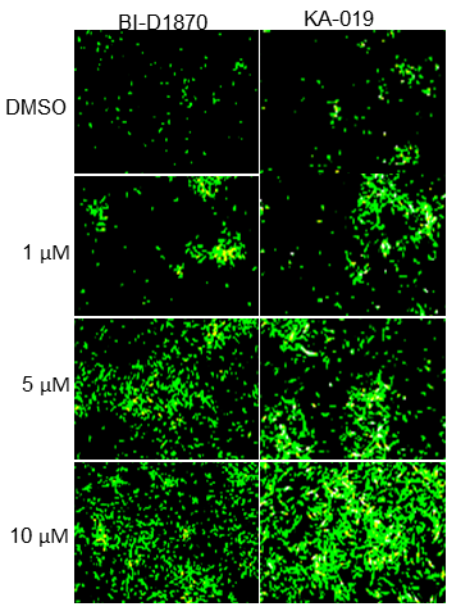
BI-D1870
KA-019
DMSO
1 µM
5 µM
10 µM

3.3.6 KA-019 represses vaccinia virus infection in a similar fashion to BI-D1870

BI-D1870 was tested with several different viruses – HSV1-1716, VSVΔ51 and Vaccinia. All analogs have been tested with HSV1-1716 and VSVΔ51 (**Supplemental Figure 2 and 3**), and KA-019 was found to increase the infection of both of these viruses. To see if KA-019 would continue to act in the same manner as BI-D1870, it was tested in combination with vaccinia virus.

4T1 cells were infected with VACV-GFP at 0.1 MOI and treated with increasing concentrations of both BI-D1870 and KA-019 (**Figure 22 A-C**) for 48 hours. KA-019 shows a repression of the infection of vaccinia, just like BI-D1870. GFP production is seen to decrease in the entire well of the plate (**Figure 22 A**) for both cells treated with BI-D1870 and KA-019. To confirm that this repression seen by KA-019 is consistent with BI-D1870, further testing with Myxoma and Adenovirus should be done. GFP cluster analysis was performed by the Incucyte, and the data further analyzed by an unpaired t-test performed with GraphPad. A significant p-value of <0.0001 was calculated between the control (DMSO) and 5 μM and 10 μM of both compounds. These results show that KA-019 has a similar mechanism of action to BI-D1870 as it can increase HSV1-1716 and VSVΔ51 infection, but repress vaccinia.

Figure 22. The effect of BI-D1870 and KA-019 on vaccinia virus (VACV). (A - C) 4T1 cells were infected with VACV-GFP at 0.1 MOI and treated with increasing concentrations of BI-D1870 and KA-019 (DMSO, 1 μM, 5 μM, 10 μM). p-values were calculated with an unpaired t-test, where **** < 0.0001. Fluorescence microscopy images were taken 48 hours after infection.

A

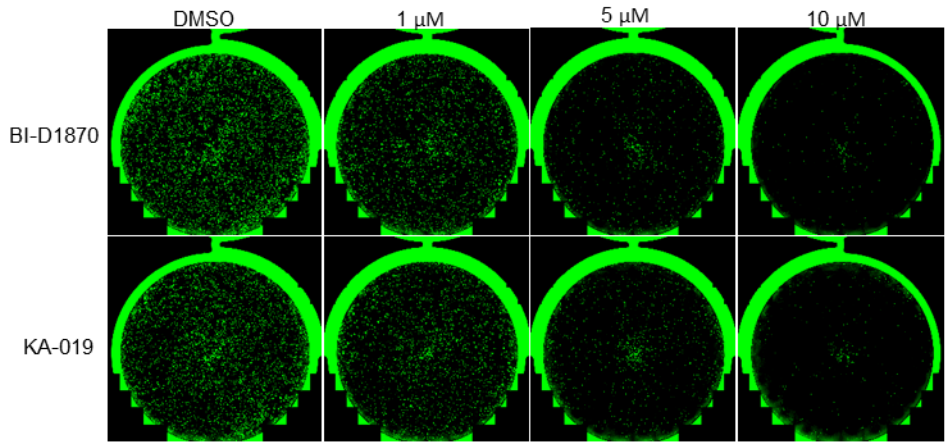
DMSO
1 µM
5 µM
10 µM
BI-D1870
KA-019

B

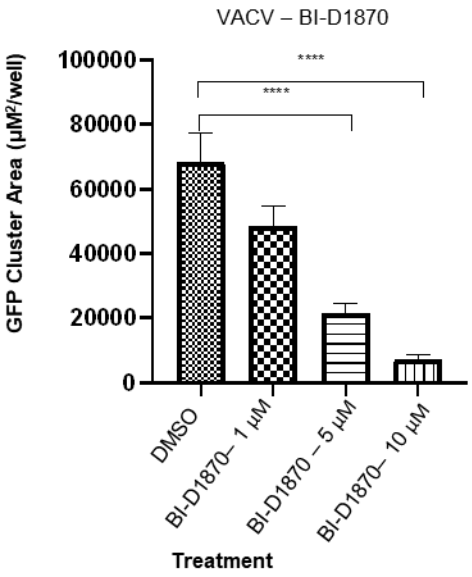
VACV – BI-D1870
GFP Cluster Area (µM²/well)
100000
80000
60000
40000
20000
0
****
****
DMSO
BI-D1870– 1 µM
BI-D1870 – 5 µM
BI-D1870– 10 µM
Treatment

C

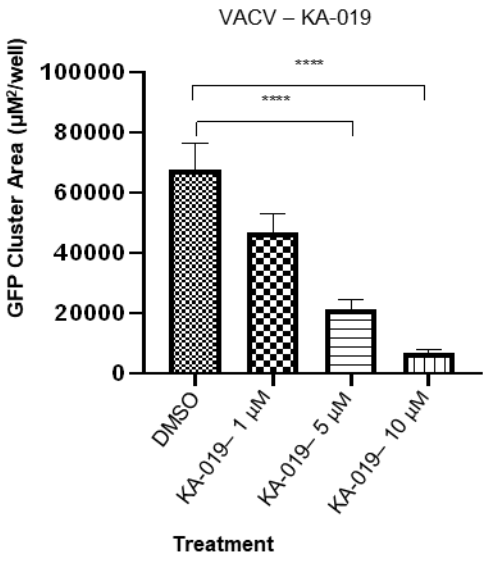
VACV – KA-019
GFP Cluster Area (µM²/well)
100000
80000
60000
40000
20000
0
****
****
DMSO
KA-019– 1 µM
KA-019– 5 µM
KA-019– 10 µM
Treatment

Chapter 4: Discussion

Oncolytic viral therapy is a new avenue of cancer treatment undergoing extensive research. OVs can selectively kill tumour cells and produce a long lasting anti-tumour immune response.[17] T-VEC, an OV approved by the FDA, is currently being used in the clinic and has shown to have a 16.3% response rate.[23] A recently published Phase III trial for the treatment of stage IIIB/C-IV melanoma with T-VEC reported a complete response rate of 61.5 %, and overall response rate of 88.5% in 26 patients.[128] Louie et al reported a complete response rate of 39% out of 121 patients.[129] While these response rates are encouraging, there is still room for improvement. In order to do this, OVs must be used in conjunction with another therapy to get a complete response. Many researchers are focusing on small molecule inhibitors such as sunitinib, ipiliminumab, as well as chemotherapeutics.[17,82] The focus of our OV research is to ensure that there is a safe and viable option to help increase the infectivity of the virus.

In order to ensure the best outcome and avoid serious adverse events, it is essential to understand how these drug works in combination with the virus. Chemotherapeutics have cytotoxic properties that inhibit DNA replication, the cell cycle or disrupt microtubules, which when combined with OVs can produce more oncolysis. In addition to this, some chemotherapies have strong immunosuppressive effects which can impact the infection of OVs and the anti-tumour response.[12] Other small molecules, like HDAC inhibitors, mTOR inhibitors, and JAK inhibitors can also dampen the anti-viral response, allowing for an increase in viral infection.[67,130,131] BI-D1870, a RSK inhibitor, was found to increase viral infection through the previous work of members of the Alain lab. It was originally found that rpS6, a downstream target of mTOR and RSK, remained phosphorylated in the presence of mTOR inhibitors in cells that had been also infected with HSV1-1716. Therefore, because RSK also phosphorylates rpS6,

BI-D1870, a RSK inhibitor, was though to prevent this from happening, and would stop the increase in viral infection. However, when HSV1-1716 infected cells were treated with BI-D1870, the results were opposite: the infection of HSV1-1716 increased.

I hypothesized that BI-D1870 could increase the infection of both HSV1-1716 and VSVΔ51. My results show that my hypothesis is correct and human glioblastoma cells (U343), human renal cell adenocarcinoma cells (786-0), murine breast carcinoma cells (EMT-6 and 4T1) all showed an increase in HSV1-1716 and VSVΔ51 infection when treated with BI-D1870. Normal human fibroblasts (GM38) and murine mammary epithelial cells (NMuMG), did not show an increase in the infection of HSV1-1716 when treated with BI-D1870. However, the infection of VSVΔ51 showed an increase in normal cells when treated with BI-D1870. But when NMuMG cells are compared to NT2196 cells infected with VSVΔ51, this increase in infection is negligible. Additional experiments must be done to verify that HSV1-1716 and VSVΔ51 do not have a significant increase in viral infection when treated with BI-D1870 in normal cells.

The next set of experiments performed were to assess if nanoparticles (NPs) could be used to delivery BI-D1870 to cancer cells. Nanoparticles can be used as a delivery system for drugs to the tumour microenvironment. Several different kinds of NP-based drug delivery systems have been reported to be successful, and can improve therapeutic effectiveness.[132,133] To determine whether or not nanoparticles could improve the delivery of BI-D1870, Dr. Suresh Gadde at the Department of Biochemistry, Microbiology and Immunology at the University of Ottawa synthesized PLGA-PEG nanoparticles that were either empty or encapsulated BI-D1870. These NPs were tested in combination with HSV1-1716 and showed an increase in infection similar to that of the ‘naked’ BI-D1870. For this particular experiment, GFP images were taken with the Evos microscope, and it would be beneficial to repeat this experiment using the Incucyte

in order to analyze the GFP cluster area and determine if there is any change in the amount of infection between the encapsulated and 'naked' BI-D1870. Nanoparticles may improve delivery *in vivo* as it will protect the drug from being metabolized and can also be used to encapsulate the oncolytic virus to prevent targeting by neutralizing antibodies.[134] Preliminary *in vivo* studies show that VSVΔ51 in combination with BI-D1870 enhanced viral infection in the tumour, as well as other parts of the mouse. Additional *in vivo* studies must include experiments to assess specificity, as well as further testing into dosing and utilizing nanoparticles for delivery.

While BI-D1870 is the most used RSK inhibitor in the literature, there are several other inhibitors that are more selective to RSK.[112] LJI308 inhibits RSK1, 2, 3 and 4 with IC_{50} of 6 nM, 4 nM, and 13 nM, and nearly 100% of target binding at 10 μM. While BI-D1870 can bind RSK2 to 99.9%, it can also bind to several other kinases (such as PLK1 and PLK3) to a similar extent.[120] BIX-02565 was found to inhibit RSK2 with IC_{50} of 1 nM, and was reported to inhibit 5 other kinases with >80% inhibition at 3 μM.[108] Fmk inhibits the C-terminal domain in contrast to the other RSK inhibitors which inhibit the N-terminal domain. Fmk inhibits RSK2 with IC_{50} of 15 nM,[119] and cannot inhibit RSK3.[112] SL0101 has been found to inhibit the N-terminal domain and is a more selective RSK inhibitor than BI-D1870, only inhibiting a few other kinases (such as Aurora B and PIM3). However, SL0101 is not as potent of an inhibitor as the others with an IC_{50} of 89 nM.[95] All 4 of these RSK inhibitors were tested in combination with HSV1 and found to have no effect upon infection. However, SL0101 appears to induce cell death of U343 cells even at 10 μM with the western blot showing less GAPDH proteins compared DMSO treated cells. Despite this, these results show that BI-D1870 is the only RSK inhibitor that increases viral

infection of HSV1-1716, indicating that the inhibition of RSK does not play a main role in the mechanism of action.

To complete these findings, LN-18, a glioma cell line, was used as RSK1 and RSK2 are the two main isoforms of RSK prevalent in this cell line. RSK1 and 2 were knocked out using CRISPR-Cas9.[112] When tested, these knockout cell lines all showed an increase in viral infection when treated with BI-D1870, including the wild type cells. However, while the wild type, RSK1 knockout (k/o) cells and the double knockout (dko) cells (RSK1 and RSK2) showed similar levels of GFP cluster area as analyzed by the Incucyte, the RSK 2 k/o cells did not. In fact, the RSK2 k/o cells showed an increase in infection closer to that of the DMSO treated cells. The western blot indicated that the WT, RSK1, RSK2 and dko cells all had similar increases in viral proteins. The difference could be from blotting technique or exposure times. Additional experiments should be performed to assess the extent of the increase of viral infection in RSK2 k/o cells. These results cannot rule out RSK2 as a player in the mechanism of action. However, with the increase in infection of HSV1-1716 in combination with BI-D1870 in LN-18 WT, RSK1 and the dko cells, this suggests that the inhibition of RSK is not the main way in which BI-D1870 increases viral infection.

It is known that BI-D1870 has several off targets,[94] and considering that RSK inhibition may not be the main mechanism of action, the other targets may be the answer. In order to find which off targets were specific to BI-D1870, a literature search was performed with search terms 'RSK inhibitor.' The off targets of each RSK inhibitor was recorded and then compared using a Venn diagram. The results of this search provided a list of suggested off target kinases specific to BI-D1870. One of these kinases was SLK, a kinase the Sabourin lab works with and have created an SLKΔ3-6 knock out cell line, impairing its function.[121] Upon infection with HSV1-1716-GFP,

VSVΔ51-RFP and treatment with BI-D1870, these WT and SLKΔ3-6 cell lines showed a similar increase in infection. Further research into the off targets of BI-D1870 revealed that SLK is not a specific off target of BI-D1870 and is also inhibited by RSK inhibitor BIX-02565. In order to find whether one of these off targets is behind the mechanism of action, a high-throughput screen as described in Diallo et al, may be of assistance. Inhibitors of each of the off target kinases would be tested on cells, and infected with VSVΔ51 or a control. Cells would then be incubated with Alamar blue and fluorescence assessed to determine cytotoxicity of each drug in the presence and absence of the virus.[70]

Other small molecules being used in combination with oncolytic viruses work through blocking the anti-viral response. Bridle et al reported that an HDAC inhibitor, MS-275, dampened the immune response and boosted viral infection of VSVΔ51.[137] Other inhibitors, such as JAK2 inhibitor, TG101348, and JAK1/2 inhibitor, ruxolitinib, decreased IFNα,ß-inducible genes, JAK1 and STAT expression, and increase VSVΔ51 expression.[131] It would be prudent to perform some of these same experiments, such as reverse-transcription PCR for IFN responsive genes, immunoblotting for various anti-viral proteins such as JAK1 or STAT,[131] detection of VSV or HSV1 neutralizing antibodies, or a T cell functional assay[137] in order to determine if BI-D1870 works through a similar mechanism.

The second part of my project looked at synthesizing BI-D1870 and analogs in order to improve upon the increase of infection and perhaps obtain some information about mechanism of action through process of elimination on the compound itself. In order to create analogs, I looked at how it fits into the binding pocket of RSK and other kinases. I found that there were two main binding modes, one in which the phenol is buried in the binding pocket, and one in which it is outside the binding pocket. This allowed me to design several different analogs with Dr. Chris

Boddy. All analogs were synthesized by Dr. Kim Apperley. The patented synthesis[109] was improved upon and cut down when we realized that isopentylamine worked just as well, if not better, than benzylamine and yielded the same result in fewer steps. The last step where the scaffold is attached to the difluoro-hydroxyl-amine was modified by Dr. Apperley where it was found that dioxane and HCl at 100°C over a 48 hour reflux provided a small yield of the product. The amine oxidized very quickly and was hard to synthesize. Luckily, Dr. Apperely was able to produce enough of in-house made BI-D1870 (also known as KA-007) to be used.

The first series of analogs looked at the phenol and surrounding fluorines to determine its importance. The first analog (KA-001), with only a benzyl group, does not have anything for hydrogen bonding within the binding pocket, and so should not have any effect upon viral infection. In contrast to the hypothesis, KA-001 appears to exert a small positive effect on viral infection. The western blot shows a slight increase in viral proteins between the cells treated with DMSO and those treated with 10 μM of KA-001, this is correlated with the GFP images which show a small increase in fluorescence. However, the analysis done by the Incucyte of GFP cluster area from the whole well indicates that there is no difference between cells treated with DMSO and KA-001. The second analog (KA-004), has both fluorines present but no hydroxyl group. Fluorines cannot hydrogen bond or form van der Waal forces as their electrons are held tightly in towards the nucleus.[138] If the kinase to which BI-D1870 binds and produces this increase in infection is similar to that of RSK, this analog will probably not bind as well in the binding pocket, and subsequently should not increase infection. The results indicate that KA-004 does not increase the viral infection, however, it appears as though it may repress infection. Western immunoblotting, GFP images and cluster area analysis from the Incucyte indicate that there is less virus present in cells treated with 10 μM of KA-004 than those treated with DMSO.

Additional experiments are needed to confirm that these results are correct. The third analog (KA-005), is the opposite of KA-004, and only has the hydroxyl group and no fluorines. Hydroxyl groups have the ability to form hydrogen bonds within the binding pocket, and so there could be a possible increase in viral infection. My results show that KA-005 does increase viral infection, however not to the same extent as BI-D1870. The western blot, GFP images and analysis have increases above that of the cells treated with DMSO. This indicates that the hydroxyl group is important in the function of BI-D1870 within the binding pocket to create hydrogen bonds. These results show that BI-D1870 is most likely binding to a kinase in a similar binding mode to that of RSK.

KA-006 is a similar analog to KA-005, however the hydroxyl group is methylated. There is still the ability for hydrogen bonding to take place, and so I hypothesized that this analog would also show an increase in viral infection. However, even though GFP images and western blot show this hypothesis to be valid, the GFP cluster area analysis indicates that the increase is the same as the cells treated with DMSO. The hydrogen bond could be weaker than that of KA-005 resulting in a weaker increase in viral infection. KA-013, the first analog in the second set of series I, is the first half of the compound with a hydroxyl group instead of an amine. This analog is smaller than BI-D1870 and has lots of potential for hydrogen bonding in the binding pocket. Despite this, the results of the western blot, GFP images, and GFP cluster analysis are all in accord and show that there is no increase of viral infection.

KA-019 goes back to the original scaffold, however the fluorines and phenol are replaced by a triazole group. In the literature, triazoles are used to mimic phenol groups,[139] and as a triazole can form many hydrogen bonds, KA-019 was hypothesized to increase viral infection. The results clearly show that KA-019 has a greater effect upon viral infection than BI-D1870.

This analog, with the addition of the triazole group fulfills the aim of the second half of my project – to synthesize an analog that performs better than BI-D1870 in increasing viral infection. When cells are infected with HSV1-1716 or VSVΔ51 and treated with 10 μM KA-019, there is a greater increase in viral infection in comparison to BI-D1870. When analyzed through an unpaired t test with GraphPad, the result is significant with a p value of 0.0001. The same repression of vaccinia virus is seen with KA-019, indicating that the two compounds have the same or similar mechanisms of action. Further work into mechanism of action of BI-D1870 and KA-019 must be completed.

The next analog to be synthesized was KA-020, which has a trifluoromethyl group in the same position as the phenol. This is a bulky group with no place for hydrogen bonds to form, leading to weak or no binding. KA-020 did not have any impact upon the viral infection of either HSV1-1716 or VSVΔ51. KA-021, a compound very similar to KA-006 with the methylated hydroxyl group, but with the presence of fluorines. While KA-006 showed a very slight increase in infection, KA-021 shows no increase or decrease in infection. The methyl group on KA-006 could rotate around within the binding pocket allowing for hydrogen bonds to occur, with the addition of the fluorines in KA-021, there is no room for this to happen. Therefore, KA-021 does not bind or has very weak binding, resulting in no effect on viral infection. The last analog to be synthesized as part of Series I was KA-022. This compound has a chlorine in the same place as the phenol group of BI-D1870, without any ability to form hydrogen bonds or other dipole forces, it cannot bind as well into the pocket, therefore resulting in less infection as the results show. Overall, my results show that BI-D1870 and new analog KA-019 can increase the viral infection of HSV1-1716 and VSVΔ51 through an unknown mechanism of action.

Conclusion and future directions:

Effective cancer immunotherapy depends on the immune response within the tumour microenvironment. Oncolytic viruses are able to evade the immune system and can be used for therapeutic purposes to induce host anti-tumour immunity by replicating in tumour cells and inducing ICD. The release of antigens and danger factors can promote the innate and adaptive immune response against the virus and the tumour.[140] However, this stimulation of the immune system can also work against the virus, leading to rapid clearance, hindering the efficiency of treatment. New compounds called oncolytic viral sensitizers can enhance the infectivity and efficacy of oncolytic viruses. The results from the first aim of my project found that BI-D1870, a RSK inhibitor, enhances the infection of HSV1-1716 and VSVΔ51 in cancer cells, but not in normal cells. The mechanism of action of this compound is still elusive, however, the results from this project show that the inhibition of RSK is not the main mechanism of action, but RSK2 could play a role. The second aim of my project was to synthesize new analogs based on BI-D1870 to aid in understanding the mechanism of action and to develop a compound that was superior. My results from this aim found an analog that enhanced the viral infection of HSV1-1716 and VSVΔ51 to a greater extent than BI-D1870, and acted in a similar manner when tested with VACV.

Despite the progress that has been made in this project, there are still issues that need to be addressed. VSVΔ51 was found to elicit an increase in infection in normal cells when treated with BI-D1870. Further testing should be done to ensure that this response is minor in comparison to the effect upon cancer cells. Other normal cell lines, human and murine, should also be tested with HSV1-1716 and VSVΔ51 in combination with both BI-D1870 and KA-019. As there are several other oncolytic viruses and combination treatments in clinical trials, these

viruses, such as reovirus and measles virus, should be tested with both BI-D1870 and KA-019 to determine if there is a positive or negative response. The results of these experiments may shed some light upon the mechanism of action. Future experiments looking into the mechanism of action should include further testing of the role of RSK2, as well as the anti-viral response. *In vivo* experiments with BI-D1870 to assess delivery to tumour tissues should be done, as well as the evaluation of pharmaco-kinetics and –dynamics. The use of nanoparticles could be especially useful for delivery of BI-D1870 or KA-019 *in vivo*, increasing the amount of drug present in the tumour, which will assist in a more robust viral infection.

The second aim of this project, namely synthesizing and testing Series II analogs, must be completed. The purpose of these compounds is to determine whether the double ring scaffold can be modified and if this will increase or repress the infection of HSV1-1716 and VSVΔ51. One analog in the second series will have a probe or fluorophore attached. If this analog does not affect the increase in viral infection induced by KA-019, it can be used for click chemistry – a reaction in which specific molecules can be 'pulled down' and located when the probe or fluorophore attaches.[141] Finally, identifying a target kinase will aid in the pursuit of the mechanism of action of BI-D1870 and KA-019.

References

1. Canadian cancer society. Canadian Cancer Society. *2018* Available at: http://www.cancer.ca/en/?region=on. (Accessed: 17th July 2018)

2. Chaurasiya, S., Chen, N. & Warner, S. Oncolytic Virotherapy versus Cancer Stem Cells: A Review of Approaches and Mechanisms. *Cancers (Basel).* **10,** 124 (2018).

3. Hanahan, D. & Weinberg, R. A. The hallmarks of cancer. *Cell* **100,** 57–70 (2000).

4. Hanahan, D. & Weinberg, R. A. Hallmarks of cancer: the next generation. *Cell* **144,** 646–74 (2011).

5. Pavlova, N. N. & Thompson, C. B. The Emerging Hallmarks of Cancer Metabolism. *Cell Metab.* **23,** 27–47 (2016).

6. Kroemer, G. & Pouyssegur, J. Tumor Cell Metabolism: Cancer's Achilles' Heel. *Cancer Cell* **13,** 472–482 (2008).

7. Izuo, M. Medical history: Seishu Hanaoka and his success in breast cancer surger under general anesthesia two hundred years ago. *Breast Cancer* **11,** 319–324 (2004).

8. Connell, P. & Hellman, S. Advances in radiotherapy and implications for the next century: a historical perspective. *Cancer Res.* **69,** 383–392 (2009).

9. Baskar, R., Lee, K. A., Yeo, R. & Yeoh, K.-W. Cancer and radiation therapy: current advances and future directions. *Int. J. Med. Sci.* **9,** 193–9 (2012).

10. Mould, R. F. Priority for radium therapy of benign conditions and cancer. *Curr. Oncol.* **14,** 118–22 (2007).

11. DeVita, V. J. & Chu, E. A history of cancer chemotherapy. *Cancer Res.* **68,** 8643–8653 (2008).

12. Wennier, S. T., Liu, J. & McFadden, G. Bugs and drugs: oncolytic virotherapy in combination with chemotherapy. *Curr. Pharm. Biotechnol.* **13,** 1817–33 (2012).

13. Kalyn, R. Overview of targeted therapies in oncology. *Oncol Pharm Pr.* **13,** 199–205 (2007).

14. Marelli, G., Howells, A., Lemoine, N. R. & Wang, Y. Oncolytic Viral Therapy and the Immune System: A Double-Edged Sword Against Cancer. *Front. Immunol.* **9,** 1–8 (2018).

15. Moore, A. Effects of viruses on tumors. *Annu. Rev. Microbiol.* **8,** 393–410 (1954).

16. Russell, L. & Peng, K. The emerging role of oncolytic virus therapy against cancer. *Chinese Clin. Oncol.* **7,** 16–16 (2018).

17. Lichty, B. D., Breitbach, C. J., Stojdl, D. F. & Bell, J. C. Going viral with cancer immunotherapy. *Nat. Rev. Cancer* **14,** 559–67 (2014).

18. Atherton, M. J. & Lichty, B. D. Evolution of oncolytic viruses: novel strategies for cancer treatment. *Immunotherapy* **5,** 1191–206 (2013).

19. Russel, S., Peng, K. & Bell, J. Oncolytic virotherapy. *Nat. Biotechnol.* **30,** 658–670 (2012).

20. Cattaneo, R., Miest, T., Shashkova, E. V & Barry, M. A. Reprogrammed viruses as cancer therapeutics: targeted, armed and shielded. *Nat. Rev. Microbiol.* **6,** 529–40 (2008).

21. EA Chiocca and SD Rabkin. Oncolytic Viruses and Their Application to Cancer Immunotherapy. *Cancer Immunol. Res.* **2,** 295–300 (2014).

22. Kaur, B., Cripe, T. P. & Chiocca, E. A. ‘Buy one get one free’: armed viruses for the treatment of cancer cells and their microenvironment. *Curr. Gene Ther.* **9,** 341–55 (2009).

23. Kaufman, H., Kohlhapp, F. & Zloza, A. Oncolytic viruses: a new class of immunotherapy drugs. *Nat. Rev. Drug Discov.* **14,** 642–662 (2015).

24. Harland, J., Dunn, P., Cameron, E., Conner, J. & Brown, S. M. The herpes simplex virus (HSV) protein ICP34.5 is a virion component that forms a DNA-binding complex with proliferating cell nuclear antigen and HSV replication proteins. *J. Neurovirol.* **9,** 477–88 (2003).

25. Takaoka, A. & Yanai, H. Interferon signalling network in innate defence. *Cell. Microbiol.* **8,** 907–22 (2006).

26. Inoue, H. & Tani, K. Multimodal immunogenic cancer cell death as a consequence of anticancer cytotoxic treatments. *Cell Death Differ.* **21,** 39–49 (2014).

27. Melcher, A., Parato, K., Rooney, C. M. & Bell, J. C. Thunder and lightning: immunotherapy and oncolytic viruses collide. *Mol. Ther.* **19,** 1008–16 (2011).

28. Cunningham, A. L., Donaghy, H., Harman, A. N., Kim, M. & Turville, S. G. Manipulation of dendritic cell function by viruses. *Curr. Opin. Microbiol.* **13,** 524–9 (2010).

29. Leveille, S., Goulet, M.-L., Lichty, B. D. & Hiscott, J. Vesicular stomatitis virus oncolytic treatment interferes with tumor-associated dendritic cell functions and abrogates tumor antigen presentation. *J. Virol.* **85,** 12160–9 (2011).

30. Melroe, G., DeLuca, N. & Knipe, D. Herpes simplex virus 1 has multiple mechanisms for

blocking virus-induced interferon production. *J. Virol.* **78,** 8411–8420 (2004).

31. tenOever, B. R., Servant, M. J., Grandvaux, N., Lin, R. & Hiscott, J. Recognition of the measles virus nucleocapsid as a mechanism of IRF-3 activation. *J. Virol.* **76,** 3659–69 (2002).

32. Allan, K. J., Stojdl, D. F. & Swift, S. L. High-throughput screening to enhance oncolytic virus immunotherapy. *Oncolytic virotherapy* **5,** 15–25 (2016).

33. Weaver, B. K., Kumar, K. P. & Reich, N. C. Interferon regulatory factor 3 and CREB-binding protein/p300 are subunits of double-stranded RNA-activated transcription factor DRAF1. *Mol. Cell. Biol.* **18,** 1359–68 (1998).

34. Hoang, H.-D., Graber, T. E. & Alain, T. Battling for Ribosomes: Translational Control at the Forefront of the Antiviral Response. *J. Mol. Biol.* **430,** 1965–1992 (2018).

35. He, B. *et al.* Suppression of the phenotype of gamma(1)34.5- herpes simplex virus 1: failure of activated RNA-dependent protein kinase to shut off protein synthesis is associated with a deletion in the domain of the alpha47 gene. *J. Virol.* **71,** 6049–54 (1997).

36. Yokota, S. *et al.* Herpes simplex virus type 1 suppresses the interferon signaling pathway by inhibiting phosphorylation of STATs and janus kinases during an early infection stage. *Virology* **286,** 119–24 (2001).

37. Wang, F. *et al.* S6K-STING interaction regulates cytosolic DNA-mediated activation of the transcription factor IRF3. *Nat. Immunol.* **17,** 514–522 (2016).

38. Elde, N. C., Child, S. J., Geballe, A. P. & Malik, H. S. Protein kinase R reveals an evolutionary model for defeating viral mimicry. *Nature* **457,** 485–9 (2009).

39. Buijs, P. R. A., Verhagen, J. H. E., Eijck, C. H. J. Van & Hoogen, B. G. Van Den. Oncolytic viruses : From bench to bedside with a focus on safety. *Hum. Vaccin. Immunother.* **11,** 1573–1584 (2015).

40. Akhtar, J. & Shukla, D. Viral entry mechanisms: cellular and viral mediators of herpes simplex virus entry. *FEBS J.* **276,** 7228–7236 (2009).

41. Mercer, J. & Helenius, A. Virus entry by macropinocytosis. *Nat. Cell Biol.* **11,** 510–520 (2009).

42. Smith, Miles C., Boutell, Chris, Davido, D. J. HSV-1 ICP0: paving the way for viral replication. *Future Virol.* **6,** 421–429 (2011).

43. Toda, M., Martuza, R. L. & Rabkin, S. D. Tumor growth inhibition by intratumoral inoculation of defective herpes simplex virus vectors expressing granulocyte-macrophage colony-stimulating factor. *Mol. Ther.* **2,** 324–9 (2000).

44. Kaufman, H. L. & Bines, S. D. OPTIM trial: a Phase III trial of an oncolytic herpes virus encoding GM-CSF for unresectable stage III or IV melanoma. *Future Oncol.* **6,** 941–9 (2010).

45. Andtbacka, R. H. I. *et al.* Talimogene Laherparepvec Improves Durable Response Rate in Patients With Advanced Melanoma. *J. Clin. Oncol.* **33,** 2780–8 (2015).

46. Zemp, F., Rajwani, J. & Mahoney, D. J. Rhabdoviruses as vaccine platforms for infectious disease and cancer. *Biotechnol. Genet. Eng. Rev.* **8725,** 1–17 (2018).

47. Ahmed, M. *et al.* Ability of the Matrix Protein of Vesicular Stomatitis Virus To Suppress Beta Interferon Gene Expression Is Geneticaly Correlated with the Inhibition of Host

RNA and Protein Synthesis. *J. Virol.* **77,** 4646–4657 (2003).

48. Stojdl, D. F. *et al.* VSV strains with defects in their ability to shutdown innate immunity are potent systemic anti-cancer agents. *Cancer Cell* **4,** 263–75 (2003).

49. Balachandran, S. & Barber, G. N. Vesicular stomatitis virus (VSV) therapy of tumors. *IUBMB Life* **50,** 135–8 (2000).

50. Lemay, G. [Taming our enemies to make them our allies: cancer 'virotherapy']. *Med. Sci. (Paris).* **28,** 339–40 (2012).

51. Alain, T. *et al.* Vesicular stomatitis virus oncolysis is potentiated by impairing mTORC1-dependent type I IFN production. *Proc. Natl. Acad. Sci.* **107,** 1576–1581 (2010).

52. Jacobs, B. L. *et al.* Vaccinia virus vaccines: past, present and future. *Antiviral Res.* **84,** 1–13 (2009).

53. Arulanandam, R. *et al.* Microtubule disruption synergizes with oncolytic virotherapy by inhibiting interferon translation and potentiating bystander killing. *Nat. Commun.* **6,** (2015).

54. Ikeda, K. *et al.* Complement depletion facilitates the infection of multiple brain tumors by an intravascular, replication-conditional herpes simplex virus mutant. *J. Virol.* **74,** 4765–75 (2000).

55. Wakimoto, H., Fulci, G., Tyminski, E. & Chiocca, E. A. Altered expression of antiviral cytokine mRNAs associated with cyclophosphamide's enhancement of viral oncolysis. *Gene Ther.* **11,** 214–23 (2004).

56. Currier, M. A. *et al.* Efficacy and safety of the oncolytic herpes simplex virus rRp450

alone and combined with cyclophosphamide. *Mol. Ther.* **16,** 879–85 (2008).

57. Ikeda, K. *et al.* Oncolytic virus therapy of multiple tumors in the brain requires suppression of innate and elicited antiviral responses. *Nat. Med.* **5,** 881–7 (1999).

58. Maitra, R. *et al.* Oncolytic reovirus preferentially induces apoptosis in KRAS mutant colorectal cancer cells, and synergizes with irinotecan. *Oncotarget* **5,** 2807–19 (2014).

59. Ottolino-Perry, K. *et al.* Oncolytic vaccinia virus synergizes with irinotecan in colorectal cancer. *Mol. Oncol.* **9,** 1539–52 (2015).

60. Lin, S.-F. *et al.* Synergy of a herpes oncolytic virus and paclitaxel for anaplastic thyroid cancer. *Clin. Cancer Res.* **14,** 1519–28 (2008).

61. Liikanen, I. *et al.* Oncolytic adenovirus with temozolomide induces autophagy and antitumor immune responses in cancer patients. *Mol. Ther.* **21,** 1212–23 (2013).

62. Eisenberg, D. P. *et al.* 5-fluorouracil and gemcitabine potentiate the efficacy of oncolytic herpes viral gene therapy in the treatment of pancreatic cancer. *J. Gastrointest. Surg.* **9,** 1068-77; discussion 1077–9 (2005).

63. Sei, S. *et al.* Synergistic antitumor activity of oncolytic reovirus and chemotherapeutic agents in non-small cell lung cancer cells. *Mol. Cancer* **8,** 47 (2009).

64. Piacentini, P. *et al.* Trichostatin A enhances the response of chemotherapeutic agents in inhibiting pancreatic cancer cell proliferation. *Virchows Arch.* **448,** 797–804 (2006).

65. Nguyên, T. L.-A. *et al.* Chemical targeting of the innate antiviral response by histone deacetylase inhibitors renders refractory cancers sensitive to viral oncolysis. *Proc. Natl. Acad. Sci. U. S. A.* **105,** 14981–6 (2008).

66. Kelly, W. K. & Marks, P. A. Drug insight: Histone deacetylase inhibitors--development of the new targeted anticancer agent suberoylanilide hydroxamic acid. *Nat. Clin. Pract. Oncol.* **2,** 150–7 (2005).

67. Liu, T.-C., Castelo-Branco, P., Rabkin, S. D. & Martuza, R. L. Trichostatin A and oncolytic HSV combination therapy shows enhanced antitumoral and antiangiogenic effects. *Mol. Ther.* **16,** 1041–7 (2008).

68. Alvarez-Breckenridge, C. A. *et al.* The histone deacetylase inhibitor valproic acid lessens NK cell action against oncolytic virus-infected glioblastoma cells by inhibition of STAT5/T-BET signaling and generation of gamma interferon. *J. Virol.* **86,** 4566–77 (2012).

69. Bridle, B. W. *et al.* Potentiating cancer immunotherapy using an oncolytic virus. *Mol. Ther.* **18,** 1430–9 (2010).

70. Diallo, J.-S. *et al.* A high-throughput pharmacoviral approach identifies novel oncolytic virus sensitizers. *Mol. Ther.* **18,** 1123–9 (2010).

71. Cataldi, M., Shah, N. R., Felt, S. A. & Grdzelishvili, V. Z. Breaking resistance of pancreatic cancer cells to an attenuated vesicular stomatitis virus through a novel activity of IKK inhibitor TPCA-1. *Virology* **485,** 340–54 (2015).

72. Selman, M. *et al.* Multi-modal Potentiation of Oncolytic Virotherapy by Vanadium Compounds. *Mol. Ther.* **26,** 56–69 (2018).

73. Felt, S. A., Droby, G. N. & Grdzelishvili, V. Z. Ruxolitinib and Polycation Combination Treatment Overcomes Multiple Mechanisms of Resistance of Pancreatic Cancer Cells to

Oncolytic Vesicular Stomatitis Virus. *J. Virol.* **91,** (2017).

74. Kim, D.-S. *et al.* Smac mimetics and oncolytic viruses synergize in driving anticancer T-cell responses through complementary mechanisms. *Nat. Commun.* **8,** 344 (2017).

75. Beug, S. T. *et al.* Smac mimetics and innate immune stimuli synergize to promote tumor death. *Nat. Biotechnol.* **32,** 182–90 (2014).

76. Dobson, C. C. *et al.* Oncolytic virus synergizes with Smac mimetic compounds to induce rhabdomyosarcoma cell death in a syngeneic murine model. *Oncotarget* **8,** 3495–3508 (2017).

77. Heo, J. *et al.* Sequential therapy with JX-594, a targeted oncolytic poxvirus, followed by sorafenib in hepatocellular carcinoma: preclinical and clinical demonstration of combination efficacy. *Mol. Ther.* **19,** 1170–9 (2011).

78. Arulanandam, R. *et al.* Microtubule disruption synergizes with oncolytic virotherapy by inhibiting interferon translation and potentiating bystander killing. *Nat. Commun.* **6,** 6410 (2015).

79. Ilkow, C. S., Swift, S. L., Bell, J. C. & Diallo, J.-S. From scourge to cure: tumour-selective viral pathogenesis as a new strategy against cancer. *PLoS Pathog.* **10,** e1003836 (2014).

80. Hodi, F. S. *et al.* Improved survival with ipilimumab in patients with metastatic melanoma. *N. Engl. J. Med.* **363,** 711–23 (2010).

81. Royal, R. E. *et al.* Phase 2 trial of single agent Ipilimumab (anti-CTLA-4) for locally advanced or metastatic pancreatic adenocarcinoma. *J. Immunother.* **33,** 828–33 (2010).

82. Zamarin, D. *et al.* Localized oncolytic virotherapy overcomes systemic tumor resistance to immune checkpoint blockade immunotherapy. *Sci. Transl. Med.* **6,** 226ra32 (2014).

83. Puzanov, I. *et al.* Talimogene Laherparepvec in Combination With Ipilimumab in Previously Untreated, Unresectable Stage IIIB-IV Melanoma. *J. Clin. Oncol.* **34,** 2619–26 (2016).

84. Kelly, E. & Russell, S. J. History of oncolytic viruses: genesis to genetic engineering. *Mol. Ther.* **15,** 651–9 (2007).

85. Alberts, P. *et al.* Long-term treatment with the oncolytic ECHO-7 virus Rigvir of a melanoma stage IV M1c patient, a small cell lung cancer stage IIIA patient, and a histiocytic sarcoma stage IV patient-three case reports. *APMIS* **124,** 896–904 (2016).

86. Ries, S. & Korn, W. M. ONYX-015: mechanisms of action and clinical potential of a replication-selective adenovirus. *Br. J. Cancer* **86,** 5–11 (2002).

87. Reid, T. *et al.* Intra-arterial administration of a replication-selective adenovirus (dl1520) in patients with colorectal carcinoma metastatic to the liver: a phase I trial. *Gene Ther.* **8,** 1618–26 (2001).

88. Hecht, J. R. *et al.* A phase I/II trial of intratumoral endoscopic ultrasound injection of ONYX-015 with intravenous gemcitabine in unresectable pancreatic carcinoma. *Clin. Cancer Res.* **9,** 555–61 (2003).

89. Galanis, E. *et al.* Phase I-II trial of ONYX-015 in combination with MAP chemotherapy in patients with advanced sarcomas. *Gene Ther.* **12,** 437–45 (2005).

90. Geevarghese, S. K. *et al.* Phase I/II study of oncolytic herpes simplex virus NV1020 in

patients with extensively pretreated refractory colorectal cancer metastatic to the liver. *Hum. Gene Ther.* **21,** 1119–28 (2010).

91. Chesney, J. *et al.* Randomized, Open-Label Phase II Study Evaluating the Efficacy and Safety of Talimogene Laherparepvec in Combination With Ipilimumab Versus Ipilimumab Alone in Patients With Advanced, Unresectable Melanoma. *J. Clin. Oncol.* **36,** 1658–1667 (2018).

92. Neise, D. *et al.* The p90 ribosomal S6 kinase (RSK) inhibitor BI-D1870 prevents gamma irradiation-induced apoptosis and mediates senescence via RSK- and p53-independent accumulation of p21WAF1/CIP1. *Cell Death Dis.* **4,** 1–11 (2013).

93. Sapkota, G. P. *et al.* BI-D1870 is a specific inhibitor of the p90 RSK (ribosomal S6 kinase) isoforms *in vitro* and *in vivo*. *Biochem. J.* **401,** 29–38 (2007).

94. Bain, J. *et al.* The selectivity of protein kinase inhibitors: a further update. *Biochem. J.* **408,** 297–315 (2007).

95. Smith, J. A. *et al.* Identification of the first specific inhibitor of p90 ribosomal S6 kinase (RSK) reveals an unexpected role for RSK in cancer cell proliferation. *Cancer Res.* **65,** 1027–1034 (2005).

96. Clark, D. E. *et al.* The serine/threonine protein kinase, p90 ribosomal S6 kinase, is an important regulator of prostate cancer cell proliferation. *Cancer Res.* **65,** 3108–16 (2005).

97. Zaru, R., Edgar, A. J., Hanauer, A. & Watts, C. Structural and functional basis for p38-MK2-activated Rsk signaling in toll-like receptor-stimulated dendritic cells. *Mol. Cell. Biol.* **35,** 132–40 (2015).

98. Kritsky, M. S. *et al.* Excited flavin and pterin coenzyme molecules in evolution. *Biochemistry. (Mosc).* **75,** 1200–16 (2010).

99. Chen, S. & Mackintosh, C. Differential regulation of NHE1 phosphorylation and glucose uptake by inhibitors of the ERK pathway and p90RSK in 3T3-L1 adipocytes. *Cell. Signal.* **21,** 1984–93 (2009).

100. Degen, M., Barron, P., Natarajan, E., Widlund, H. R. & Rheinwald, J. G. RSK Activation of Translation Factor eIF4B Drives Abnormal Increases of Laminin γ2 and MYC Protein during Neoplastic Progression to Squamous Cell Carcinoma. *PLoS One* **8,** e78979 (2013).

101. Karelina, K., Alzate-Correa, D. & Obrietan, K. Ribosomal S6 kinase regulates ischemia-induced progenitor cell proliferation in the adult mouse hippocampus. *Exp. Neurol.* **253,** 72–81 (2014).

102. Edgar, A. J., Trost, M., Watts, C. & Zaru, R. A combination of SILAC and nucleotide acyl phosphate labelling reveals unexpected targets of the Rsk inhibitor BI-D1870. *Biosci. Rep.* **34,** 29–41 (2014).

103. Pambid, M. R. *et al.* Overcoming resistance to Sonic Hedgehog inhibition by targeting p90 ribosomal S6 kinase in pediatric medulloblastoma. *Pediatr. Blood Cancer* **61,** 107–15 (2014).

104. Chiu, C.-F. *et al.* Antitumor effects of BI-D1870 on human oral squamous cell carcinoma. *Cancer Chemother. Pharmacol.* **73,** 237–2347 (2014).

105. Nguyen, T. L. Targeting RSK: an overview of small molecule inhibitors. *Anticancer. Agents Med. Chem.* **8,** 710–6 (2008).

106. Roux, P. P. & Topisirovic, I. Regulation of mRNA translation by signaling pathways. *Cold Spring Harb. Perspect. Biol.* **4,** (2012).

107. Takada, I., Yogiashi, Y. & Makishima, M. The ribosomal S6 kinase inhibitor BI-D1870 ameliorated experimental autoimmune encephalomyelitis in mice. *Immunobiology* **221,** 188–192 (2016).

108. Kirrane, T. M. *et al.* Indole RSK inhibitors. Part 2: Optimization of cell potency and kinase selectivity. *Bioorganic Med. Chem. Lett.* **22,** 738–742 (2012).

109. Hoffmann, M. *et al.* Novel dihydropteridinones, method for producing the same and the use thereof as medicaments. 103 (2003).

110. Zakaria, C. *et al.* Active-site mTOR inhibitors augment HSV1-dICP0 infection in cancer cells via dysregulated eIF4E/4E-BP axis. *PLoS Pathog.* **14,** e1007264 (2018).

111. Gadde, S. *et al.* Development of Therapeutic Polymeric Nanoparticles for the Resolution of Inflammation. *Adv. Healthc. Mater.* **3,** 1448–1456 (2014).

112. Roffé, M., Lupinacci, F. C., Soares, L. C., Hajj, G. N. & Martins, V. R. Two widely used RSK inhibitors, BI-D1870 and SL0101, alter mTORC1 signaling in a RSK-independent manner. *Cell. Signal.* **27,** 1630–1642 (2015).

113. Eichner, L. J. *et al.* miR-378 ∗ Mediates Metabolic Shift in Breast Cancer Cells via the PGC-1β/ERRγ Transcriptional Pathway. *Cell Metab.* **12,** 352–361 (2010).

114. Grottkau, B. E., Cai, X., Wang, J., Yang, X. & Lin, Y. Polymeric nanoparticles for a drug delivery system. *Curr. Drug Metab.* **14,** 840–6 (2013).

115. De Jong, W. H. & Borm, P. J. A. Drug delivery and nanoparticles:applications and

hazards. *Int. J. Nanomedicine* **3,** 133–49 (2008).

116. Singh, S. K., Singh, S., Lillard, J. W. & Singh, R. Drug delivery approaches for breast cancer. *Int. J. Nanomedicine* **12,** 6205–6218 (2017).

117. Heo, J. *et al.* Randomized dose-finding clinical trial of oncolytic immunotherapeutic vaccinia JX-594 in liver cancer. *Nat. Med.* **19,** 329–36 (2013).

118. Ranki, T. *et al.* Phase I study with ONCOS-102 for the treatment of solid tumors - an evaluation of clinical response and exploratory analyses of immune markers. *J. Immunother. cancer* **4,** 17 (2016).

119. Cohen, M. S., Zhang, C., Shokat, K. M. & Taunton, J. Structural Bioinformatics-Based Design of Selective, Irreversible Kinase Inhibitors. *Science (80-.).* **308,** 1318–1321 (2005).

120. Aronchik, I. *et al.* Novel Potent and Selective Inhibitors of p90 Ribosomal S6 Kinase Reveal the Heterogeneity of RSK Function in MAPK-Driven Cancers. *Mol. Cancer Res.* **12,** (2014).

121. Al-Zahrani, K. N., Baron, K. D. & Sabourin, L. A. Ste20-like kinase SLK, at the crossroads: a matter of life and death. *Cell Adh. Migr.* **7,** 1–10

122. Pryce, Benjamin R., Al-Zahrani, Khalid N., Dufresne, Sebastien, Belkina, Natalya, Labreche, Cedrik, Patino-Lopez, Genaro, Frenette, Jerome, Shaw, Stephen, Sabourin, L. A. Deletion of the Ste20-like kinase SLK in skeletal muscle results in a progressive myopathy and muscle weakness. *Skelet. Muscle* **7,** 1–13 (2017).

123. Wan, Y., Simovic, B. & Walsh, S. Mechanistic insights into the oncolytic activity of

vesicular stomatitis virus in cancer immunotherapy. *Oncolytic Virotherapy* 157 (2015). doi:10.2147/OV.S66079

124. Finkelshtein, D., Werman, A., Novick, D., Barak, S. & Rubinstein, M. LDL receptor and its family members serve as the cellular receptors for vesicular stomatitis virus. *Proc. Natl. Acad. Sci.* **110,** 7306–7311 (2013).

125. Agelidis, A. M., Shukla, D. & Sciences, V. Cell entry mechanisms of HSV: what we have learned in recent years. *Future Virol.* **10,** 1145–1154 (2015).

126. Jain, R. *et al.* Discovery of Potent and Selective RSK Inhibitors as Biological Probes. *J. Med. Chem.* **58,** 6766–83 (2015).

127. Puleo, David E., Kucera, Kaury, Hammaren, Henrik M., Ungureanu, Daniela, Newton, Ana S., Silvennoinen, Olli, Jorgensen, William L., Schlessinger, J. Identification and Characterization of JAK2 Pseudokinase Domain Small Molecule Binders. *ACS Med. Chem. Lett.* **8,** 618–621 (2017).

128. Franke, V. *et al.* High Response Rates for T-VEC in Early Metastatic Melanoma (Stage IIIB/C-IVM1a). *Int. J. cancer* (2019). doi:10.1002/ijc.32172

129. Louie, R. J. *et al.* Real World Outcomes of Talimogene Laherparepvec Therapy: A Multi-Institutional Experience. *J. Am. Coll. Surg.* (2019). doi:10.1016/j.jamcollsurg.2018.12.027

130. Lun, X. Q. *et al.* Targeting human medulloblastoma: oncolytic virotherapy with myxoma virus is enhanced by rapamycin. *Cancer Res.* **67,** 8818–27 (2007).

131. Escobar-Zarate, D., Liu, Y.-P., Suksanpaisan, L., Russell, S. J. & Peng, K.-W. Overcoming cancer cell resistance to VSV oncolysis with JAK1/2 inhibitors. *Cancer Gene*

Ther. **20,** 582–9 (2013).

132. Edgar, J. Y. C. & Wang, H. Introduction for Design of Nanoparticle Based Drug Delivery Systems. *Curr. Pharm. Des.* **23,** 2108–2112 (2017).

133. Ashfaq, U. A., Riaz, M., Yasmeen, E. & Yousaf, M. Z. Recent Advances in Nanoparticle-Based Targeted Drug-Delivery Systems Against Cancer and Role of Tumor Microenvironment. *Crit. Rev. Ther. Drug Carrier Syst.* **34,** 317–353 (2017).

134. Yokoda, R. *et al.* Oncolytic virus delivery: from nano-pharmacodynamics to enhanced oncolytic effect. *Oncolytic virotherapy* **6,** 39–49 (2017).

135. Lemay, C. G. *et al.* Harnessing oncolytic virus-mediated antitumor immunity in an infected cell vaccine. *Mol. Ther.* **20,** 1791–9 (2012).

136. Roberts, A., Buonocore, L., Price, R., Forman, J. & Rose, J. K. Attenuated vesicular stomatitis viruses as vaccine vectors. *J. Virol.* **73,** 3723–32 (1999).

137. Bridle, B. W. *et al.* HDAC inhibition suppresses primary immune responses, enhances secondary immune responses, and abrogates autoimmunity during tumor immunotherapy. *Mol. Ther.* **21,** 887–94 (2013).

138. Purser, S., Moore, P. R., Swallow, S. & Gouverneur, V. Fluorine in medicinal chemistry. *Chem. Soc. Rev.* **37,** 320–30 (2008).

139. Menendez, C. *et al.* Chemical synthesis and biological evaluation of triazole derivatives as inhibitors of InhA and antituberculosis agents. *Eur. J. Med. Chem.* **52,** 275–283 (2012).

140. Bommareddy, P. K., Shettigar, M. & Kaufman, H. L. Integrating oncolytic viruses in combination cancer immunotherapy. *Nat. Rev. Immunol.* **18,** 498–513 (2018).

141. Kolb, H. C., Finn, M. G. & Sharpless, K. B. Click Chemistry: Diverse Chemical Function from a Few Good Reactions. *Angew. Chem. Int. Ed. Engl.* **40,** 2004–2021 (2001).

Contributions of Collaborators

Experiments performed with HSV1-1716 and HSV1-ICP0-null in combination with BI-D1870 in Figure 4, nanoparticle experiments (Figure 11), and VACV infection in combination with BI-D1870 (Figure 12) were executed by Nick Yelle.

Vickey Gilcrest conducted the experiments with HSV1-1716 and VSVΔ51 in combination with BI-D1870 in Figures 5 and 9, and infection with VACV in combination with BI-D1870 and KA-019 in Figure 23.

In vivo experiments in Figure 10 A, B were performed by Dr. Shawn Beug and Nathalie Earl at the Children's Hospital of Eastern Ontario Research Institute (CHEORI); Figure 10 C experiments performed by Dr. Fabrice LeBoeuf at the OHRI; and Figure 10 E, F experiments were performed by Dr. Xuequing Lun at the University of Calgary.

Members of the Robin Parks lab at the OHRI performed infections with adenovirus in combination with BI-D1870 in Figure 11.

Dr. Marceline Côté at the University of Ottawa, Department of Biochemistry and Microbiology, conducted the experiment comparing the relative infection of VSV-G between cells treated with DMSO and 5 μM BI-D1870 in Figure 17 A.

Dr. Chris Boddy at the University of Ottawa, Department of Chemistry and director of the Biochemistry program identified the areas of modification on BI-D1870 in Figure 18 B, created the images of BI-D1870 docking in RSK and JAK2 in Figure 19, and designed the analogs in Figure 20.

Dr. Kim Apperley, Coordinator for Canadian Institutes of Health Research, synthesized all Series I analogs for experiments in Figures 21, 22 and 23.

Appendices

Supplemental Figure 1. RSK is not the main mechanism of action by which BI-D1870 can increase viral infection. (A – D) RSK k/o cell lines were infected with HSV1-1716-GFP at 0.01 MOI and treated with increasing concentrations of BI-D1870 (1μM, 5 μM, 10 μM) for 48 hours. GFP cluster analysis was performed by the Incucyte and GraphPad.

A

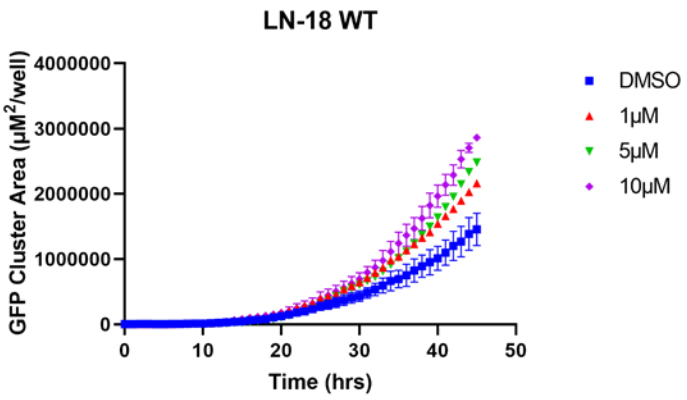
LN-18 WT
GFP Cluster Area (µM²/well)
4000000
3000000
2000000
1000000
0
0
10
20
30
40
50
Time (hrs)
DMSO
1µM
5µM
10µM

B

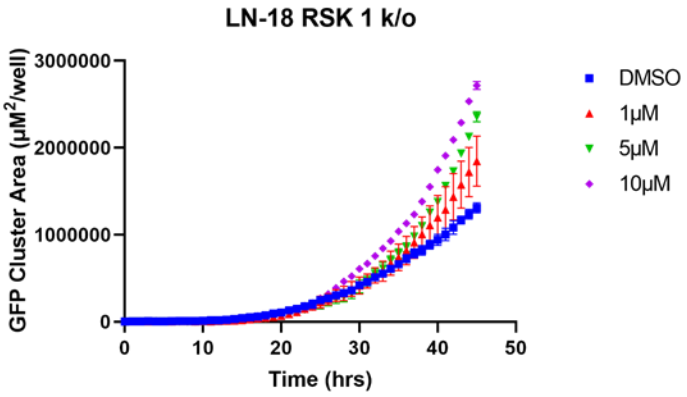
LN-18 RSK 1 k/o
GFP Cluster Area (µM²/well)
3000000
2000000
1000000
0
0
10
20
30
40
50
Time (hrs)
DMSO
1µM
5µM
10µM

C

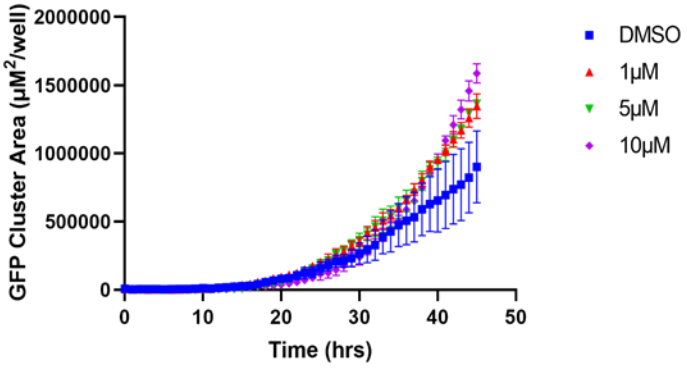
LN-18 RSK 2 k/o
GFP Cluster Area (µM²/well)
2000000
1500000
1000000
500000
0
0
10
20
30
40
50
Time (hrs)
DMSO
1µM
5µM
10µM

D

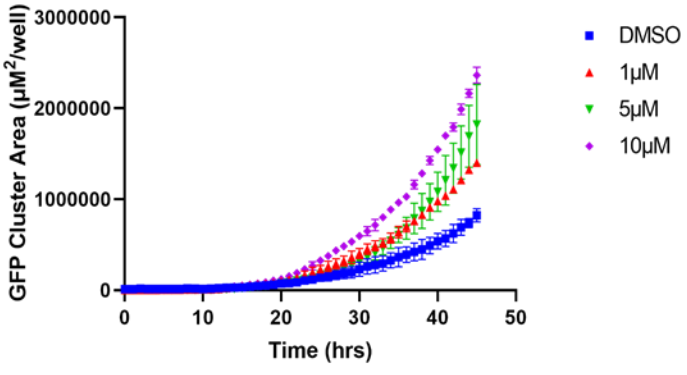
LN-18 RSK dko
GFP Cluster Area (µM²/well)
3000000
2000000
1000000
0
0
10
20
30
40
50
Time (hrs)
DMSO
1µM
5µM
10µM

Supplemental Figure 2. The effect of Series I.I analogs on VSVΔ51 infection. (A, B) Murine breast carcinoma cells (4T1) were infected with VSVΔ51-GFP at 0.1 MOI and treated with increasing concentrations of each of Series I.I analog (KA-001, KA-004, KA-005, KA-006, KA-007). (A) GFP cluster area (μM^2/well over time) was analyzed of each analog at 10 μM and graphed. (B) GFP images of VSVΔ51 infection after 24 hours.

A

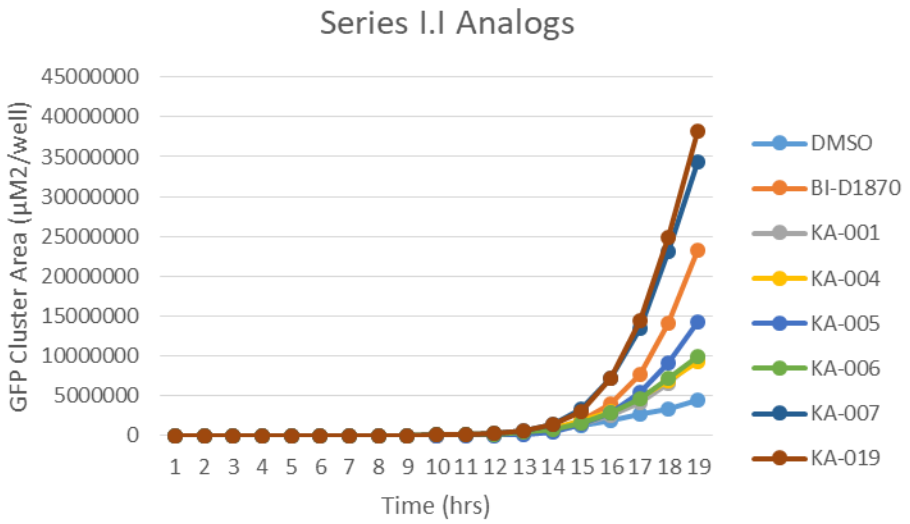
Series I.I Analogs
GFP Cluster Area (µM2/well)
45000000
40000000
35000000
30000000
25000000
20000000
15000000
10000000
5000000
0
1 2 3 4 5 6 7 8 9 10 11 12 13 14 15 16 17 18 19
Time (hrs)
DMSO
BI-D1870
KA-001
KA-004
KA-005
KA-006
KA-007
KA-019

B

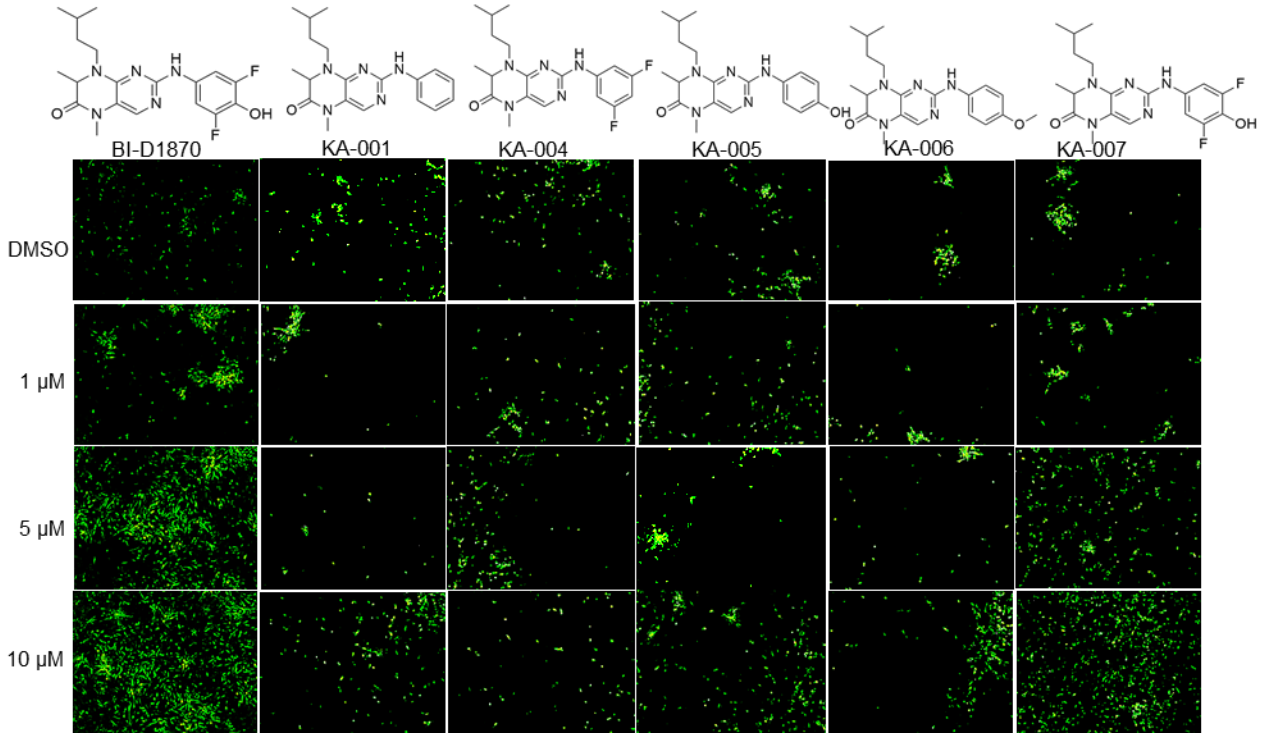
BI-D1870
KA-001
KA-004
KA-005
KA-006
KA-007
DMSO
1 µM
5 µM
10 µM

Supplemental Figure 3. The effect of Series I.II analogs on VSVΔ51 infection. (A, B) Murine breast carcinoma cells (4T1) were infected with VSVΔ51-GFP at 0.1 MOI and treated with increasing concentrations of each of Series I.II analog (KA-013, KA-019, KA-020, KA-021, KA-022). (A) GFP cluster area (μM^2/well over time) was analyzed of each analog at 10 μM and graphed. (B) GFP images of VSVΔ51 infection after 24 hours.

A

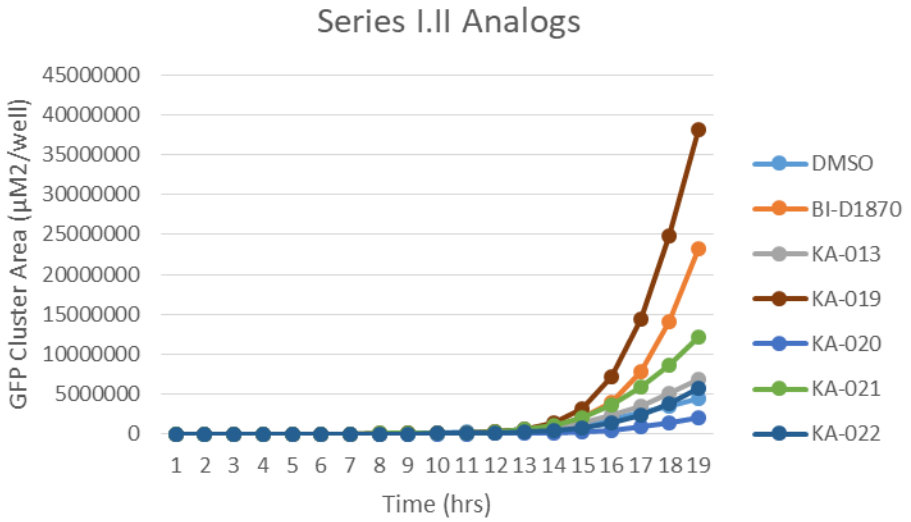
Series I.II Analogs
GFP Cluster Area (µM2/well)
45000000
40000000
35000000
30000000
25000000
20000000
15000000
10000000
5000000
0
1 2 3 4 5 6 7 8 9 10 11 12 13 14 15 16 17 18 19
Time (hrs)
DMSO
BI-D1870
KA-013
KA-019
KA-020
KA-021
KA-022

B

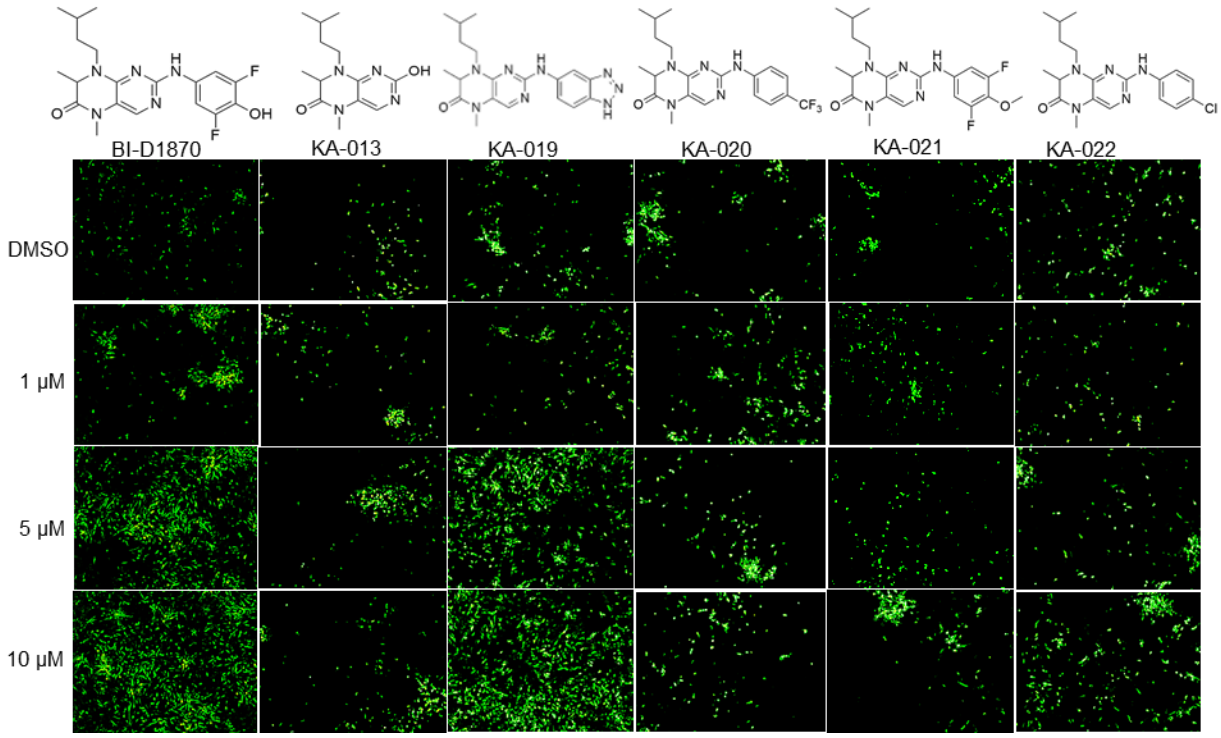
BI-D1870
KA-013
KA-019
KA-020
KA-021
KA-022
DMSO
1 µM
5 µM
10 µM

NMR Data

KA-001

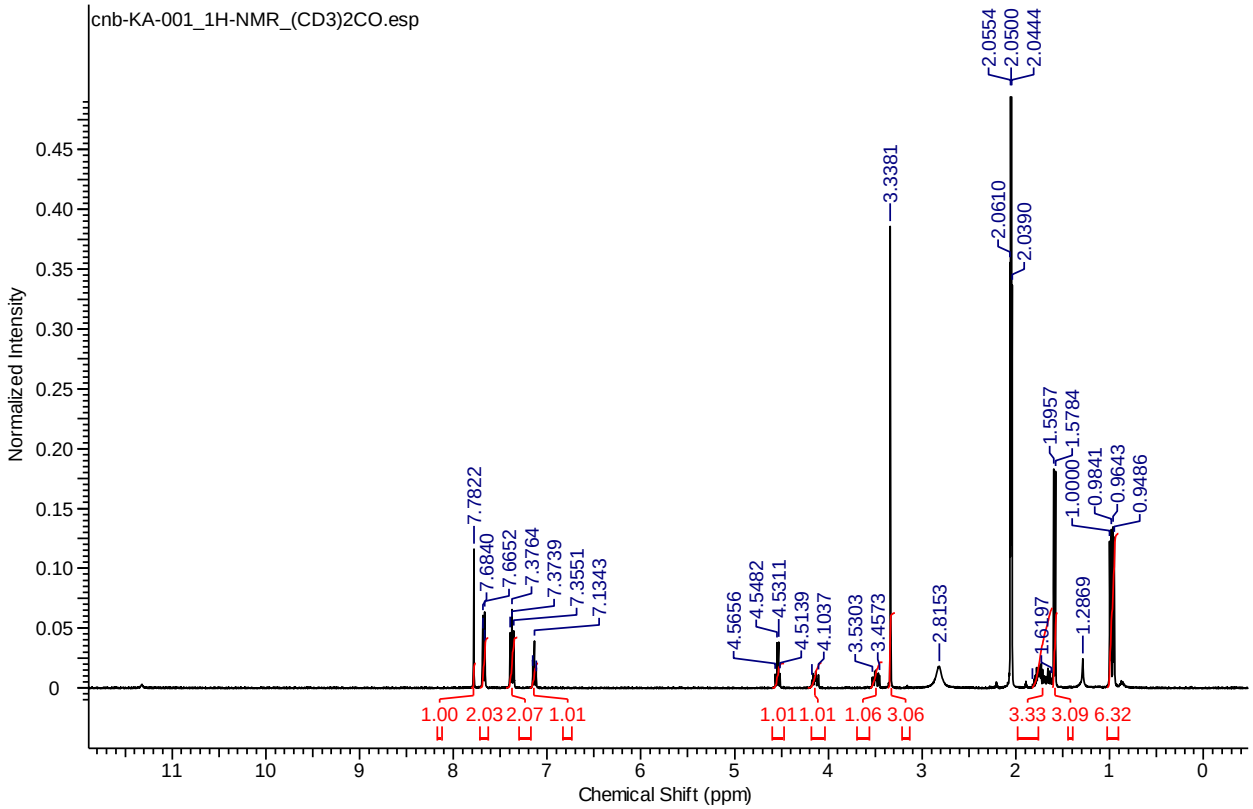

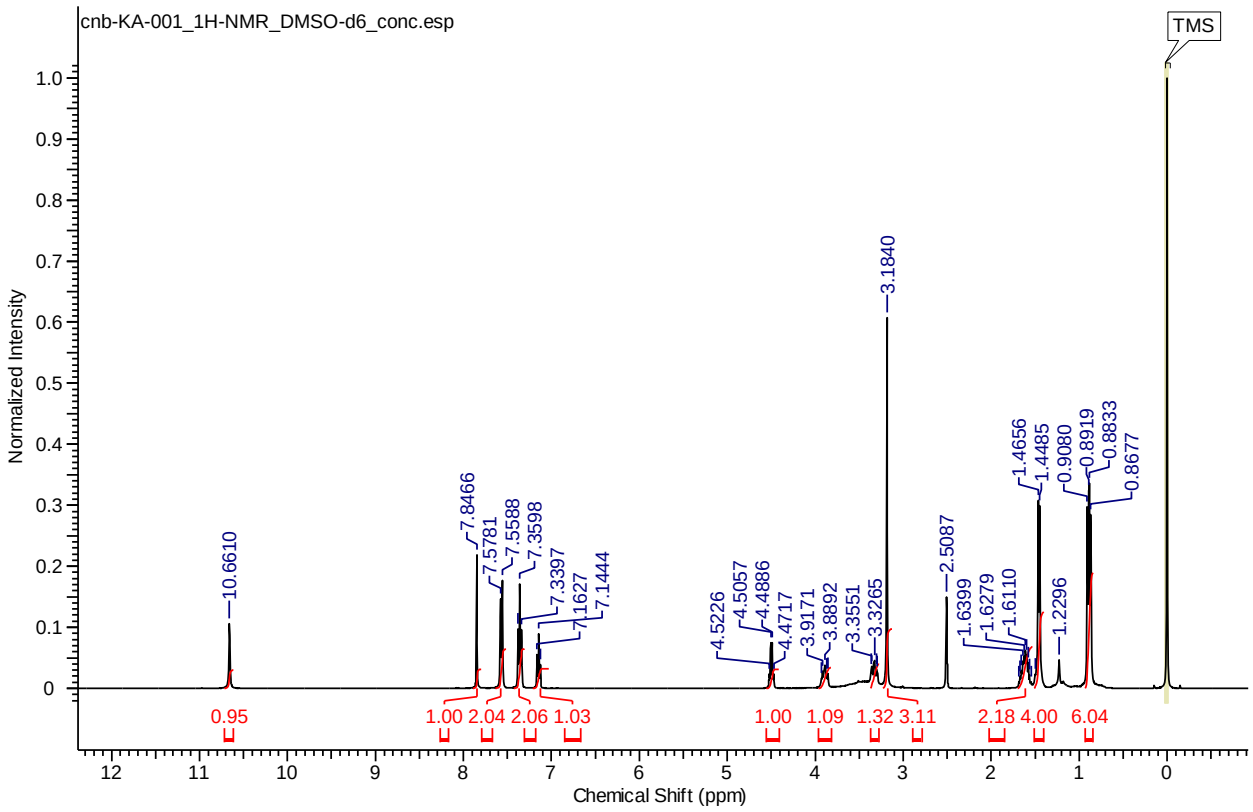
cnb-KA-001_1H-NMR_DMSO-d6_conc.esp
TMS
Normalized Intensity
Chemical Shift (ppm)
10.6610
7.8466
7.5781
7.5588
7.3598
7.3397
7.1627
7.1444
4.5226
4.5057
4.4886
4.4717
3.9171
3.8892
3.3551
3.3265
3.1840
2.5087
1.6399
1.6279
1.6110
1.4656
1.4485
1.2296
0.9080
0.8919
0.8833
0.8677
0.95
1.00 2.04 2.06 1.03
1.00 1.09 1.32 3.11
2.18 4.00 6.04

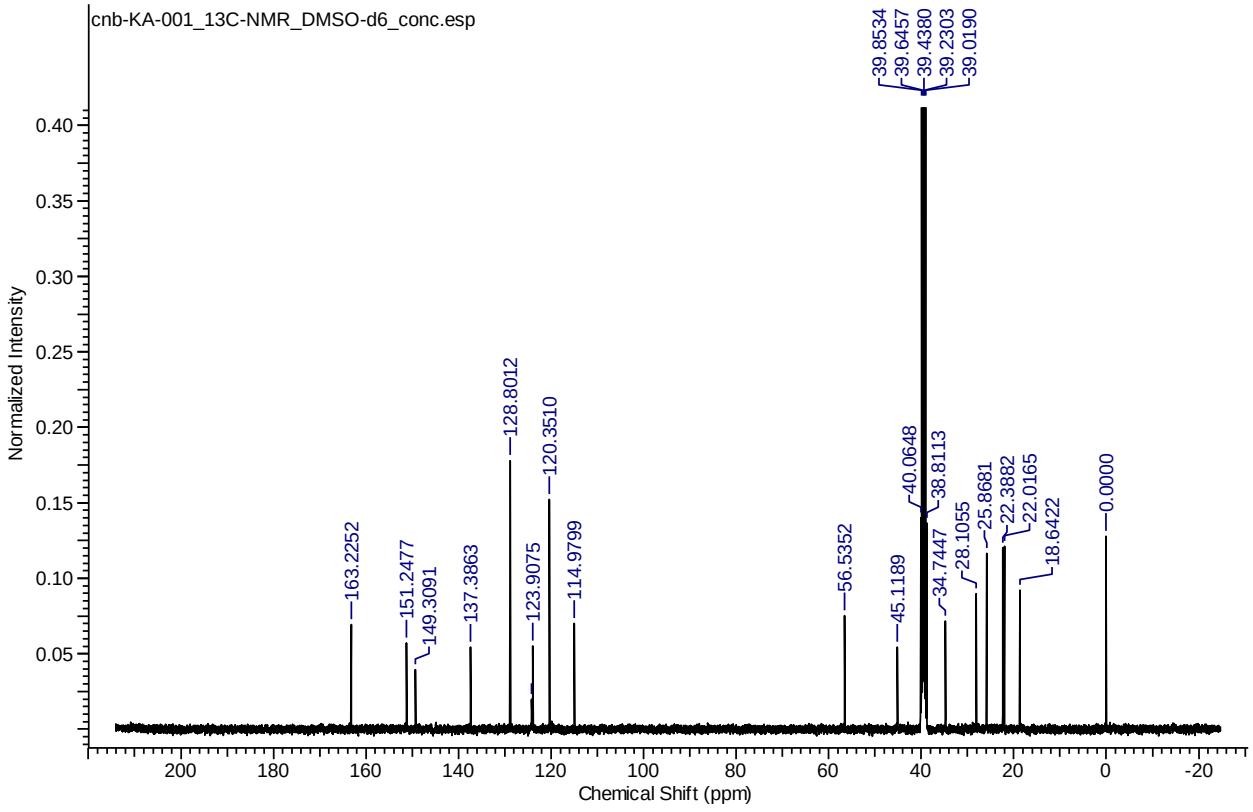
cnb-KA-001_13C-NMR_DMSO-d6_conc.esp
Normalized Intensity
Chemical Shift (ppm)
39.8534
39.6457
39.4380
39.2303
39.0190
163.2252
151.2477
149.3091
137.3863
128.8012
123.9075
120.3510
114.9799
56.5352
45.1189
40.0648
38.8113
34.7447
28.1055
25.8681
22.3882
22.0165
18.6422
0.0000

KA-004

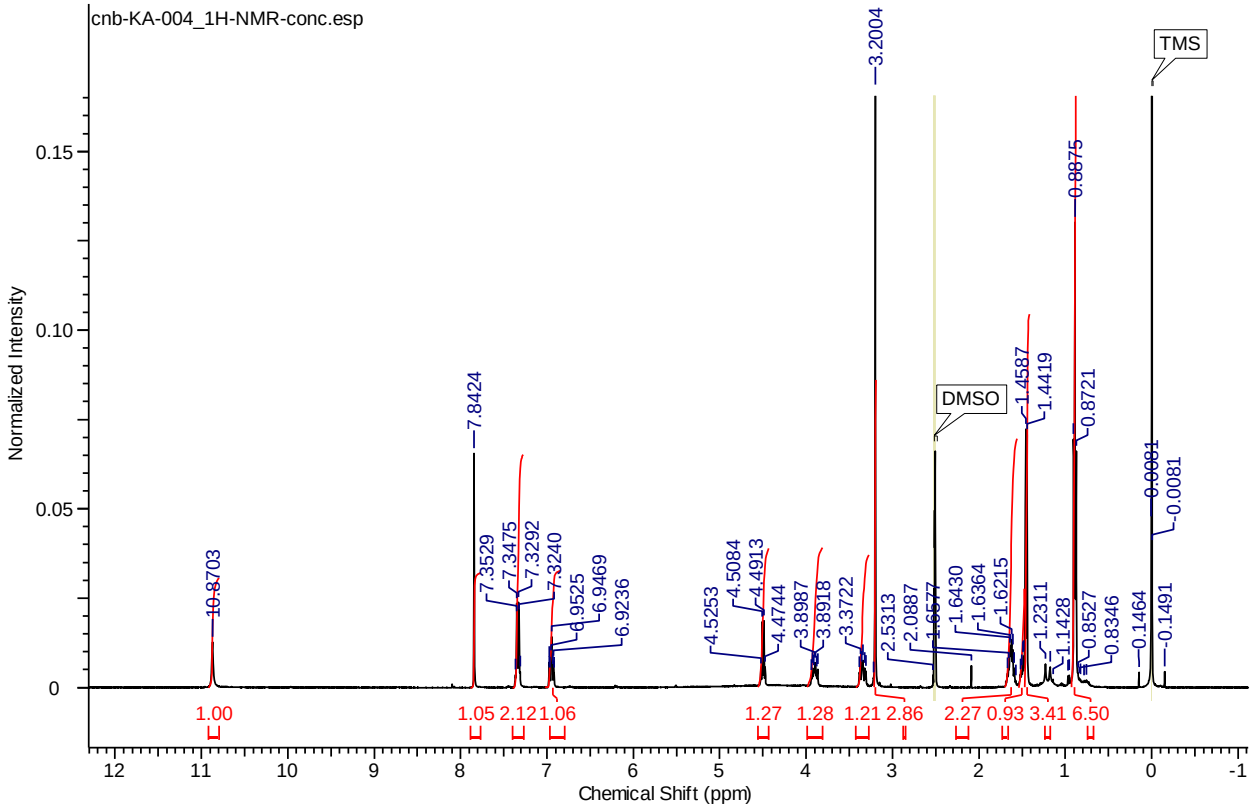
cnb-KA-004_1H-NMR-conc.esp
Normalized Intensity
Chemical Shift (ppm)
TMS
DMSO
3.2004
0.8875
7.8424
1.4587
1.4419
0.8721
0.0081
10.8703
7.3529
7.3475
7.3292
7.3240
6.9525
6.9469
6.9236
4.5253
4.5084
4.4913
4.4744
3.8987
3.8918
3.3722
2.5313
2.0887
1.6677
1.6430
1.6364
1.6215
1.2311
1.1428
0.8527
0.8346
0.1464
0.1491
1.00
1.05
2.12
1.06
1.27
1.28
1.21
2.86
2.27
0.93
3.41
6.50

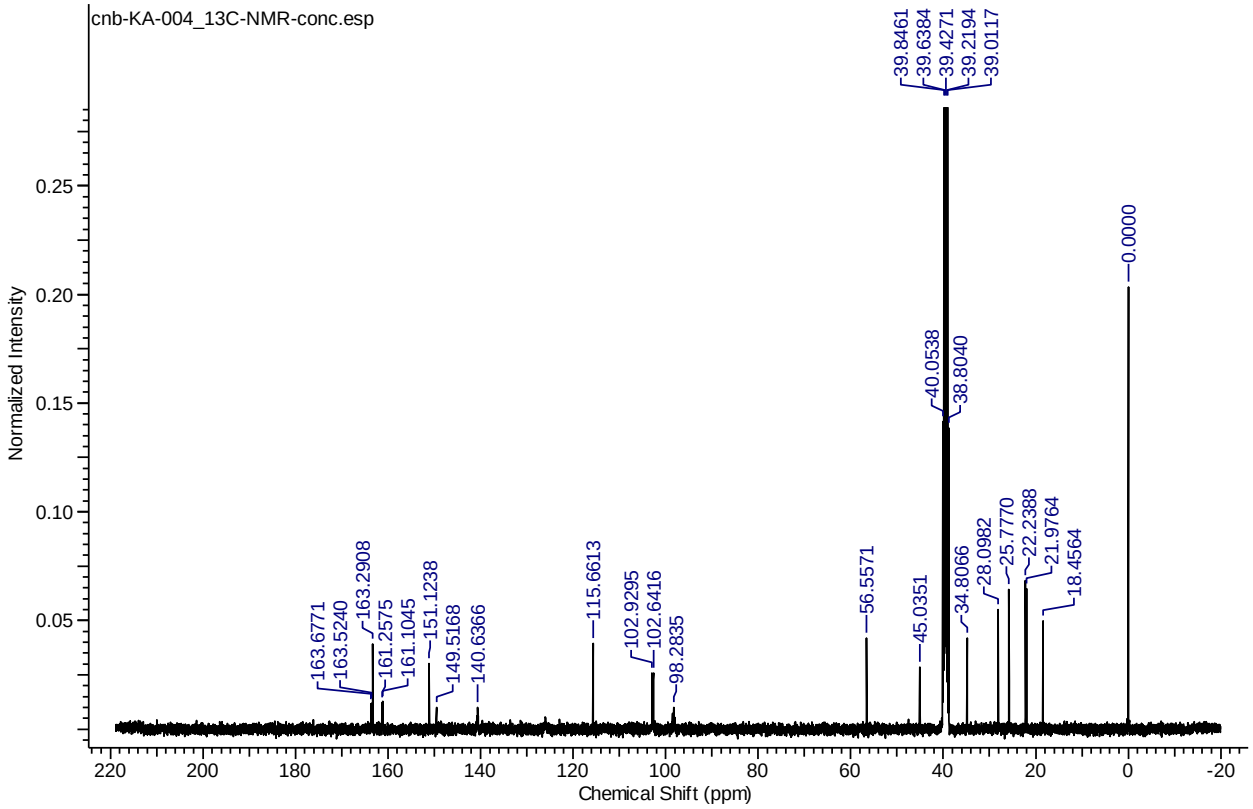
cnb-KA-004_13C-NMR-conc.esp
Normalized Intensity
Chemical Shift (ppm)
39.8461
39.6384
39.4271
39.2194
39.0117
0.0000
40.0538
38.8040
163.6771
163.5240
163.2908
161.2575
161.1045
151.1238
149.5168
140.6366
115.6613
102.9295
102.6416
98.2835
56.5571
45.0351
34.8066
28.0982
25.7770
22.2388
21.9764
18.4564

KA-005

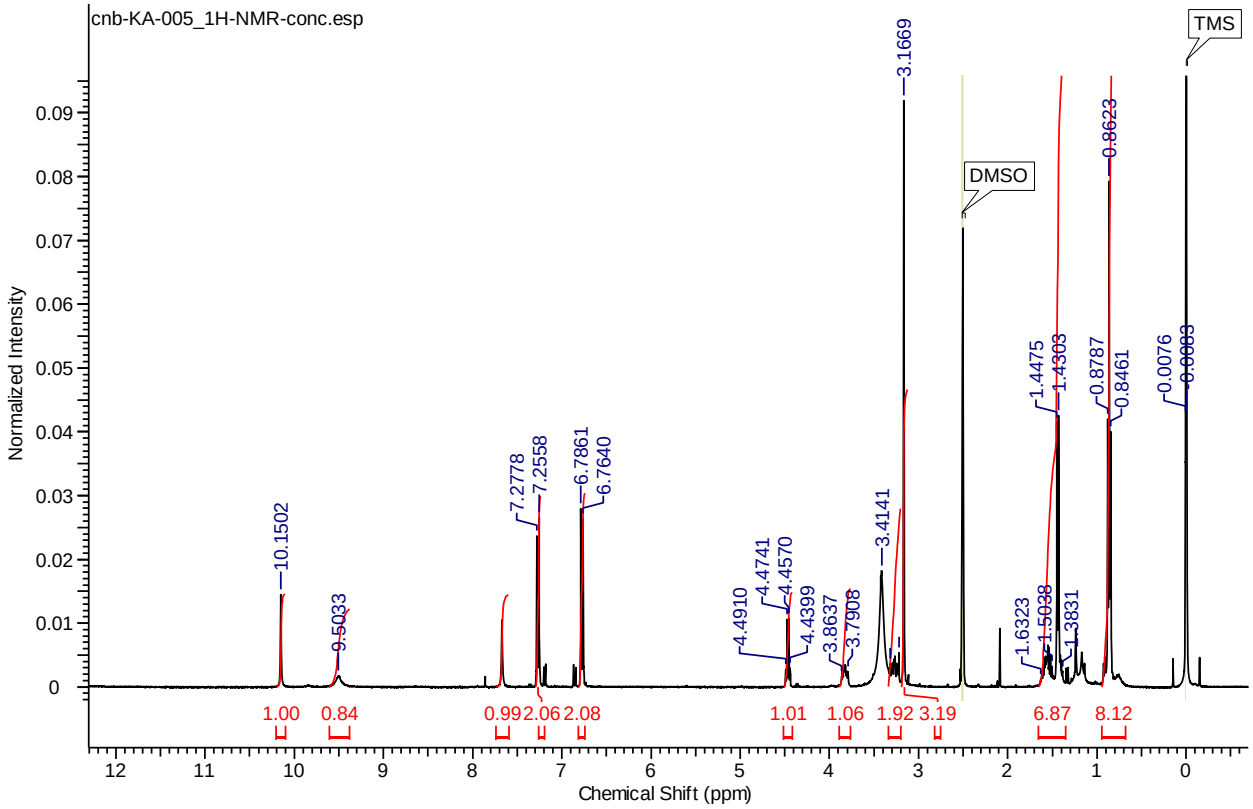
cnb-KA-005_1H-NMR-conc.esp
Normalized Intensity
Chemical Shift (ppm)
TMS
DMSO
3.1669
0.8623
10.1502
9.5033
7.2778
7.2558
6.7861
6.7640
4.4910
4.4741
4.4570
4.4399
3.8637
3.7908
3.4141
1.6323
1.5038
1.4475
1.4303
1.3831
0.8787
0.8461
0.0076
0.0003
1.00
0.84
0.99
2.06
2.08
1.01
1.06
1.92
3.19
6.87
8.12

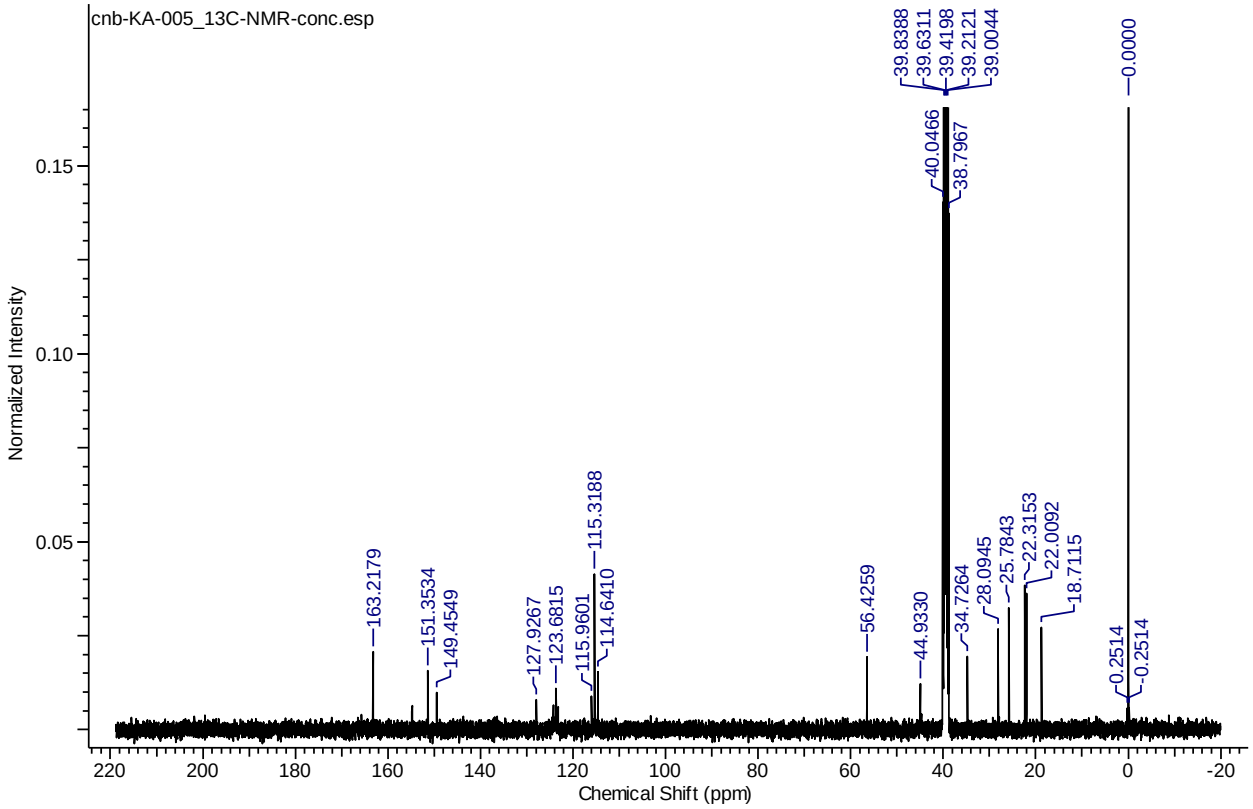
cnb-KA-005_13C-NMR-conc.esp
Normalized Intensity
Chemical Shift (ppm)
39.8388
39.6311
39.4198
39.2121
39.0044
40.0466
38.7967
0.0000
163.2179
151.3534
149.4549
127.9267
123.6815
115.9601
115.3188
114.6410
56.4259
44.9330
34.7264
28.0945
25.7843
22.3153
22.0092
18.7115
0.2514
-0.2514

KA-006

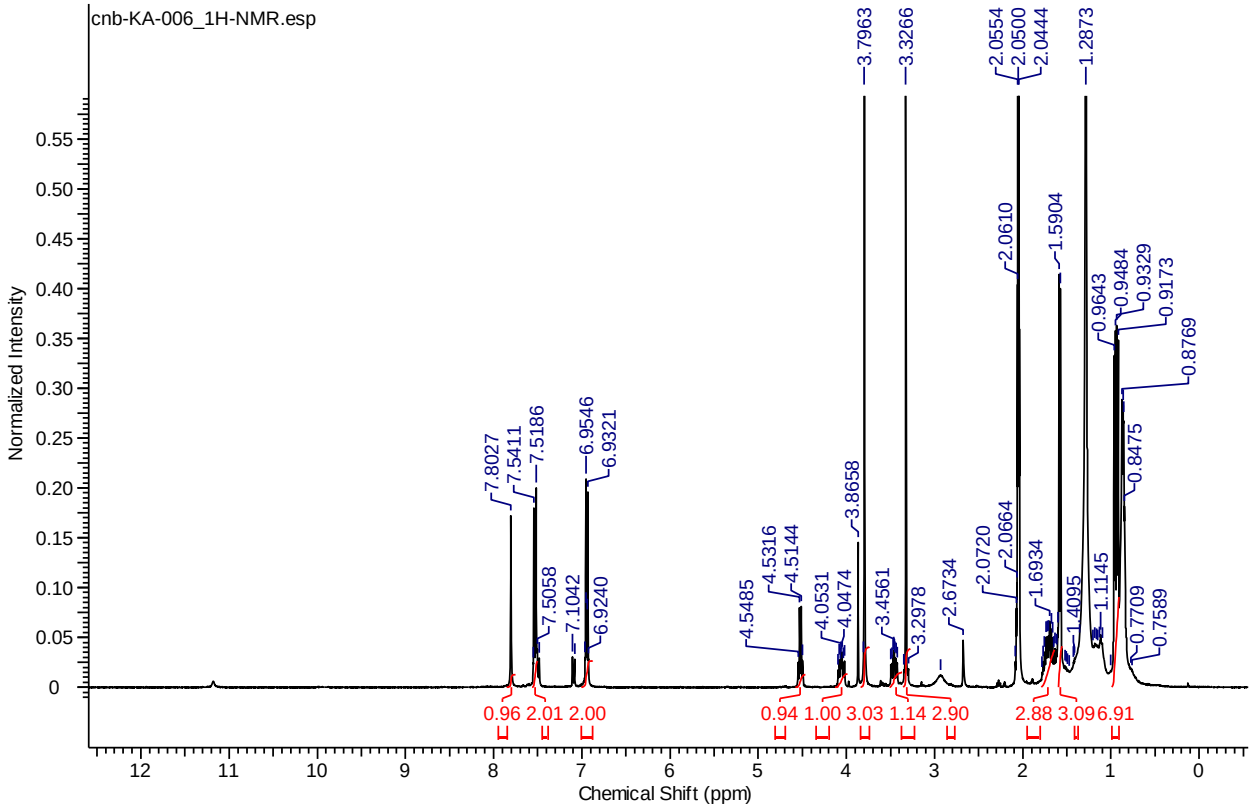
cnb-KA-006_1H-NMR.esp
Normalized Intensity
Chemical Shift (ppm)
7.8027
7.5411
7.5186
7.5058
7.1042
6.9546
6.9321
6.9240
4.5485
4.5316
4.5144
4.0531
4.0474
3.8658
3.7963
3.4561
3.3266
3.2978
2.6734
2.0720
2.0664
2.0610
2.0554
2.0500
2.0444
1.6934
1.5904
1.4095
1.2873
1.1145
0.9643
0.9484
0.9329
0.9173
0.8769
0.8475
0.7709
0.7589
0.96 2.01 2.00
0.94 1.00 3.03 1.14 2.90
2.88 3.09 6.91

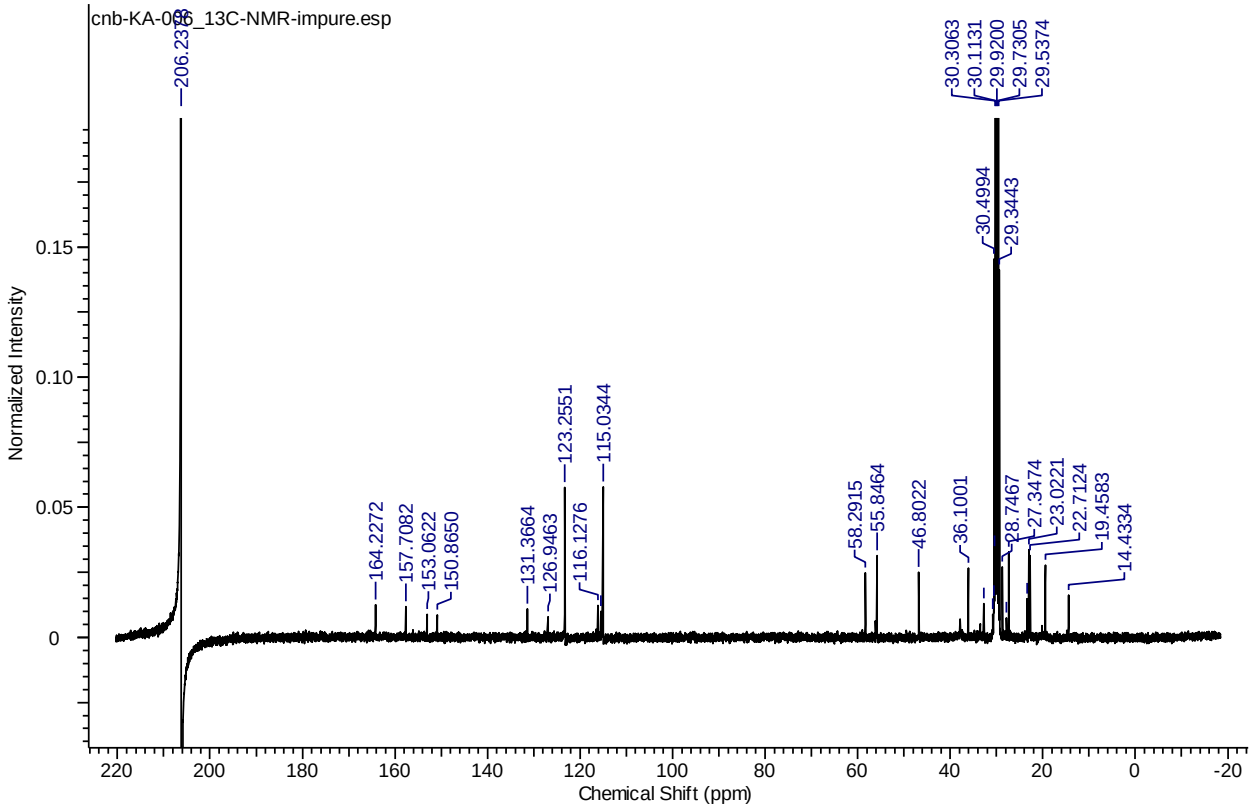
cnb-KA-006_13C-NMR-impure.esp
Normalized Intensity
Chemical Shift (ppm)
206.2378
164.2272
157.7082
153.0622
150.8650
131.3664
126.9463
123.2551
116.1276
115.0344
58.2915
55.8464
46.8022
36.1001
30.4994
30.3063
30.1131
29.9200
29.7305
29.5374
29.3443
28.7467
27.3474
23.0221
22.7124
19.4583
14.4334

KA-007

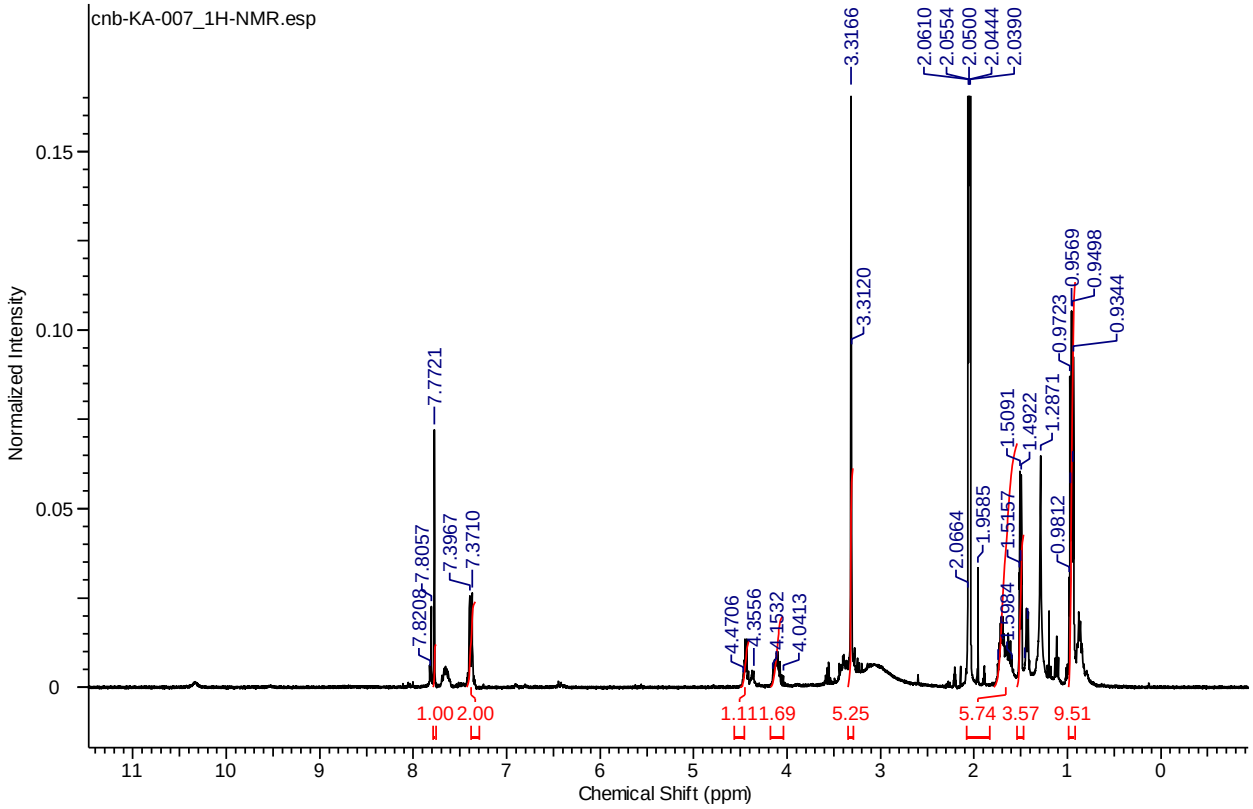
cnb-KA-007_1H-NMR.esp
Normalized Intensity
Chemical Shift (ppm)
0.15
0.10
0.05
0
11
10
9
8
7
6
5
4
3
2
1
0
7.8209
7.8057
7.7721
7.3967
7.3710
4.4706
4.3556
4.1532
4.0413
3.3166
3.3120
2.0664
1.9585
1.5157
1.5091
1.4922
1.2871
0.9812
0.9723
0.9569
0.9498
0.9344
1.00
2.00
1.11
1.69
5.25
5.74
3.57
9.51

KA-013

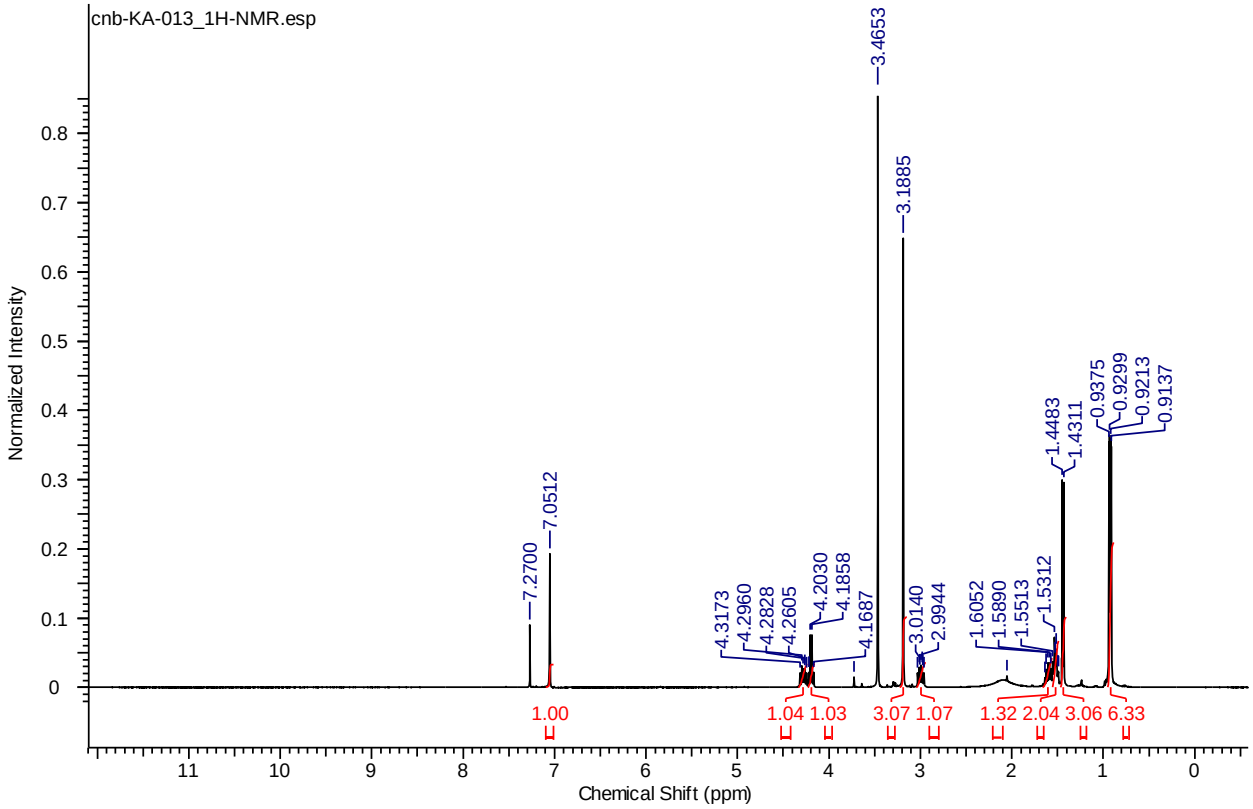
cnb-KA-013_1H-NMR.esp
Normalized Intensity
Chemical Shift (ppm)
3.4653
3.1885
7.2700
7.0512
4.3173
4.2960
4.2828
4.2605
4.2030
4.1858
4.1687
3.0140
2.9944
1.6052
1.5890
1.5513
1.5312
1.4483
1.4311
0.9375
0.9299
0.9213
0.9137
1.00
1.04
1.03
3.07
1.07
1.32
2.04
3.06
6.33

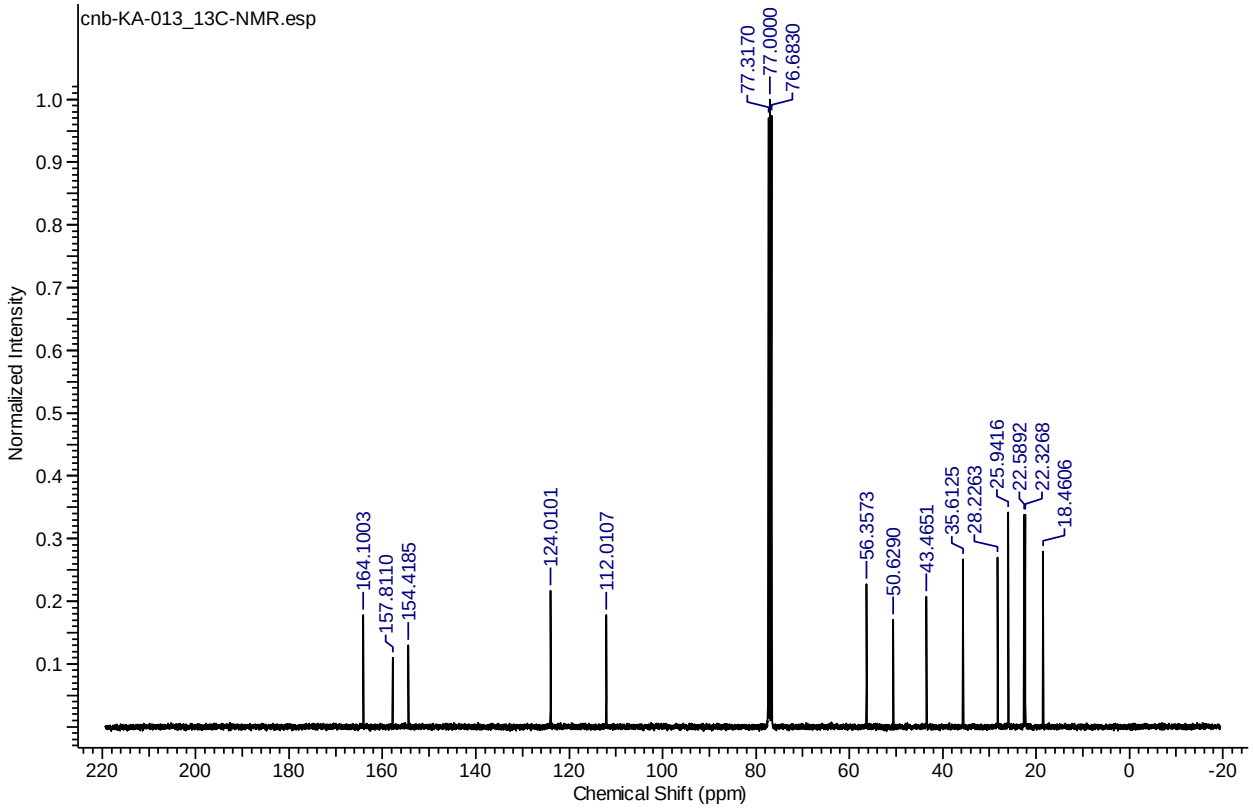
cnb-KA-013_13C-NMR.esp
Normalized Intensity
Chemical Shift (ppm)
77.3170
77.0000
76.6830
164.1003
157.8110
154.4185
124.0101
112.0107
56.3573
50.6290
43.4651
35.6125
28.2263
25.9416
22.5892
22.3268
18.4606

KA-019

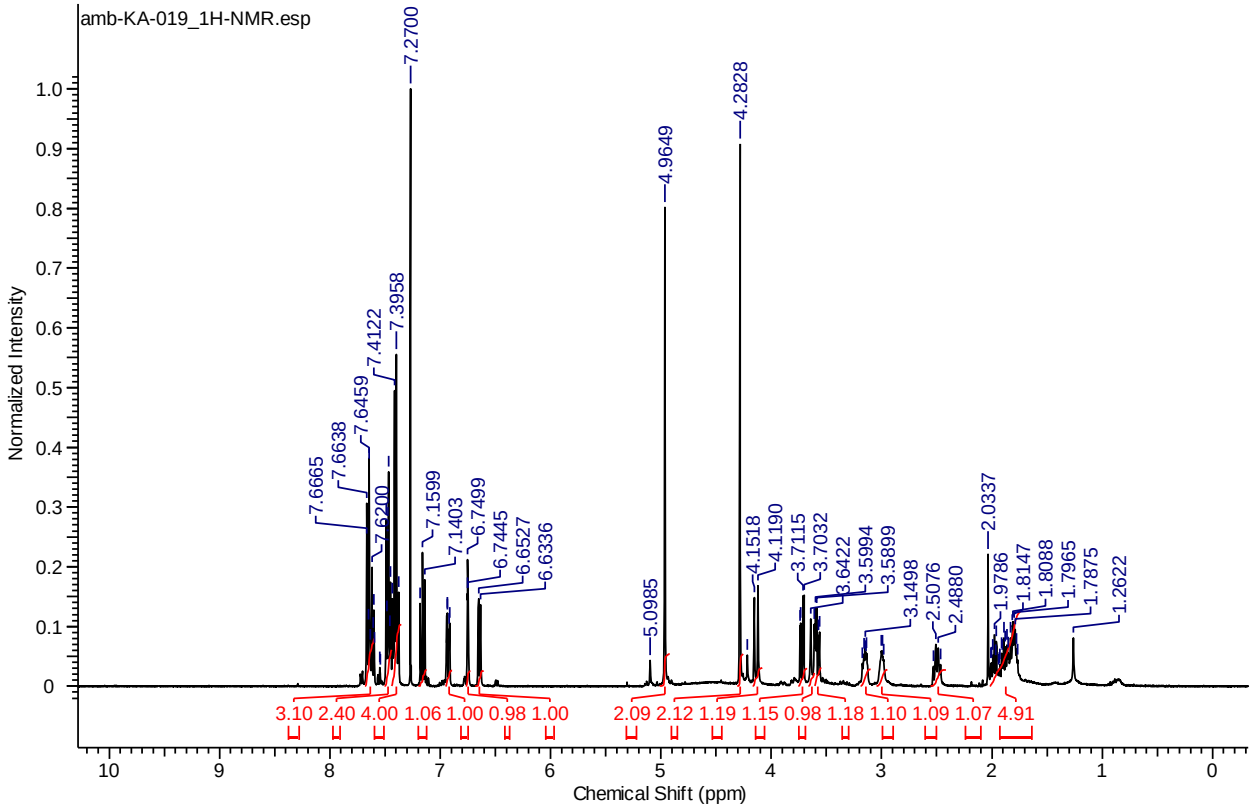
amb-KA-019_1H-NMR.esp
Normalized Intensity
Chemical Shift (ppm)
7.2700
4.9649
4.2828
7.4122
7.3958
7.6459
7.6638
7.6665
7.6200
7.1599
7.1403
6.7499
6.7445
6.6527
6.6336
5.0985
4.1518
4.1190
3.7115
3.7032
3.6422
3.5994
3.5899
3.1498
2.5076
2.4880
2.0337
1.9786
1.8147
1.8088
1.7965
1.7875
1.2622
3.10 2.40 4.00 1.06 1.00 0.98 1.00
2.09 2.12 1.19 1.15 0.98 1.18 1.10 1.09 1.07 4.91

KA-020A

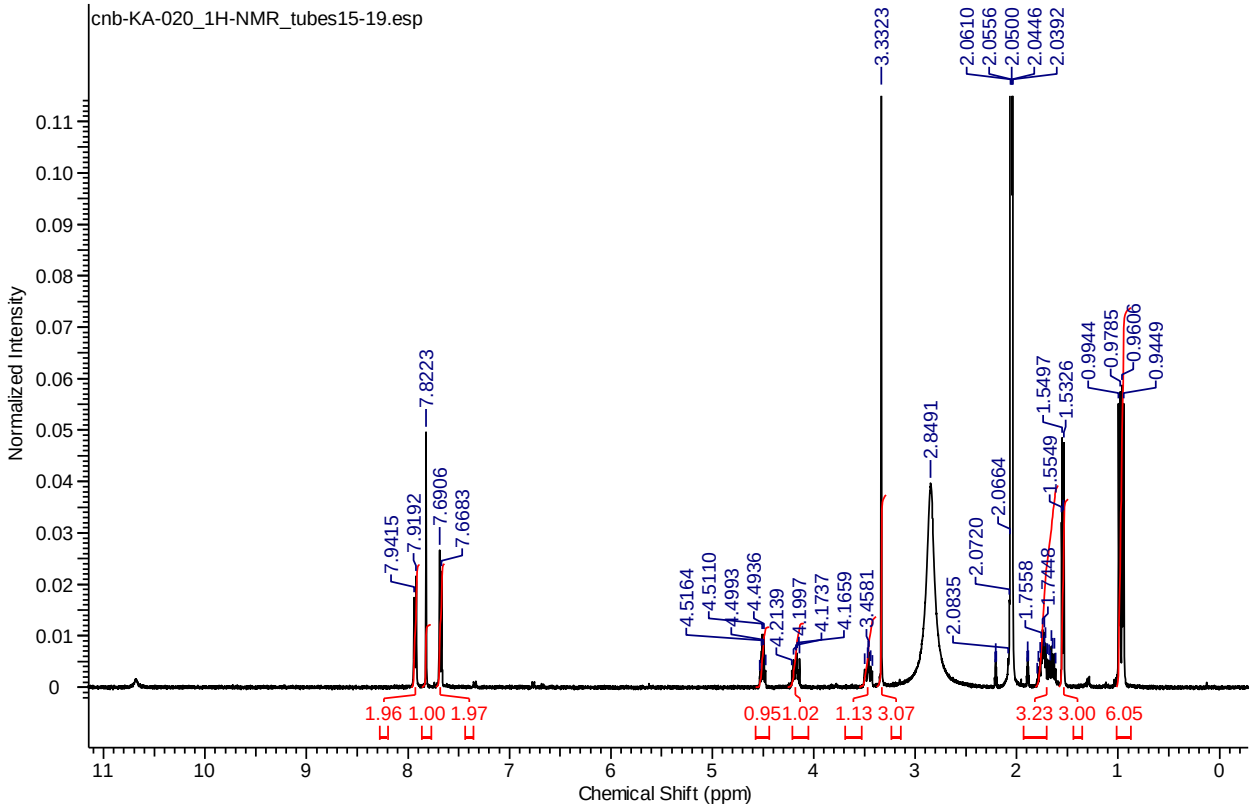
cnb-KA-020_1H-NMR_tubes15-19.esp
Normalized Intensity
Chemical Shift (ppm)
7.9415
7.9192
7.8223
7.6906
7.6683
4.5164
4.5110
4.4993
4.4936
4.2139
4.1997
4.1737
4.1659
3.4581
3.3323
2.8491
2.0835
2.0720
2.0664
2.0610
2.0556
2.0500
2.0446
2.0392
1.7558
1.7448
1.5549
1.5497
1.5326
0.9944
0.9785
0.9606
0.9449
1.96 1.00 1.97
0.95 1.02 1.13 3.07
3.23 3.00 6.05

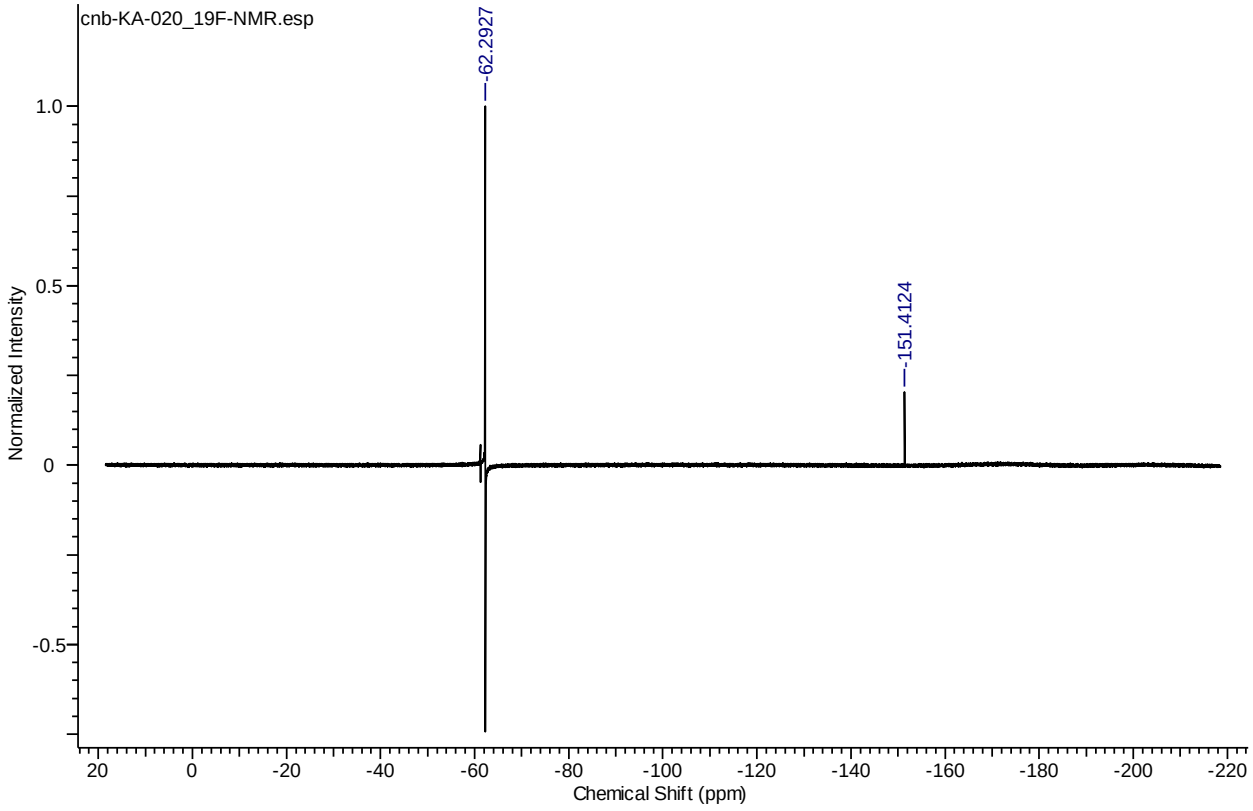
cnb-KA-020_19F-NMR.esp
Normalized Intensity
Chemical Shift (ppm)
-62.2927
-151.4124

KA-020B

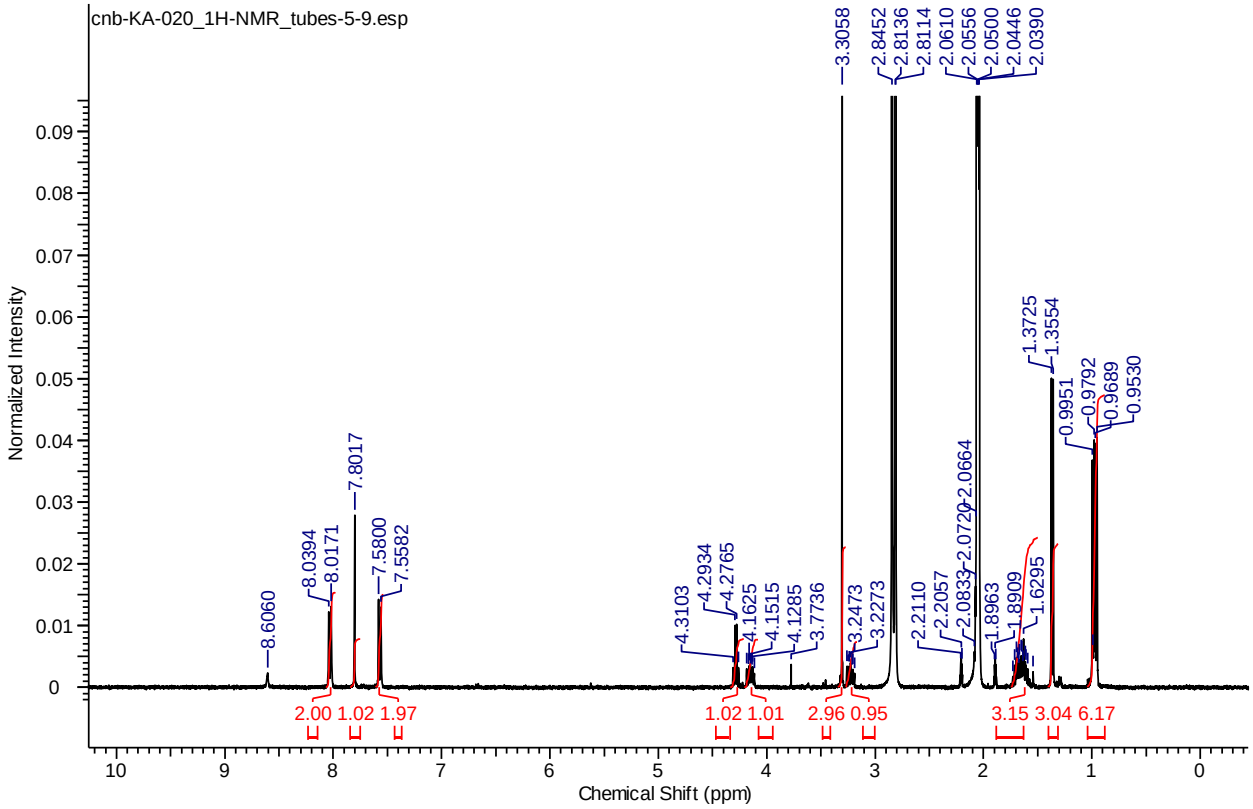
cnb-KA-020_1H-NMR_tubes-5-9.esp
Normalized Intensity
Chemical Shift (ppm)
8.6060
8.0394
8.0171
7.8017
7.5800
7.5582
4.3103
4.2934
4.2765
4.1625
4.1515
4.1285
3.7736
3.3058
3.2473
3.2273
2.8452
2.8136
2.8114
2.2110
2.2057
2.0833
2.0720
2.0664
2.0610
2.0556
2.0500
2.0446
2.0390
1.8963
1.8909
1.6295
1.3725
1.3554
0.9951
0.9792
0.9689
0.9530
2.00 1.02 1.97
1.02 1.01
2.96 0.95
3.15 3.04 6.17

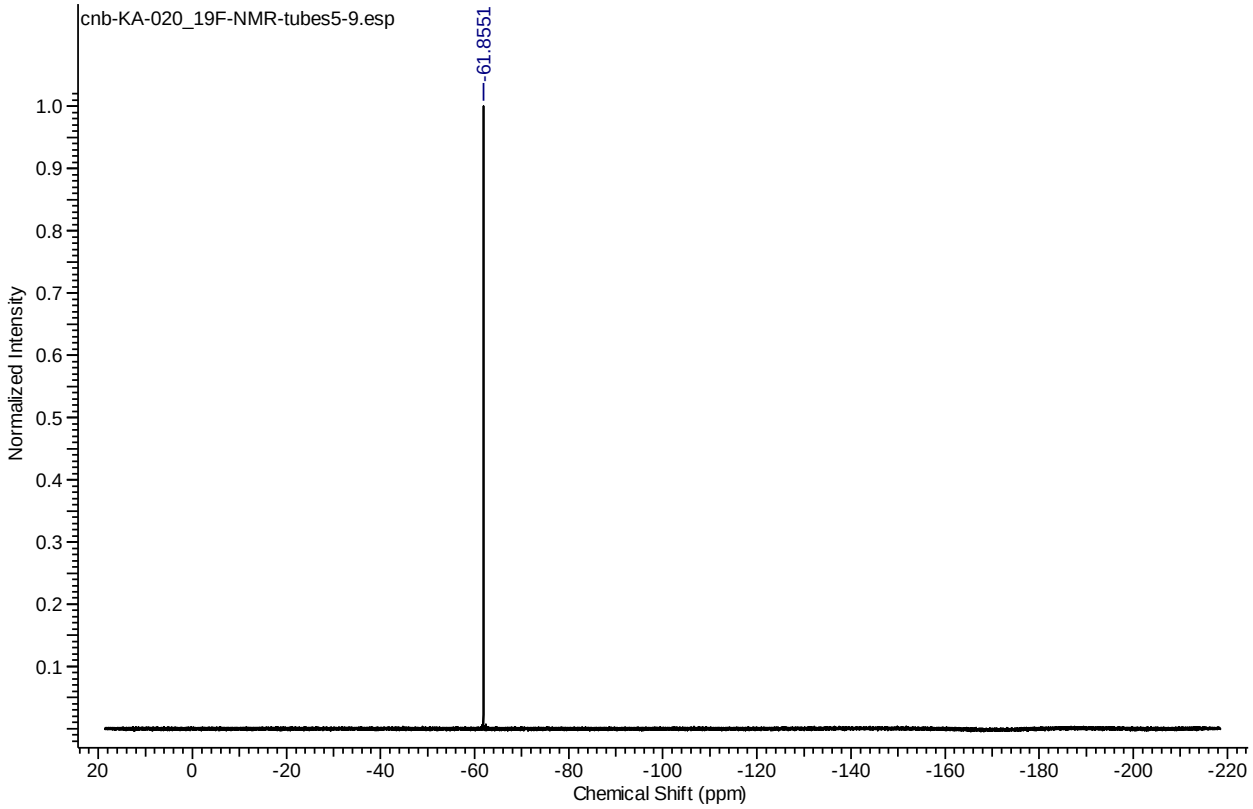
cnb-KA-020_19F-NMR-tubes5-9.esp
Normalized Intensity
Chemical Shift (ppm)
-61.8551

KA-016

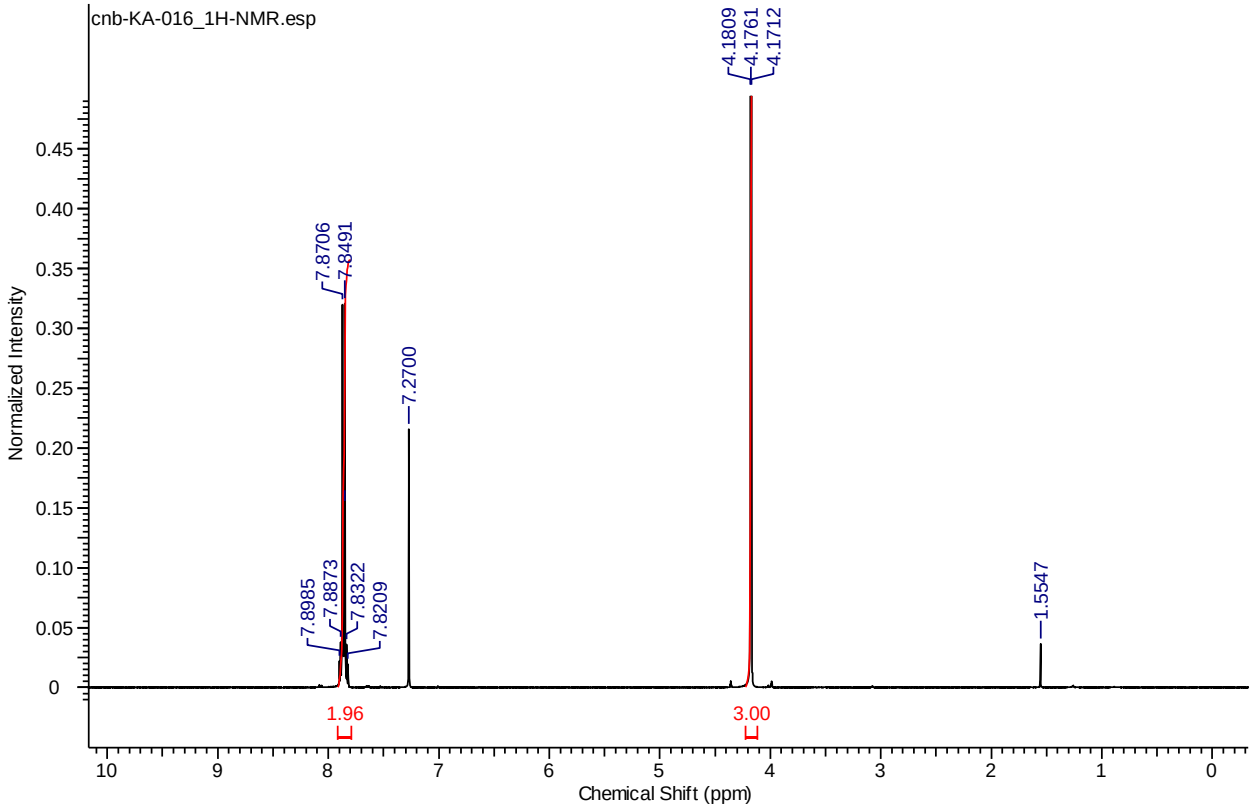
cnb-KA-016_1H-NMR.esp
Normalized Intensity
Chemical Shift (ppm)
4.1809
4.1761
4.1712
7.8706
7.8491
7.2700
7.8985
7.8873
7.8322
7.8209
1.5547
1.96
3.00

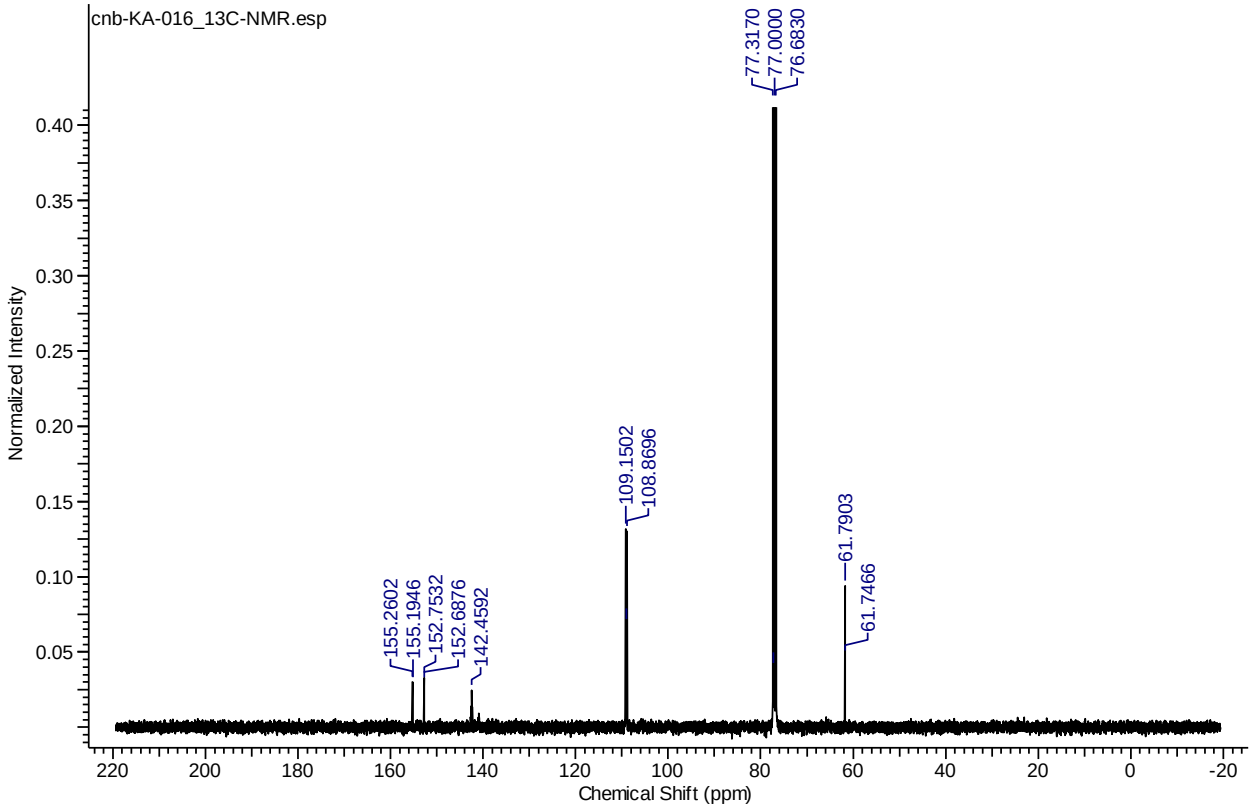
cnb-KA-016_13C-NMR.esp
Normalized Intensity
Chemical Shift (ppm)
77.3170
77.0000
76.6830
109.1502
108.8696
61.7903
61.7466
155.2602
155.1946
152.7532
152.6876
142.4592

KA-018

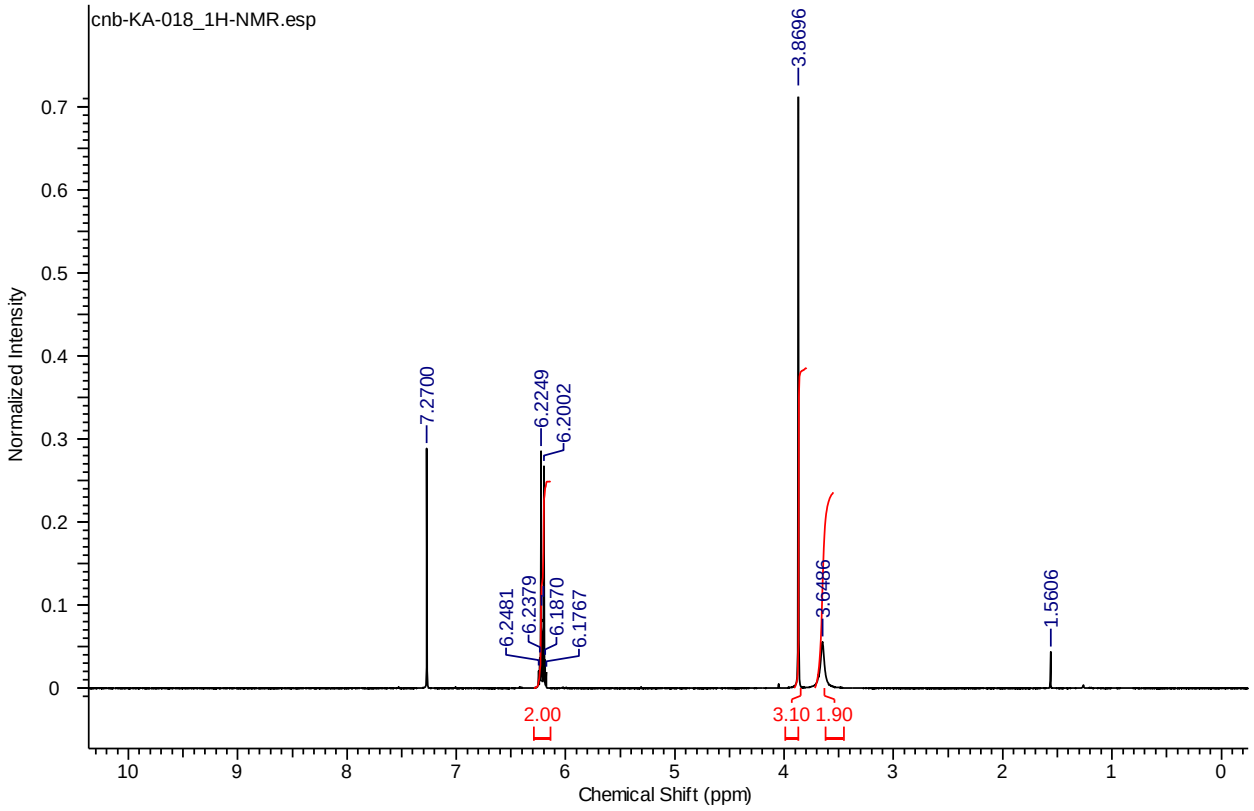
cnb-KA-018_1H-NMR.esp
Normalized Intensity
Chemical Shift (ppm)
7.2700
6.2481
6.2379
6.2249
6.2002
6.1870
6.1767
3.8696
3.6486
1.5606
2.00
3.10
1.90

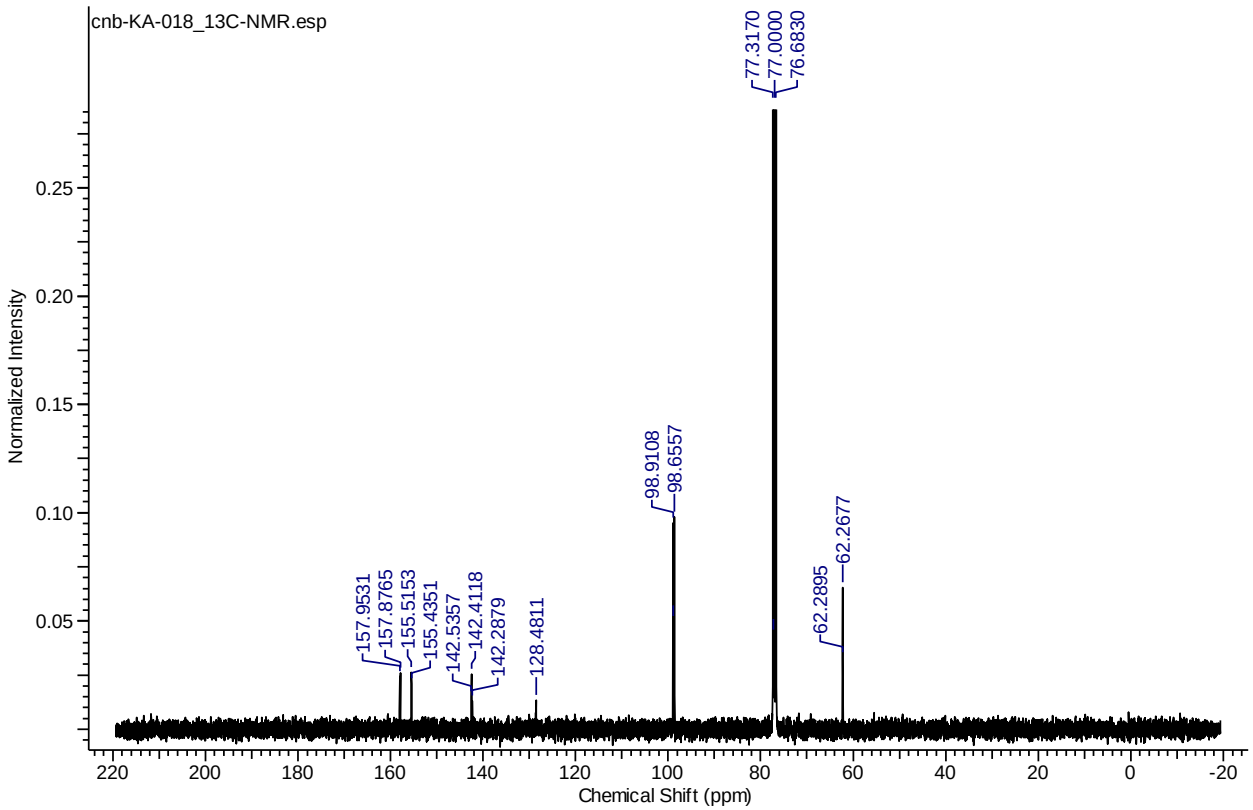
cnb-KA-018_13C-NMR.esp
77.3170
77.0000
76.6830
98.9108
98.6557
62.2677
62.2895
157.9531
157.8765
155.5153
155.4351
142.5357
142.4118
142.2879
128.4811
Normalized Intensity
Chemical Shift (ppm)

KA-021

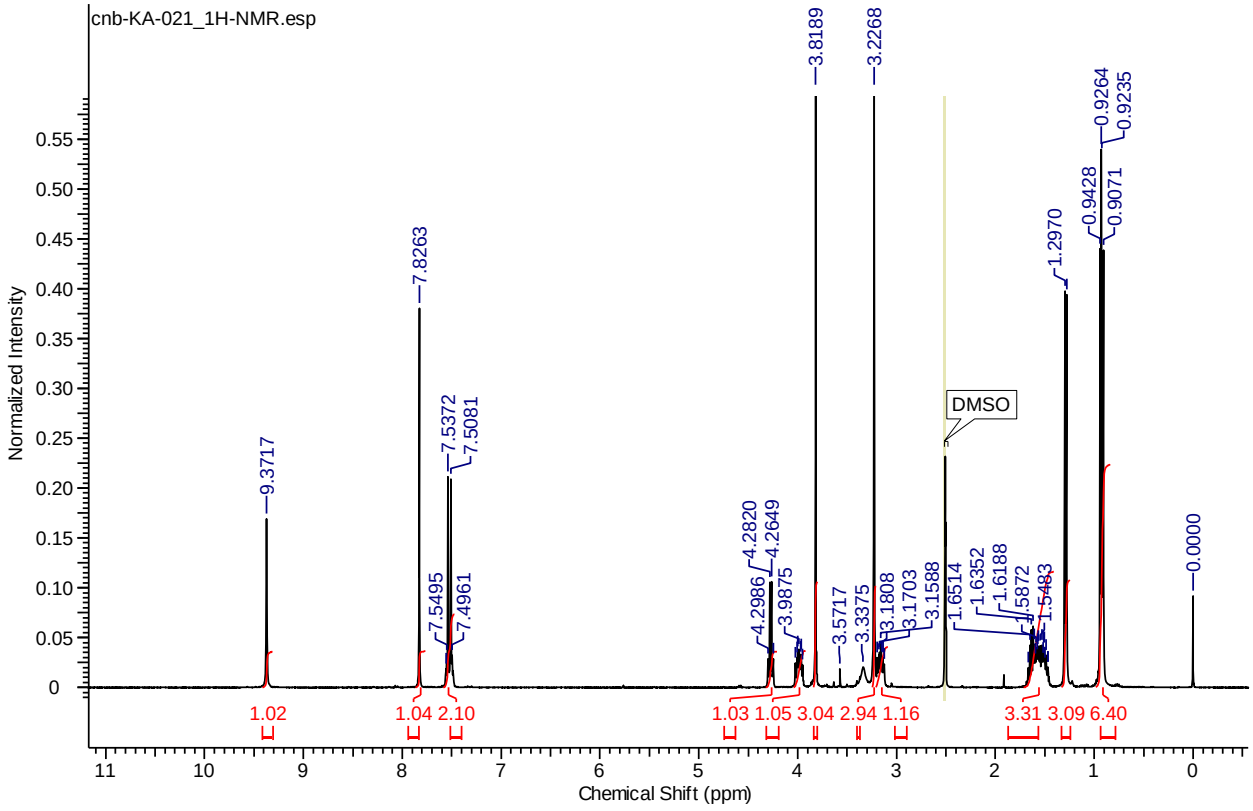
cnb-KA-021_1H-NMR.esp
3.8189
3.2268
0.9264
0.9235
0.9428
0.9071
1.2970
7.8263
7.5372
7.5081
9.3717
7.5495
7.4961
DMSO
4.2820
4.2649
4.2986
3.9875
3.5717
3.3375
3.1808
3.1703
3.1588
1.6514
1.6352
1.6188
1.5872
1.5483
0.0000
1.02
1.04
2.10
1.03
1.05
3.04
2.94
1.16
3.31
3.09
6.40
Normalized Intensity
Chemical Shift (ppm)

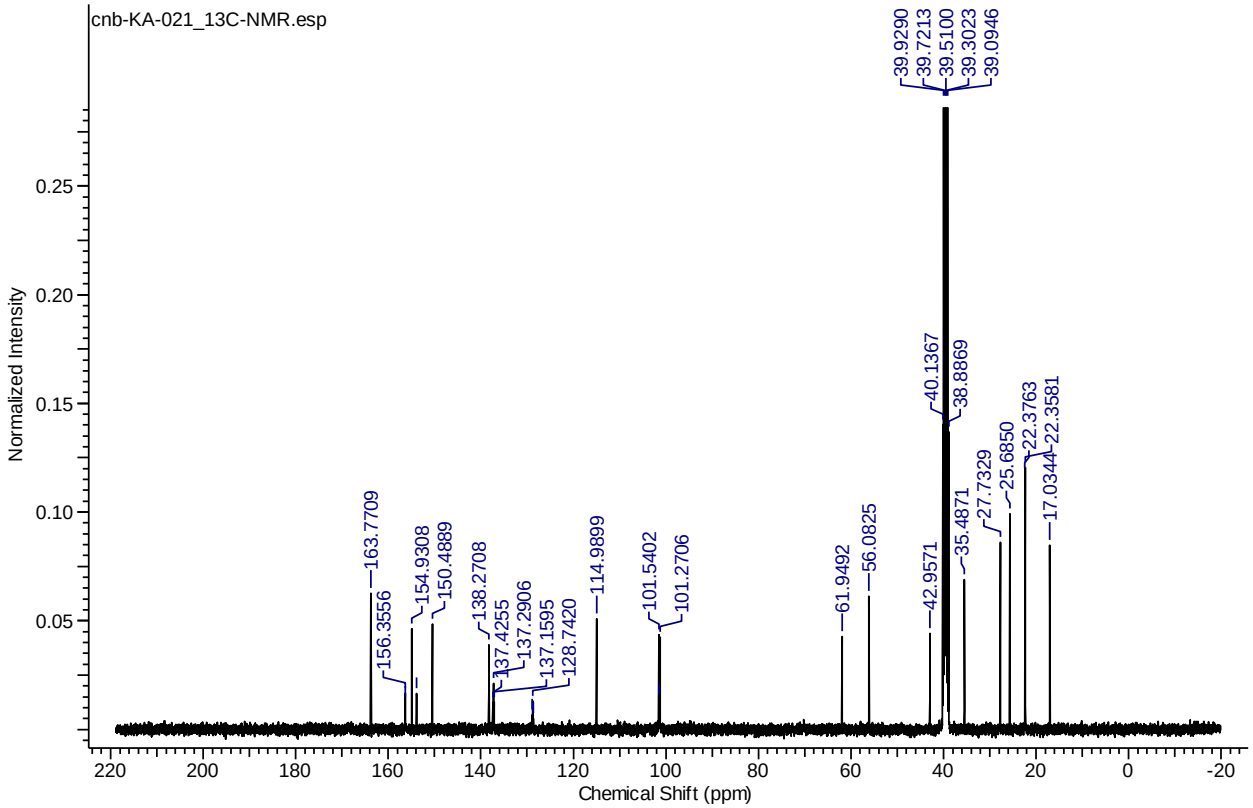
cnb-KA-021_13C-NMR.esp
Normalized Intensity
Chemical Shift (ppm)
39.9290
39.7213
39.5100
39.3023
39.0946
40.1367
38.8869
22.3763
22.3581
25.6850
27.7329
17.0344
35.4871
42.9571
163.7709
156.3556
154.9308
150.4889
138.2708
137.4255
137.2906
137.1595
128.7420
114.9899
101.5402
101.2706
61.9492
56.0825

KA-022

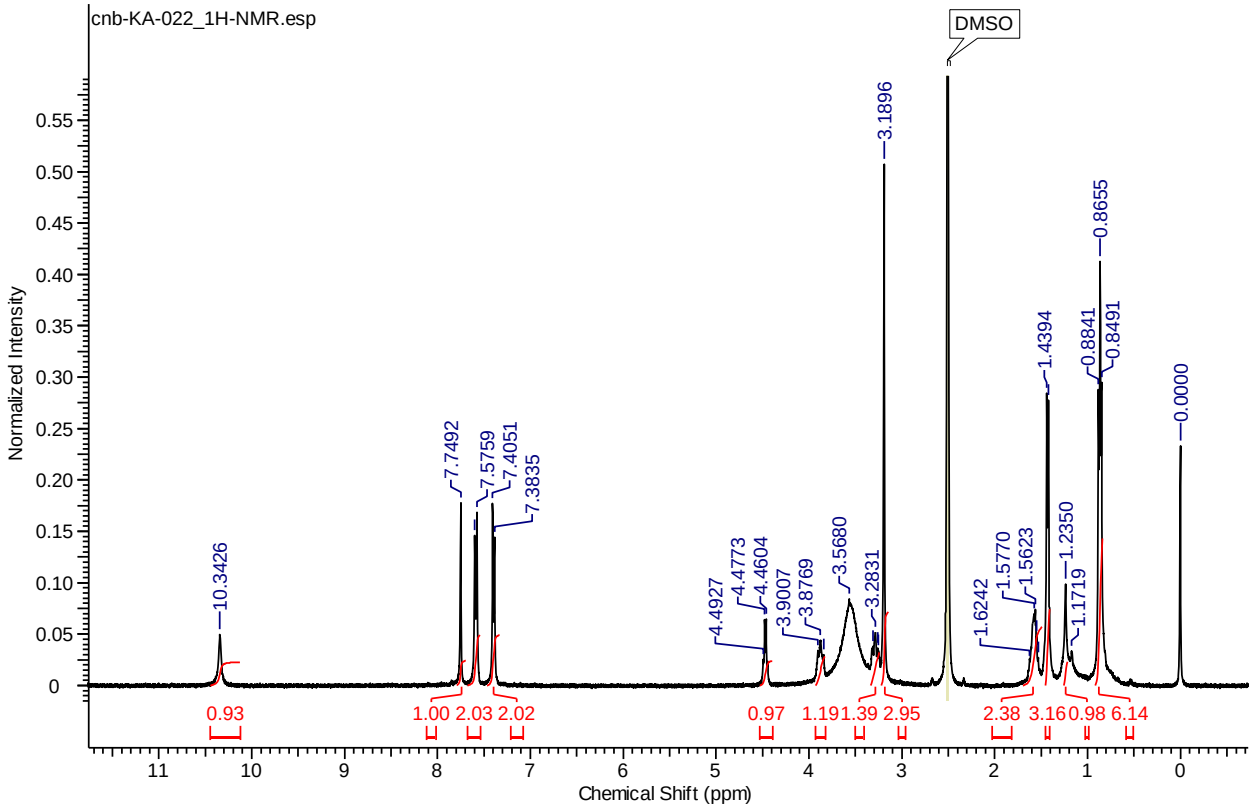
cnb-KA-022_1H-NMR.esp
Normalized Intensity
Chemical Shift (ppm)
DMSO
3.1896
0.8655
1.4394
0.8841
0.8491
0.0000
10.3426
7.7492
7.5759
7.4051
7.3835
4.4927
4.4773
4.4604
3.9007
3.8769
3.5680
3.2831
1.6242
1.5770
1.5623
1.2350
1.1719
0.93
1.00
2.03
2.02
0.97
1.19
1.39
2.95
2.38
3.16
0.98
6.14

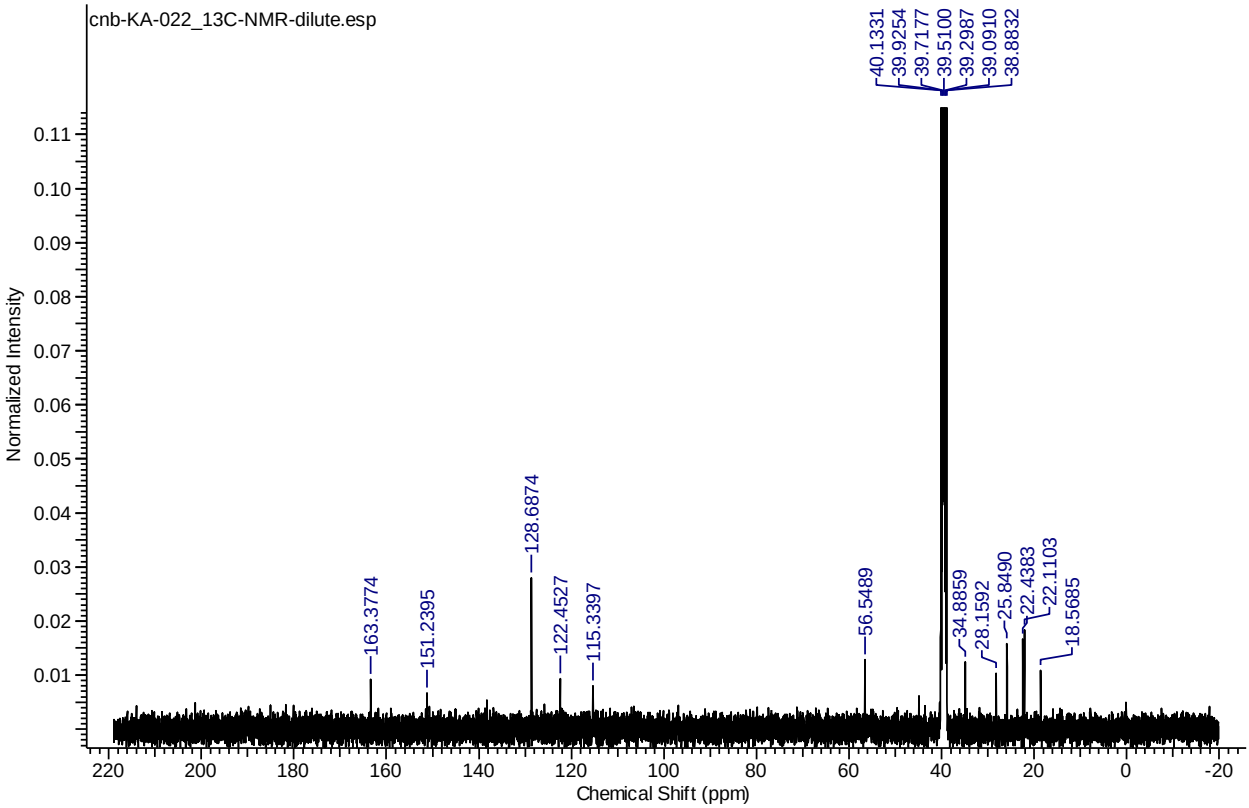
cnb-KA-022_13C-NMR-dilute.esp
Normalized Intensity
Chemical Shift (ppm)
40.1331
39.9254
39.7177
39.5100
39.2987
39.0910
38.8832
163.3774
151.2395
128.6874
122.4527
115.3397
56.5489
34.8859
28.1592
25.8490
22.4383
22.1103
18.5685

Compound 23

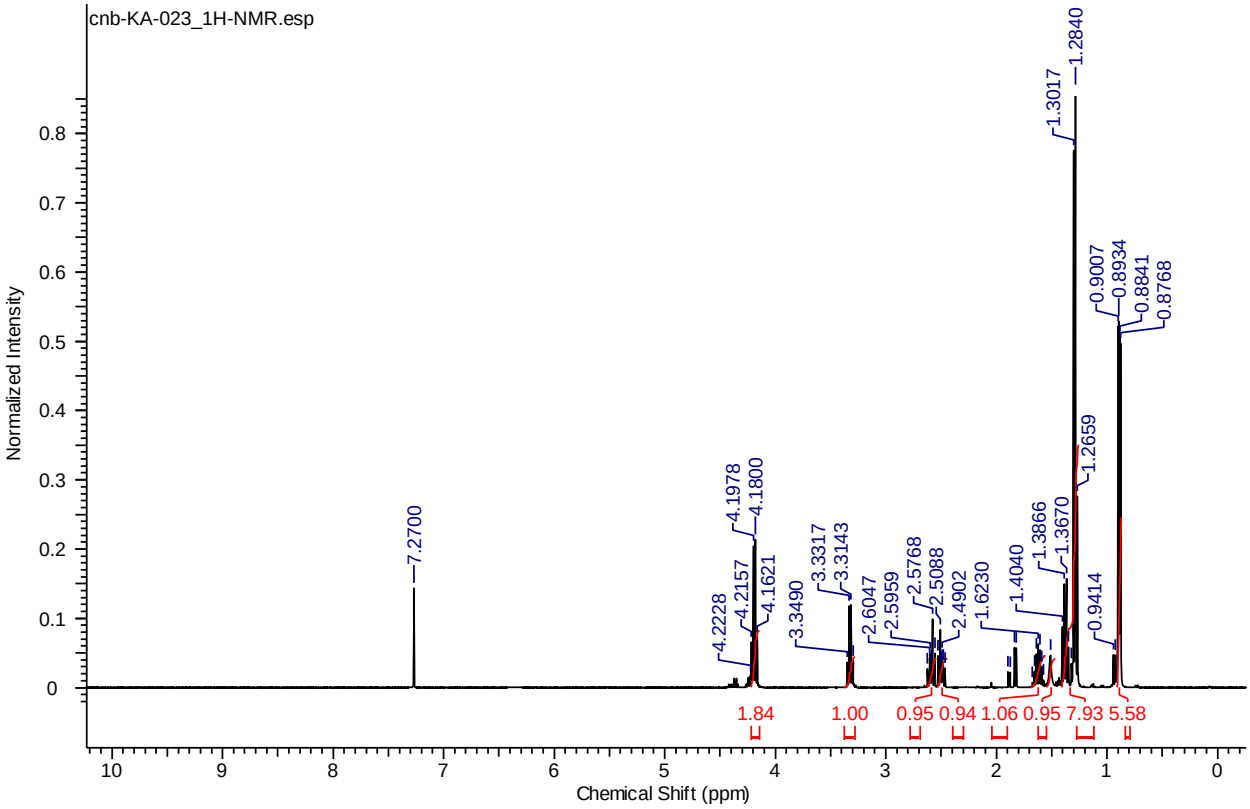
cnb-KA-023_1H-NMR.esp
Normalized Intensity
Chemical Shift (ppm)
7.2700
4.1978
4.1800
4.2157
4.2228
4.1621
3.3490
3.3317
3.3143
2.6047
2.5959
2.5768
2.5088
2.4902
1.6230
1.4040
1.3866
1.3670
1.3017
1.2840
1.2659
0.9414
0.9007
0.8934
0.8841
0.8768
1.84
1.00
0.95
0.94
1.06
0.95
7.93
5.58

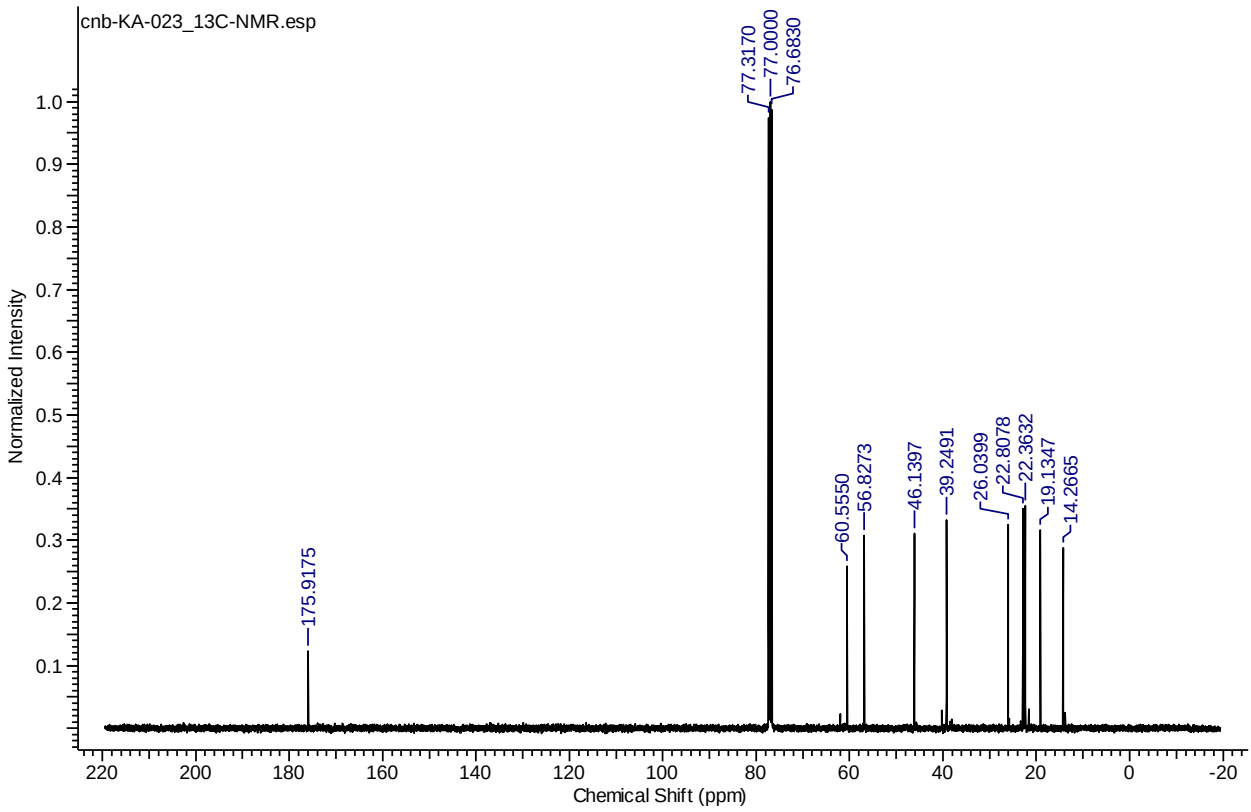
cnb-KA-023_13C-NMR.esp
Normalized Intensity
Chemical Shift (ppm)
77.3170
77.0000
76.6830
175.9175
60.5550
56.8273
46.1397
39.2491
26.0399
22.8078
22.3632
19.1347
14.2665

Compound 24

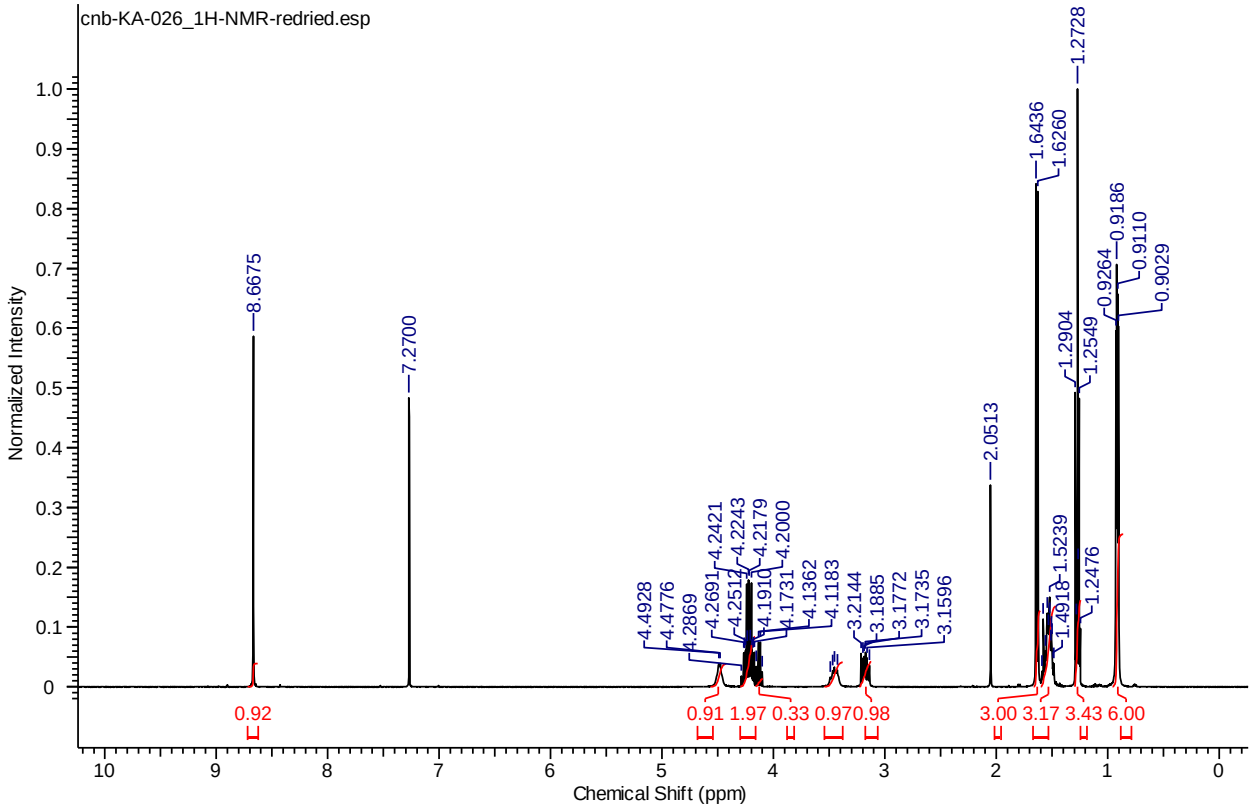
cnb-KA-026_1H-NMR-redried.esp
Normalized Intensity
Chemical Shift (ppm)
8.6675
7.2700
4.4928
4.4776
4.2869
4.2691
4.2514
4.2421
4.2243
4.2179
4.2000
4.1910
4.1731
4.1362
4.1183
3.2144
3.1885
3.1772
3.1735
3.1596
2.0513
1.6436
1.6260
1.5239
1.4918
1.2728
1.2904
1.2549
1.2476
0.9264
0.9186
0.9110
0.9029
0.92
0.91 1.97 0.33 0.97 0.98
3.00 3.17 3.43 6.00

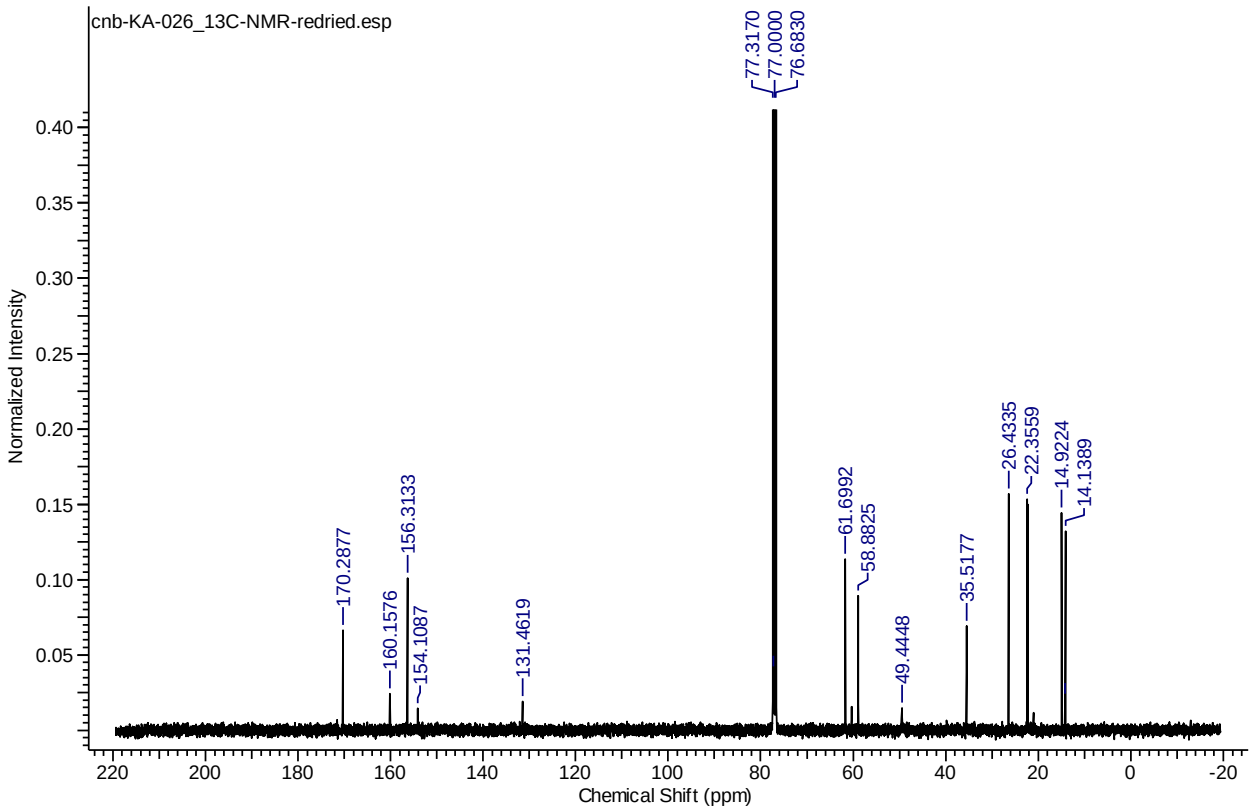
cnb-KA-026_13C-NMR-redried.esp
Normalized Intensity
Chemical Shift (ppm)
77.3170
77.0000
76.6830
170.2877
160.1576
156.3133
154.1087
131.4619
61.6992
58.8825
49.4448
35.5177
26.4335
22.3559
14.9224
14.1389

Compound 25

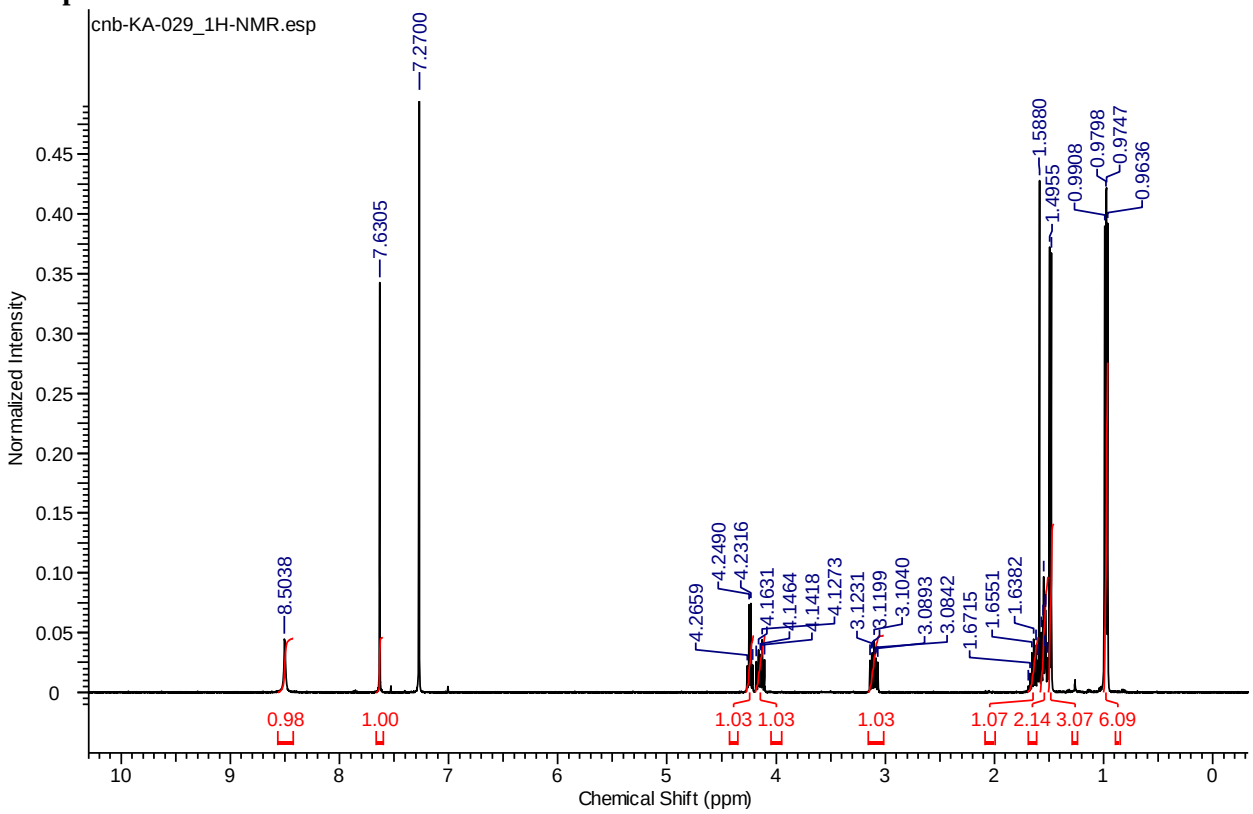
cnb-KA-029_1H-NMR.esp
Normalized Intensity
Chemical Shift (ppm)
8.5038
7.6305
7.2700
4.2659
4.2490
4.2316
4.1631
4.1464
4.1418
4.1273
3.1231
3.1199
3.1040
3.0893
3.0842
1.6715
1.6551
1.6382
1.5880
1.4955
0.9908
0.9798
0.9747
0.9636
0.98
1.00
1.03
1.03
1.03
1.07
2.14
3.07
6.09

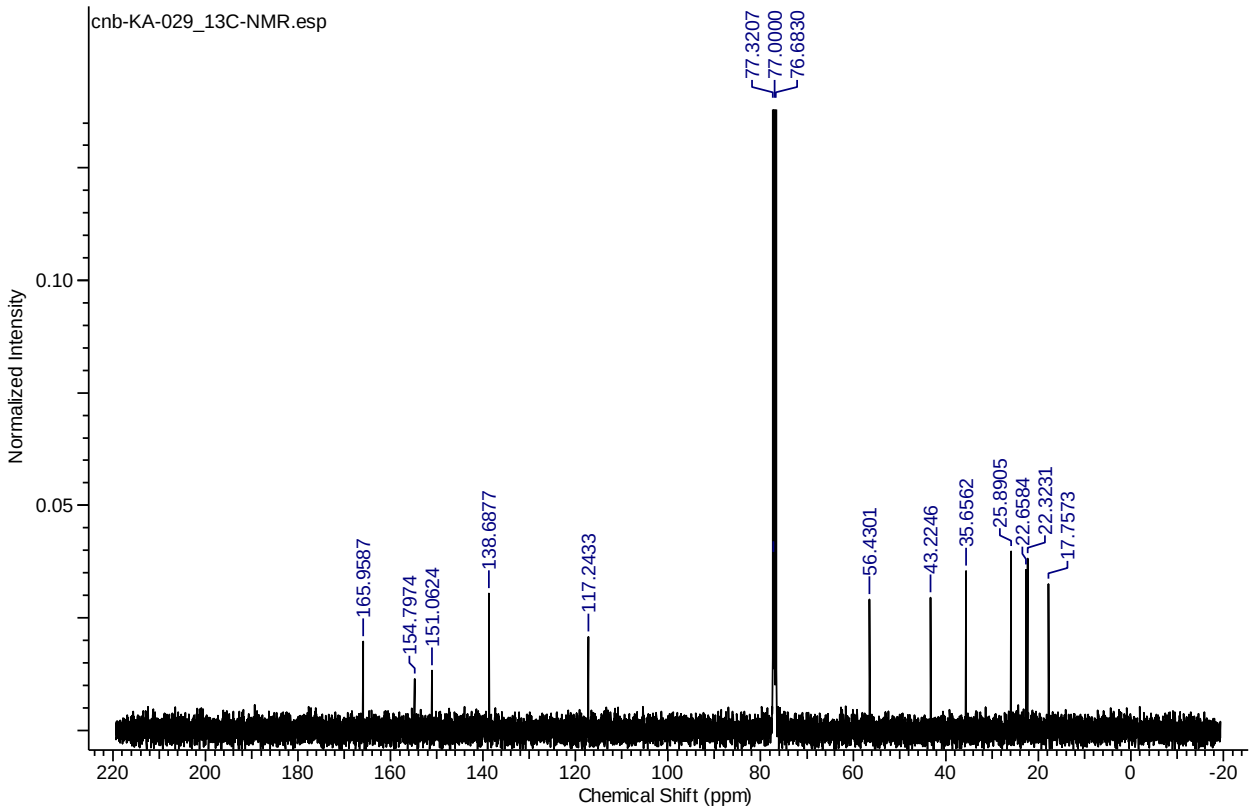
cnb-KA-029_13C-NMR.esp
77.3207
77.0000
76.6830
165.9587
154.7974
151.0624
138.6877
117.2433
56.4301
43.2246
35.6562
25.8905
22.6584
22.3231
17.7573
Normalized Intensity
0.10
0.05
220
200
180
160
140
120
100
80
60
40
20
0
-20
Chemical Shift (ppm)